Applied Thermal Engineering

sCO2 POWER PLANTS FOR WASTE HEAT RECOVERY: DESIGN OPTIMIZATION AND PART-LOAD OPERATION STRATEGIES

--Manuscript Draft--

Manuscript Number:	ATE-D-20-03999R1
Article Type:	VSI:CO2 technologies:Original Research Papers
Keywords:	Waste heat recovery; energy harvesting; Supercritical carbon dioxide; Part-load operation; System optimization; Techno-economic analysis
Corresponding Author:	Marco Astolfi ITALY
First Author:	Dario Alfani
Order of Authors:	Dario Alfani
	Marco Binotti
	Paolo Silva
	Ennio Macchi
	Marco Astolfi
Abstract:	This paper focuses on the potential of supercritical carbon dioxide closed cycle for waste heat recovery applications. The valorization of waste heat released from glass, steel and cement production facilities is recognized as one of the most effective solutions for the reduction of carbon footprint of the industrial sector. Common solutions rely on steam Rankine cycles and organic Rankine cycles while only few sCO2 power plants have been manufactured and operated so far as this technology has not yet reached the technical and commercial maturity. In spite of the large interest on sCO2 power plant from industry, institutions and academia, the role of this solution in future waste heat recovery applications is still unclear, highlighting the need of research studies focused on the performance assessment of these novel systems in both design and off-design conditions. This paper aims at bridging the gap between preliminary numerical studies and the design of real power systems by focusing on different aspects scarcely investigated in literature. The first section of this study deals with cycle design and provides a full description of the numerical complexity related to sCO2 power plant optimization, with a detailed description of the assumptions and the models implemented for the design of cycle components. Five different cycle configurations for the exploitation of a heat source consisting of a 50 kg/s stream of flue gas at 550°C have been analyzed and optimized: results are presented with a set of sensitivity analyses and the most promising configurations are analyzed from both a thermodynamic and a techno-economic perspective. Simple recuperative cycle, simple recuperative cycle with recuperator bypass and turbine split flow configurations are compared in detail proving that sCO2 technology can reach overall efficiencies up to 27.5%, a value higher than ORC for the same power output (around 6 MWel), and with a similar specific cost (2000 $/kW). Simple recuperated cycle with recuperator bypass is selected as the most promising configuration and it is further studied in off design conditions in the second section of the paper. Five different part-load strategies have been implemented allowing to assess the part-load performance of the selected cycle, considering both variable CO2 inventory and constant CO2 inventory systems. Results highlight that sCO2 recuperative cycles equipped with a CO2 storage vessel present a very high and almost constant efficiency down to 50% of the normalized flue gases mass flow rate, while a lower efficiency is expected for constant inventory systems. Both solutions can be operated down to 30% load with no difficulties on system components and with a minimum plant efficiency still competitive against ORC technology.
Suggested Reviewers:	Ty Neises ty.neises@nrel.gov
	Ambra Giovannelli

	ambra.giovannelli@uniroma3.it
	David Sanchez ds@us.es
Response to Reviewers:	

General comment from the Authors to Editor and Reviewers

The authors would like to thank the Editor for the suggestions and the selection of three very expert reviewers. Their comments allowed us to improve the clarity of the manuscript pointing out several sentences that were misleading for the readers. In this document we provide an answer to all the reviewers comments and we clearly reported in ***yellow*** the sentences that have been modified following their suggestions. The revised manuscript includes more changes(always highlighted in yellow) implemented thanks to reviewers observations. It was not an easy task, as demonstrated by the length of this document, and we hope the reviewers will appreciate the effort in following their comments regarding the content and they will understand our reasons behind the need of keeping some parts unchanged from the point of view of paper structure. In particular, we are aware of the length of the paper, but we previously discussed with ATE editorial board members who confirmed us that this Journal has removed the page limit. Regarding your suggestions, reviewer 2 did not highlighted the need of length reduction, while reviewer 1 and 3 suggested to cut on different sections which did not allow us to understand how to properly modify the paper. Moreover, reviewer #3 asked to expand some parts in order to ensure replicability. This was particularly challenging because providing more information on model structure in both design and part load without going through all the equations and further increase the length of the paper was not easy. We propose the following flow diagrams which we believe summarize all the interconnections between assumptions, calculated values, results and optimization routine. Some minor comments are still open and, if reviewers would like to provide us more information about them, we will be glad to include them in the final version.

Thanks a lot again for your time and your valuable comments,

The authors

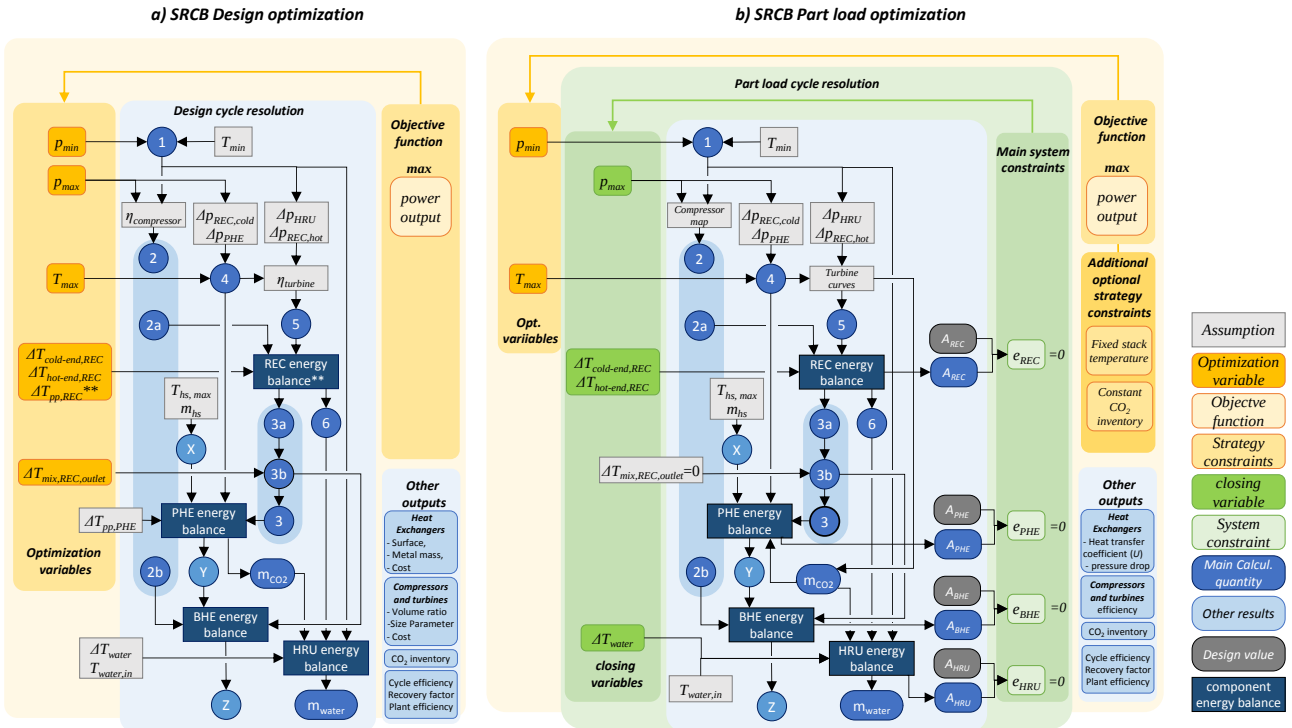

Editor

1. The Abstract should contain answers to the following questions:

What problem was studied and why is it important? What methods were used? What are the important results? What conclusions can be drawn from the results? What is the novelty of the work and where does it go beyond previous efforts in the literature? Please include specific and quantitative results in your Abstract, while ensuring that it is suitable for a broad audience. References, figures, tables, equations and abbreviations should be avoided.

Thanks for the comment, we revised the abstract and we think that now the abstract includes what is requested. The goal of the paper is clearly stated as well as the main numerical results. Let us know if something else in specific should be changed and we will make our best to improve this section.

---

2. The originality of the paper needs to be stated clearly. It is of importance to have sufficient results to justify the novelty of a high-quality journal paper. The Introduction should make a compelling case for why the study is useful along with a clear statement of its novelty or originality by providing relevant information and providing answers to basic questions such as: What is already known in the open literature? What is missing (i.e., research gaps)? What needs to be done, why and how? Clear statements of the novelty of the work should also appear briefly in the Abstract and Conclusions sections.

Thanks for the comment, we revised the last paragraph of the introduction trying to follow Editor suggestion. The new version is reported below:

These aforementioned studies highlight the potential of sCO_2 power cycles for WHR applications and justify the academic and industrial interest in the development of this technology. However, the currently available scientific literature lacks in research studies dealing with both the cycle optimization and the evaluation of part load performance. The present work aims to investigate this topic of high relevance for WHR applications providing results that can be useful to guide studies on system dynamic or control for future sCO2 power systems. First, a fair comparison of five cycle configurations in design conditions is presented, also including techno-economic and layout complexity considerations. Optimization of each cycle configuration has been implemented considering all the free design parameters instead of fixing some of them, in order to avoid suboptimal solutions and improve the accuracy and reliability of the results. Three cycles configurations are selected and discussed in detail and techno-economic analysis highlights that considering heat exchangers mass and cost is crucial when comparing different cycle architectures. Recuperative cycle with recuperator bypass has been selected as the most promising cycle configuration for this application and it has been eventually studied in part load conditions proposing and comparing different possible control strategy options based on both constant and variable inventory solutions.

---

3. An updated and complete literature review should be conducted and should appear as part of the Introduction, while bearing in mind the work's relevance to ATE and taking into account the scope and readership of the journal. The results and findings should be compared to and discussed in the context of earlier work in the literature.

Thanks for the comment, bibliography already included 77 reference in the draft paper and introduction provides a complete description of the most relevant works in literature. Now we reduced down to 74 limiting self-citing. If Editor would like to suggest any specific reference to be included, we will be happy to read it and cite it into the text

Reviewer #1

A) This study analyzes the performance of various sCO2 cycle configurations based on the; (1) operating parameters, (2) economic evaluation and, (3) part load operation. The study is extensive but some of the information is trivial such as section 2.1, 2.2 and 4.1.

Thanks for the comment. We are glad the study has been considered extensive in content. Regarding sections highlighted we would like to underline that:

- **Section 2.1 describes the different cycle configurations. We understand that for an expert reader on sCO_2 power cycles the advantages of the recompressed cycle and the role of recuperator bypass is clear and straightforward. However, we believe that without this section a generic reader will not be able to follow the remaining part of the paper. Also, this section allows us to introduce the methodology and the thermodynamic streams indexing.**
- **Section 2.2 describes all the assumptions and the methodology and the optimization procedure. We understand that it would be relatively trivial for some readers, but it ensures the replicability of the results. Actually, Reviewer 3 suggested to provide more details on this part, so we need to find a compromise.**
- **Section 4.1 could be a bit out of the context because it does not exclusively deal with the numerical procedure. However, referring to real plant operation allows to support some of the numerical choices taken in the paper. Moreover, it is not common to have this level of discussion is a research paper and we believe that for a generic reader, especially from industry, this information could be more interesting than numerical optimization analysis. The other two reviewers did not highlight the necessity of removing this part, so we are inclined to keep it into the paper.**

B) The show the validation of the results and HX's sub routines to calculate HX area can be useful.

Thanks for the comment. As reported in the text the numerical model has been implemented on the base of the Dostal PhD Thesis model which is a common standard in CO_2 power plant modelling and integrated with some manufacturer data on plate thickness and channels hydraulic diameter. The model has been used within the H2020 sCO2-flex project and presented in different conferences (ASME TE, ORC seminars and sCO2 conference) but we included only one reference in order to limit self-citing. Results regarding the overall heat transfer coefficient are reported in Table 6 and validated as order of magnitude against the design of Fives Cryo (partner in sCO2-flex project) which detailed results on HX design are unfortunately confidential. We believe that we provided all the information in order to ensure a complete understanding of the methodology and the main results are clearly reported. However, a validation against real size equipment for this application is not possible due to the lack of experimental data. If the reviewer can share a reference which allows for model validation on PCHE we will be happy to consider it for this or future publications.

C) Authors may consider adding some of the details and figures to supplementary information such as the discussion of economic analysis and so on, so the readability and the coherence of the manuscript can be improved.

Thanks for the comment, we are aware of the length of the paper and we discussed about this with the editor before the submission. Since Applied Thermal Engineering removed the limit of max number of pages, we agreed to keep the whole paper content in a single paper (avoiding splitting it in part A & B) and limiting the use of supplementary material which is not taken into account by many readers. We will report

your observation to the Editor, however, we are not sure to be able to follow this suggestion without a clear indication of all the parts to be moved in supplementary material section or the sections that should be shortened. Regarding economic analysis we believe that is just one page long and gives interesting information on the competitiveness of CO_2 cycles against ORC which is not something easy to find. Moreover, this part also explains that from a specific cost perspective the three cycle architectures are rather similar and it guides the choice of the plant to be studied in part load operation.

D) In section 3.2, the main results discussion is focused on the isothermal mixing, however, this require more explanation and justification (See comment 6).

Thanks for the observation: Comment 6 of Reviewer 1 refers to isobaric mixing which is probably a typo. Mixing is always isobaric in design (if not a lumped pressure drop is added on the high-pressure stream) while it can be isothermal or not (and this is a design choice). Isothermal mixing is the common design criteria, supported by second law analysis considerations, and adopted in many different papers. Coherently the sensitivity analysis on ΔTpp of recuperators (3.2) adopts this assumption. However, this assumption is then modified in section 3.3 in order to explain to the readers that this is not always the optimal choice, but it is strongly influenced by the cycle layout and the application. We added a short sentence trying to be clearer about this point:

This constraint involves the adoption of a specific split or bypass ratio (depending on the cycle configuration) which may lead to suboptimal solutions.

E) The study concluded sCO2 is superior to ORC and that the simple recuperative cycle with bypass outperforms the other sCO2 cycle configurations. The key conclusion of the manuscript in the reviewers' opinion are: (a) the desired configuration of sCO2 cycle depends on the heat source but it has been reported before. (b) the metal mass of Heat exchanger (HX) or the characterization of HX's is important while comparing different sCO2 configurations, and (c) and investigating the part load operation strategies. It is recommended to emphasize on (b and c) and discussed them in the introduction. Right now, there is hardly any study in the introduction that discusses what has been done in the scope of (b) and (c).

Thanks for the comment, we modified the introduction trying to highlight these aspects as follow:

Optimization of each cycle configuration has been implemented considering all the free design parameters instead of fixing some of them in order to avoid suboptimal solutions and improve the accuracy and reliability of the results. Three cycles configurations are selected and discussed in detail and techno-economic analysis highlights that considering heat exchangers mass and cost is crucial when comparing different cycle architectures. Recuperative cycle with recuperator bypass has been selected as the most promising cycle configuration for this application and it has been eventually studied in part load conditions proposing and comparing different possible control strategy options based on both constant and variable inventory solutions.

F) The results pertaining to the part load operation are more interesting and certainly valuable for sCO2 researchers community.

Thanks for the comment, we are glad the reviewer appreciated this part of the paper.

G) Lastly, the provision of line no could have eased the mentioning of a certain manuscript section while making comments.

Thanks for the suggestion, we added line numbering.

---

1. Improving the overall readability, flow of the manuscript, and sentence structure is recommended. Check for typos and punctuation. E.g. in section 3.1, the "id" should be "is", 3.2, "similarly to the previous example". Check the color of Fig. 4 (middle)

Thanks for the comment, we revised the text trying to limit typos. If the reviewer can highlight more typos we will be glad and happy to correct them. Regarding Figure 4, we corrected the colour of HTR duty label?

---

2. Avoid lumping the references. Also, the literature survey can be improved. Some latest and pioneering work addressing the sCO2 cycle configuration analysis, applications, and development should be cited.

Thanks for the comment, the paper has now 74 cited papers which is certainly a consistent number. We tried to include the most relevant references in our opinion. If the reviewer would like to suggest any specific reference, we will take them into consideration, we will read them and we will be happy to add them in bibliography. Regarding lumping references, we tried to improve this aspect splitting them and revising the text.

---

3. The highlights focus on what has been studied. Please reiterate on key results and highlight the vital findings as well.

Thanks for the comment. We revised this part and the new proposed Highlights are formulated as follow:

- ***We optimized five sCO_2 cycle configurations for waste heat recovery application***
- ***Optimal plants reach efficiency higher than ORC (>27%) with similar specific cost (2000$/kW)***
- ***Simple recuperative cycle with bypass (SRBC) is selected as the optimal configuration***
- ***We studied the different part-load strategies for this optimal configuration (SRBC)***
- ***Variable inventory part load strategy is more efficient than constant inventory strategy***

---

4. The abstract mentions some sCO2 cycles have been operated for the valorization of waste heat. In reviewer's opinion, the sCO2 power plants are still under laboratory development stage.

Thanks for the comment. Actually Echogen in US is manufacturing sCO2 cycles also for WHR. They installed and operated some plants and so this technology TRL is pretty high and systems are already tested in relevant environment. This is also confirmed by Reviewer 2 comment.

---

5. "due to the lack of coherent and comprehensive numerical studies aimed at assessing the performance of these novel systems in both design and off-design conditions."
While the reviewer agrees sCO2 cycle studies has still a lot of scope, however, this conclusion is not that sound. Since a single research on ScienceDirect for sCO2 cycle gives numerous (100s) of results. Moreover, the abstract gives information, that is better suited for the introduction. Kindly rewrite.

Thanks for the comment, we softened this sentence in the abstract. New version is the following:

In spite of the large interest on sCO_2 power plant from industry, institutions and academia, the role of this solution in future waste heat recovery applications is still unclear, highlighting the need of research studies focused on the performance assessment of these novel systems in both design and off-design conditions.

5.b Kindly emphasize on the novelty and contribution of this study in the introduction.

Thanks for the comment. We revised the introduction trying to be clearer about this point. In particular, we added the following sentence:

These aforementioned studies highlight the potential of sCO_2 power cycles for WHR applications and justify the academic and industrial interest in the development of this technology. However, the scientific literature available today lacks in research studies dealing with both the cycle optimization and the evaluation of part load performance. The present work aims to investigate this topic of high relevance for WHR applications providing results that can be useful to guide studies on system dynamics or control for future sCO_2 power systems.

---

6. Kindly provide references to this statement "An additional hypothesis generally adopted in literature is related to the imposition of isothermal mixing processes to minimize mixing irreversibilities." Above table 2. In reviewer opinion, many researchers have investigated isobaric mixing. Further in section, 3.3, why do authors have to fix the temperature difference before mixing? For example, based on the energy balance and isobaric mixing, the state of working fluid after mixing can be calculated. In reviewers' opinion, e.g. in Fig. 1(b), the temperature 3b and 3a can be same or different based on the split ratio. In any case the state 3 can be found. Kindly elaborate on it and why the difference in mixing temperature is necessary to fix?

Thanks for the comment. Mixing in design conditions is always isobaric (if the pressure drops are not balanced a lumped pressure drop is added to the stream at high pressure) while the temperature difference between the two streams before mixing process is a design variable. This temperature difference is generally set to zero because it allows to minimize entropy generation and exergy loss in the mixing process. However, the goal of section 3.3 is to demonstrate that the hypothesis of isothermal mix is actually not correct at all times and it can lead to suboptimal design solutions. Regarding the final observation, reviewer is right and fixing a ΔTmix is the same of fixing the split ratio but our choice is more stable from numerical point of view and it allows to avoid inconsistent results during cycle optimization. We highlighted this aspect with the following text:

This constraint involves the adoption of a specific value for the split or bypass ratio (depending on the cycle configuration) which may lead to suboptimal solutions.

---

7. The TQ diagrams in Fig. 2. C2 needs elaboration

Sorry but we did not catch the suggestion. C2 diagram is similar to C1 and C3. In any case we added y-axes titles in order to improve the readability of the charts.

---

8. In section 3, is the optimization done to maximize plant effieicny?

Thanks for the comment, we believe that this point is clearly explained by sentence above equation 1:

"The optimization algorithm aims at maximizing the net power output and consequently the overall plant efficiency η_{plant} which takes into account not only the thermodynamic quality of the conversion from heat to electricity (through η_{cycle}), but also the fraction of heat exploited with respect to the total heat available from the heat source (through χ).

---

9. In sec 3.1 , Kindly explain in what temperature range the cycle efficiency is being decayed. From the figure, it keeps increasing. "However, in this temperature range the cycle efficiency decay is more marked than for the other two configurations due to the adoption of two turbines, thus reducing the main turbine inlet temperature is not convenient from thermodynamic perspective."

Thanks for the comment, we tried to be clearer with the following sentence:

In this temperature range (450°C-525°C) the cycle efficiency change is more marked than for the other two configurations because of the adoption of two turbines and larger than the relative increase of heat recovery factor χ, thus reducing the main turbine inlet temperature is not convenient from thermodynamic perspective.

---

10. Figure 4, instead of left, right or middle, the writer may use alphabets to distinguish and cite each figure.

Thanks for the comment, we changed all the figures and the reference into the text.

---

11. Check the weird question mark sign above Fig. 4 in the text.

Sorry, but we do not see the question mark in the file. Probably is a problem of file visualization.

---

12. The effect of recuperator temperature difference in SRC and SRCB is quite simple. From a simple thermodynamic perspective, reducing the PP always increases the cycle performance and efficiency at the expense of increased HX area and investment. In Fig. 3 (left), the only drawback of the reduced PP was on heat recovery, but that also merely changes from 83 to 86 %. Thus, in reviewer's opinion, for optimizing efficiencies and heat recovery, the lower the PP, the better. Why does the writer choose to show these results?

Thanks for the comment. In WHR applications is not sure that the lower DTpp results in the higher overall power production. Adopting low ΔTpp also increase the inlet temperature at the primary heat exchanger (CO_2/flue gases) with a possible reduction of heat recovery factor and a penalization of the power production. For some cycle configurations this tradeoff pushes the optimal ΔTpp towards low values, in others like the recompressed cycles towards high values highlighting that adopting always the minimum technical value of ΔTpp independently of the cycle configuration is not the optimal choice at all times.

---

13. Fig. 4 right, please mention what are solid and dashed line?

Thanks for the comment, we included the following explanation in caption:

Dashed lines in (c) represent the cold and hot extremities of the recuperators.

---

14. "Sensitivity analysis is carried out varying the pinch point temperature difference of LTR and HTR and by optimizing the performance by varying the cycle maximum temperature, the cycle maximum and minimum pressures, the ΔTcold-end,LTR, the ΔThot-end,LTR and the ΔThot-end,HTR while always considering a isothermal mixing a both LTR and HTR recuperators." The results can be added to the supplementary information.

Thanks for the comment, please refer to our answer to comment C).

---

15. Please add references to the turbomachinery efficiencies in Page 14

Thanks for the comment, actually the following sentence also includes the reference for the turbomachinery efficiency calculation: "Results can be confirmed by verifying the correctness of turbomachinery efficiency assumptions against the results attainable with correlations developed for sCO2 components as function of pressure ratio and size parameter [66]"

---

16. Plz check caption of Fig. 5. Also, add explanation? What are the dotted lines in Fig 5(a).

Thanks for the comment, please see answer to comment 13.

---

17. What are Zin, Zout and Vr in table 6? Kindly mention the symbols before using them.

Thanks for the comment, because of column size it is not possible to add the full variable explanation, but the variables are included in the nomenclature section

---

18. What is the meaning of closing variable in Table 8?

Thanks for the comment. We tried to be clearer modifying the sentence as follow:

Once the aforementioned parameters are set, the steady-state part load operating condition is obtained by solving a system of nonlinear equations each one representing the part load behavior of a component in the system (system constraints in Table 8). Table 8 also reports the selected closing variables of the off-design problem, namely those quantities, unknown a priori, that are varied by the solving algorithm in order to verify system constraints. Once the off-design problem is solved, the power output is computed and the fluid inventory variation within the system is calculated knowing the internal volume of each component, the connecting piping volume and the thermodynamic conditions of sCO_2. Table 8 only refers to the SRCB configuration which is the one selected for part load operation detailed analysis.

---

19. Please explain the acronyms for the first time you have used them.

Thanks for the comment, we checked the document and we made revision when needed

---

20. Compressor maps haven been developed for this study or is this a part of bigger study? Kindly clarify on how the figure 6 is obtained

Thanks for the comment. As reported in sentences "Turbomachinery design can be assumed coherent with the design proposed by Baker Hughes General Electric (BHGE) in the framework of sCO2-Flex project [39] adopting the following design criteria and off design performances" and "Turbine part load operative curve and off design performance is derived from BHGE calculations carried out in the frame of sCO2-Flex project [39]." The compressor map has been developed in the frame of a bigger study

---

21. What is the meaning of less optimized one in 5.1. "Strategy S1 is the less optimized one and it is reported here as term of comparison"

Thanks for the comment, we agree that the term "less optimized" is misleading. We modified the sentence as follow:

Strategy S1 is the simplest one, it does not include any optimization in order to maximize power output and it is reported here as term of comparison

---

22. In my understanding, figure 8 is plotted only for strategy S2. Why? Moreover, what is Tmax,nom? Also, add some more discussion to these figures.

Thanks for the comment, we tried to improve the description to this figure by revising the text:

Strategy S2 aims at optimizing cycle power output by varying both minimum pressure (compressor inlet) and maximum cycle temperature (turbine inlet). Figure 8.a depicts the trend of power output variation against strategy S1 attainable by the adoption of different cycle maximum temperatures and by optimizing the cycle minimum pressure (Figure 8.b) at all times.

and the figure caption:

Figure 8. (a) Net power output variation with respect to S1 strategy attainable by varying cycle maximum temperatures and optimizing cycle minimum pressure at all times, (b) corresponding optimal compressor inlet pressure for the different cycle maximum temperatures.

---

23. Has the preliminary sizing of turbomachinery conducted in this study as mention in conclusions?

Thanks for the comment, reviewer is right and we modified the sentence as follow:

a preliminary sizing heat exchanger and the definition of turbomachinery main parameters has….

Reviewer #2:

Overall, a very well-written paper. The cycle layouts cover a good range of possible arrangements of turbomachinery and heat exchangers, and the comparisons between them are fair, and the reasons for differences in performance are explained clearly. Similarly, the part-load optimization work is also well described, despite the complexity of the multiple methods for optimization.

The attached PDF includes my commentary, much of which is driven more by academic curiosity about the results than direct criticisms. There are a few editorial marks as well for completeness. I recommend publication with only a few minor edits and clean-ups.

Thanks a lot for the comment, we report below the PDF comments and the respective answers while the typo has been directly corrected in the manuscript.

---

1. Echogen's cycle is not simple recuperated - see Held, T. J., 2015, "Supercritical CO2 Cycles for Gas Turbine Combined Cycle Power Plants," Power Gen International, Las Vegas, NV. for details

Thanks for the comment, reviewer is right and Echogen adopts a dual rail cycle. We modified the sentence accordingly:

In the US this technological solution has already been proposed to the market by Echogen [42], which manufactures and commercializes sCO_2-based WHR systems also in combined heat and power solutions (CHP). Echogen technology was initially based on a simple recuperated power cycle but now adopts a more complex design, called Dual Rail configuration, which is similar to the turbine split flow cycle and allows to obtain a higher power output and a better exploitation of exhaust gases sensible heat [ref].

---

2. Glass furnace flue gas is highly particulate-loaded... maybe worse than iron & steel

Thanks for the comment, we added your observation in the column "comment"

Very high particulate load which results in high fouling factors on heat transfer surfaces

---

3. cp is a function of temperature (and composition) for real flue gases. Probably wouldn't change the outcome, but important to note, especially because the variation of CO2's cp with temperature and pressure is the cause of the temperature pinch issues in the LTR, and could also affect pinch point behavior in the BHE

Thanks for the comment, reviewer observation is very precise but we believe that accounting for cp(T) for the flue gases would not affect final results because the pretty high minimum temperature of the gases and the fact that cp reduces with temperature reduction while the opposite for CO_2. As result, in recuperator bypass pinch point can occur only at cold or hot side and not in the middle of the heat exchanger. Regarding CO_2, thermodynamic properties are precisely calculated and recuperators are discretized in order to correctly detect pinch point location.

---

4. Proximity to the critical point does not directly drive system efficiency. In fact, Reference 64 makes no such statement regarding selection of minimum cycle temperature, simply that it was chosen to avoid condensation. Modeling of the heat rejection system performance as a function of design, operating conditions (load) and ambient temperature is difficult, and incredibly important.

Thanks for the comment, reviewer is right and we cited the wrong reference. We totally agree that the design and the operation of the heat rejection system is of crucial importance for a sCO_2 power plant and it is often a very neglected topic. We prepared a research paper on this issue with a focus on dry air cooling and corrective actions in order to limit annual energy production penalization.

---

5. Please describe the rationale for this limit (I assume it is dewpoint / condensation avoidance)

The reviewer is correct, we added this information directly into the text:

and a minimum allowable temperature of 150°C in order to avoid any formation of acid condenses and fouling on heat transfer surfaces

---

6. Why are some heat exchanger dP's given in %, others in bar?

Thanks for the comment, actually this assumption came from sCO2 flex experience for boiler convective pass heat exchangers. If the reviewer can suggest a % value we will be happy to test the effect on the results and adopt it in this or future works

---

7. Strangely enough, compressibility reduces compression work (increases average fluid density during the compression process). What you really want is to increase the mean density of the fluid, but balancing that against getting the highest pressure ratio across the expander as possible.

Thanks for the comment but we are not totally sure to catch the observation but we tried to follow reviewer suggestion modifying the sentence as follow:

Cycle minimum and maximum pressures are selected considering the trade-off between the need of having high cycle expansion ratio and the need to increase compressor fluid average density by exploiting the low compressibility factor of the CO_2 in the proximity of the critical point

---

8. What is sigma_max? ASME allowable?

Thanks for the comment. Yes, it is. We added a note in the text.

---

9. I don't think anyone makes PCHEs out of Alloy 800... at these temperatures, would almost certainly be 316L

Thanks for the comment, we modified the mass of the PCHE according to your suggestion.

---

10. The exhaust temperatures are too hot for carbon steel, would need to be either a higher chrome ferritic (e.g. T22, T91) or austenitic alloy.

Thanks for the comment, we made some errors in the table due to copy&paste from another work. Thanks for having noticed it! Actually, we used Inconel 617 for PHE and BHE and copper/aluminium (tube/fins) for the HRU. Many thanks!

11. Basis is total area, or bare-tube area? What flue-gas dP was assumed to arrive at this (seems on the high side)?

Thanks for the comment, as reported in the equations the global heat transfer coefficient is related to the internal heat transfer area. We now clearly report this into the text. Pressure drop on flue gas side is neglected since flue gas blowing is not considered as an internal consumption

---

12. Pinch point limits are sometimes, but not always used as constraints. Weiland's and Held's studies, for example, use UA as an optimization variable rather than pinch point.

Thanks for the comment, we added a sentence for this new reference of Held. Unfortunately we checked on Weiland papers and we did not find the work mentioned. Can you share the exact reference with us?

An exception is represented by the work of Held [ref] where the heat exchangers UA value (overall heat transfer coefficient, U, multiplied by the heat transfer surface, A) is selected as an optimization variable rather than pinch point temperature differences.

---

13. Referred to isothermal mixing : That's not a hypothesis, it's an arbitrarily imposed constraint.

Thanks for the comment, we corrected the text accordingly.

---

14. Not necessarily true--the characteristic thermal time parameter for heat exchanger is m*cp/UA. Since m/UA is roughly constant for a given heat exchanger type (for instance, PCHEs), the thermal inertia of the heat exchangers is not a strong function of heat exchanger scale.

Thanks for the comment, this is a very precise observation. We made some research and we decided to remove that sentence, referring now only to cost and footprint.

---

15. It would have been interesting to look at performance vs cycle architecture at fixed capex. Perhaps as a follow-on study?

Thanks for the suggestion, we added a note in future steps section.

---

16. I generally disagree with the conclusions of [71] - they should not have used Mach number to determine the equivalent of cavitation margin, since it entangles the speed of sound into the problem, which is not the correct scaling for a near-liquid fluid.

Thanks for the comment, we included a new reference which states a similar conclusion. We hope you agree with this. Otherwise we will be happy to receive a suggestion from you.

---

17. So the main compressor is using VIGVs (first mention of it... also need to define "IGV")? Is there sufficient margin to ensure no cavitation at the compressor inlet? ([71]'s methodology for determining margin is OK, it's just their Ma scaling I disagree with)

Thanks for the comment, the presence of IGV is reported later at page 21 with sentence so we decided to make the highlighted sentence more general:

Both main and secondary compressor operating points are set acting on available control strategies (IGV aperture and/or rotational speed variation) in order to provide the desired mass flow rate at the….

---

18. Regarding water coled HRU: Not entirely... wet bulb temperature is more diurnally consistent than dry bulb, but will change some day-to-night, and can vary widely seasonally.

Thanks for the comment, we changed the sentence including a recent reference on this topic:

Cooling water minimum temperature (fixed): always equal to the design value according to the focus of this work on the part load analysis. Variation of minimum temperature of the cooling medium on nigh-day and seasonal base can clearly affect system performance but the penalizing effect on annual energy yield can be rather limited when water cooled or wet and dry HRU solutions are adopted [ref].

---

19. Regarding heat transfer area in off. Design: Shouldn't the heat transfer area be constant (and equal to the design value)?

Thanks for the comment, we modified the sentence as follow:

Off design heat transfer area of each heat exchanger is imposed equal to the design value and calculated considering the same discretization of the component in order to catch local variations of thermodynamic properties as reported in Eq. 5 and Eq. 6.

---

20. Referred to strategies definition- higher is the number of active constraints lower is the number of free control variables to be optimized to maximize power output Not clear what is meant by "higher" and "lower"

Thanks for the comment, we agree that the sentence was not clear enough, we tried to improve it as follow:

The activation of a specific strategy constraint involves an additional new closing variable: as result one strategy control variable must be calculated to satisfy the additional constraint instead of being varied with the aim at maximizing power output

---

21. Figure 7 (b) Dashed vs solid lines are not clear for S1 and S3

It was a problem of PDF visualization. We will check it during revision proof

---

22. Referring to part load section: It would be helpful to point out in the introductory paragraph that power is being optimized, not efficiency. Otherwise, this chart can be a little confusing at first.

Thanks for the comment, we think that this aspect is clearly reported at the beginning of the section by sentence:

“Different part-load cycle operation strategies can be implemented in order to optimize the power production and/or to meet specific operational constraints”.

---

23. reduce both the cycle minimum pressure: How does this impact the compressor cavitation margin?

Thanks for the comment, we did not check this aspect with calculations but we expect that moving on the right of the critical point (lower pressures at constant temperature) would also limit this issue.

---

24. Only cycle maximum temperature is optimized constraint while cycle minimum pressure is calculated in order to respect the stack temperature. Did the authors consider varying the PHE/BHE flow split to maintain minimum stack temperature?

Thanks for the comment, this is a very interesting suggestion, but we did not consider this option as we imposed an isothermal mixing at all times.

---

25. very similar values of net power output can be obtained with different combinations of cycle maximum temperature and minimum pressure - This is a very good observation, one that many people who do optimization studies miss!

Thanks for the comment, we appreciate!

Reviewer #3:

This paper investigates sCO2 cycles for waste-heat recovery looking into cycle optimisation, techno-economics and part load performance. The paper is very interesting, and relevant to the journal and to the special issue to which it has been submitted. The paper is on the whole also prepared to a good standard and I believe technically correct.

Thanks for the comment, we are glad the reviewer appreciated the paper.

However, I have a few reservations with the paper which should be considered by the authors before being acceptable for publication:

1. the paper is very long and a significant effort needs to be made to condense the content of the paper to ensure the discussion is concise;

Thanks for the comment, we are aware of the length of the paper and we discussed about this with the editor before the submission. Since Applied Thermal Engineering removed the limit of max number of pages, we agreed to keep the whole paper content in a single paper (avoiding splitting it in part A&B) and limiting use of supplementary material which is not taken into account by many readers. We will report your observation to the Editor, however we are not sure to be able to follow this suggestion without a clear indication of all the parts to be moved in supplementary material section or the sections that should be shortened.

---

2. throughout the paper, very limited details on the modelling are presented. I am not suggesting that every single equation needs to be shown, but in its current format I believe it would be difficult for a reader to replicate the study. I would therefore ask the authors to include some more specific details.

Thanks for the comment, we understand the need of providing all the information about system modelling in order to ensure replicability and we think that the reported information in the revised version are more adequate. We introduced a flow diagram for both the nominal and part-load modelling and reported more information about the modelling in the text by adding several sentences and rewriting the ones that were misleading or unclear. Once all the assumptions have been declared (table 2) and the free quantities (table 3) subject to optimization are defined, the solution of the cycle is just a matter of energy balance on the different components. Cycle simulation can be carried out with ad hoc numerical tools or with commercial software like Aspen or Thermoflex. We tried our best to make as clear as possible the modelling approach, but if the reviewer has some examples or suggestions about this point, we will be happy to consider it in a second step of the review.

---

3. whilst the work presented appears thorough, the analysis is only applied to a single heat-source condition, and only one cycle is considered at off-design. This does somewhat limit the conclusions to this specific case, and means it is difficult to extrapolate the results to other applications. This is slightly at odds with the statement at the end of the introduction where they mention a need for comprehensive studies.

The reviewer is right, however expanding the work to different heat sources will result in a strong increase of paper length. Moreover, the outcome would be rather similar to an already published paper of the same authors with self-citing issues. Regarding the off-design analysis to be applied to other cycle layouts, it is important to underline that this part is extremely time consuming and would require at least other 2-3 pages in the final manuscript. Moreover, we focused the off-design analysis on the cycle with the higher potential, providing a full explanation of the selection criteria. Regarding your last observation, we agree

that the sentence in the introduction is not representative of our work that cannot claim to be comprehensive (all heat sources, all cycle configurations, each one in both design and off design)

---

4. In line with my previous comment, I wonder if instead of focussing on covering thermodynamics, economics and off-design in a single paper, a better approach might be to focus on a particular aspect and look into that in more detail. In my opinion, the economics section is probably the weakest since no form of techo-economic optimisation has been completed and there is likely to be significant uncertainty in the heat exchanger sizing and component cost modelling. Therefore, that could be removed and in return more details relating to the thermodynamic modelling could be included. Perhaps by looking at other heat-source conditions, or possibly looking at more than one cycle architecture at off design.

Thanks for the comment, on the one hand we agree with the reviewer but on the other we think that expanding the work to different heat sources and considering the off design of more configurations would result in a strong increase of paper length which is something already highlighted as a weak point by the reviewers. The economic part we believe is important because it allows to clarify that sCO_2 can be competitive against ORC even if without a full technoeconomic optimization and to support the choice of the simple recuperative cycle with bypass as the most interesting configuration because it can reach high efficiency but without an excessive cost increase.

---

5. Besides those comments, a few other comments:- in the abstract, define abbreviations at first use (i.e., WHR)

Thanks for the comment, we checked the document and we made revision when needed

---

6. the abstract is too long

Thanks for the comment, however we did not have a clear indication from the Journal guidelines. We will check with the Editor.

---

7. whilst I appreciate the very comprehensive introduction, in its current format I believe it is too long. Some effort needs to be put into significantly reducing it in length and focusing on the most important features that are relevant to the study.

Thanks for the comment. Even if we recognize the introduction is quite long, we are reluctant in reducing it because we believe it is valuable. It reports a synthetic description of many studies instead of a stream of citations with no comments and provides a clear overview of this research field to the readers (especially the less knowledgeable ones).

---

8. at the end of the introduction, the motivation of the study needs further justification. For example, there are currently many thermodynamic studies on sCO2 systems within the literature - what exactly is not comprehensive about those already published?

Thanks for the comment. We revised the introduction trying to be clearer about this point. In particular we added the following sentence:

These aforementioned studies highlight the potential of sCO_2 power cycles for WHR applications and justify the academic and industrial interest in the development of this technology. However, the scientific literature available today lacks in research studies dealing with both the cycle optimization and the evaluation of part load performance. The present work aims to investigate this topic of high relevance for WHR applications providing results that can be useful to guide studies on system dynamics or control for future sCO2 power systems.

---

9. Section 2.1: better to give the precise mathematical model used to compute properties (i.e., the equation of state), rather than saying REFPROP.

Thanks for the comment, we included the following sentence:

Carbon dioxide thermodynamic properties are computed through the REFPROP 9.1 database [57] using a high fidelity 42 terms reduced Helmholtz energy equation of state [ref] allowing for an accurate evaluation of real gas effects close to the critical point of the working fluid.

---

10. the motivation for the selected heat source conditions should be enhanced.

Thanks for the comment, we added a clarification on the choice of minimum stack temperature and we think that the reported temperature values in table 1 and cited references are sufficient to support our choice. However, if reviewer can provide more details about the missing motivation, we will be happy to discuss them in the paper.

---

11. as a reviewer, I would consider myself quite knowledgeable on this topic and can appreciate all of the intricacies discussed in Section 2.2. Having said that, I do not believe readers of the paper would be able to understand fully or replicate the study. I believe more effort is needed to explain how the developed model.

Thanks for the comment, it is not easy to explain the methodology without going deep in all the calculations which is not the case as already motivated in answer to comment 2. We tried to provide a graphical explanation of the methodology for the SRCB cycle configuration. We hope the reviewer will find this adequate.

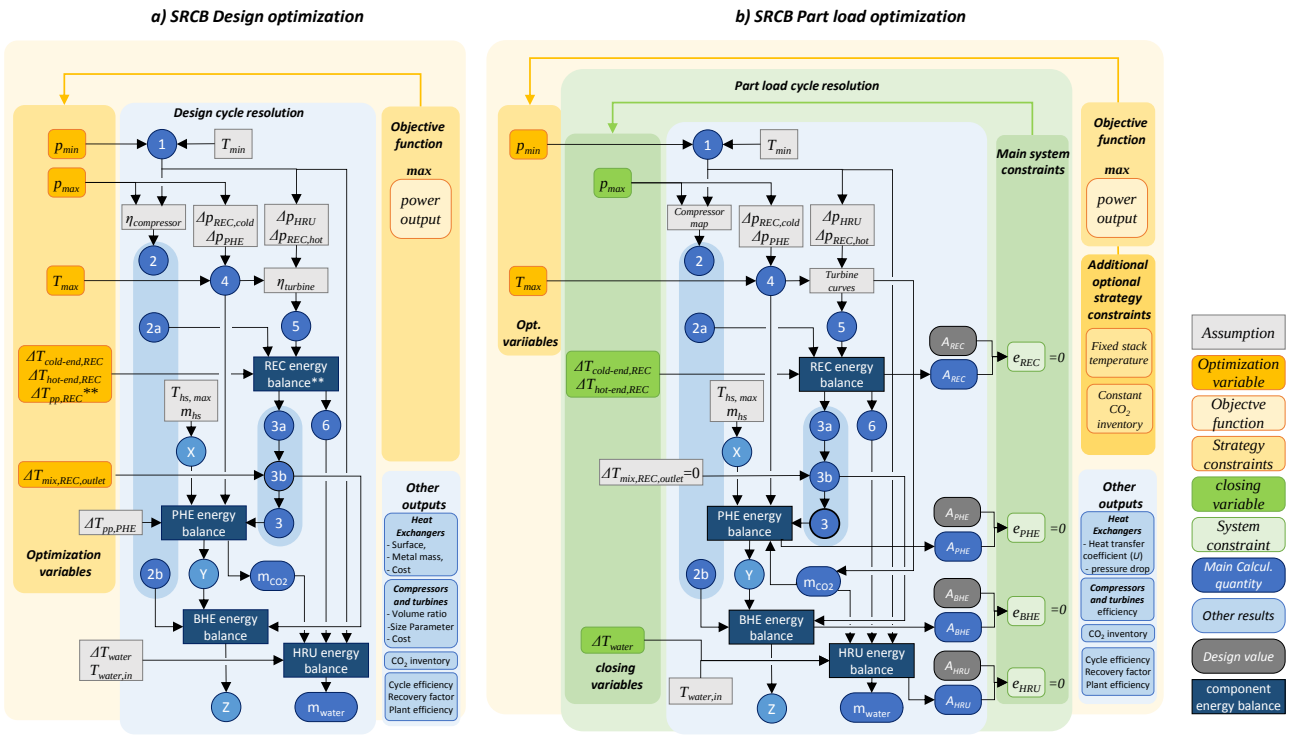

---

12. more details on the optimisation applied should be included. Both in terms of the optimiser used and the type of optimisation. For example, considering that heat-exchanger sizing is included is a single or multi-objective problem?

Thanks for the comment, we included some details about the optimization algorithms adopted.

The optimization algorithm selected to maximize the net power output of the systems is the patternsearch algorithm available in the MATLAB optimization toolbox. Patternsearch is a direct search algorithm for constrained optimization problems which evaluates, at each iteration step, the objective function over a increasing/decreasing/rotating mesh of tentative solution and it does not require gradient calculation. As result it can deal with non-continuous and non-differentiable functions and shows a good ability in avoiding local minimum/maximum. This algorithm has been preferred to simple fmincon and complex genetic or particle swarm algorithms because it shows a good compromise between computational time and accuracy of the solution

---

13. regarding the heat exchanger design, can the authors comment on the suitability of the Gnielinksi and Dittus-Boelter correlations? Particular in close proximity to the critical point where there are strong variations in the thermo-physical properties.

Thanks for the comment, the authors agree that it is not trivial to select a proper heat transfer coefficient correlation, especially in the proximity of the critical point. However, several works suggest the adoption of Dittus-Boelter and Gnielinski correlations for carbon dioxide in supercritical conditions: an example is represented by *Van Eldik, Martin; Harris, Paul Marius; Kaiser, Werner Heinrich; and Rousseau, Pieter Gerhardus, "Theoretical And Experimental Analysis Of Supercritical Carbon Dioxide Cooling" (2014). International Refrigeration and Air Conditioning Conference.Paper 1360.* http://docs.lib.purdue.edu/iracc/1360. The authors of the publication clearly states that "The Dittus and Boelter (1985) correlation predicts Nu values the best with an average relative error of 20% over the entire

Re range and with an average of 9% at 350,000 < Re < 550,000. The second best comparison was obtained by the correlation of Gnielinski (1975) with an average relative error of 45% over the entire Re range and 9.5% for Re numbers between 600,000 < Re < 700,000."

More recently, also the NETL report *C. White, S. Pidaparti, A. O'Connell and N. Weiland, "Cooling Technology Models for Indirect sCO2 Cycles," National Energy Technology Laboratory (Pittsburgh, September 2019)* suggested the Gnielinski correlation for the cooling of sCO_2.

Gnielinski correlation for HRU has been suggested by CO2 cooler manufacturer but they asked to not be cited.

---

14. It is hard to look at Fig. 2 and make immediate conclusions given the amount of information present. They are interesting results but perhaps there are more useful ways of presenting the information. Perhaps by grouping results for the most important parameters (say plant efficiency) on the same graph. That allows an easier comparison between the different cycles. Also, minor point by I presume the T-Q diagrams correspond to the optimal cycles (max. plant efficiency) for each cycle. It would be worth stating that in the caption.

Thanks for the comment, the primary scope of these charts is not to provide a comparison among the different configurations but highlight the different impact of maximum cycle temperature on different cycle architectures. However, in order to improve the possibility of easy comparison the y axes are now equal for all the cases. Moreover, we added a new line on the TQ diagrams for the optimal configuration.

---

15. It might be interesting the investigate the sensitivity of the results to the selected turbomachinery efficiencies.

Thanks for the comment, it certainly would be interesting, but it would require additional pages. In addition, the selected values of turbomachinery efficiency has been checked against correlation from literature thus we a hope that a sensitivity analysis is not mandatory in this case.

- In Section 3.5 I have a few comments:

16. firstly, as with other sections of the paper, it would be very hard for a reader to replicate the study given the limited information presented;

Thanks for the comment, we could include a table with the adopted cost correlations but this would result in further increase of paper length and increase of length in a section that Reviewer 1 suggested to reduce. Let us know if this comment is mandatory or not and if the additional table can solve the issue.

---

17. (ii) can the authors comment on the suitability of the employed cost correlations for sCO_2 applications, particularly considering that sCO2 components at this sort of scale have not really been commercialised;

Thanks for the comment, as any cost correlation the accuracy is pretty low and around ±30%. For such a novel technology errors can be even higher. This is clearly reported for turbines correlation, but it is valid also for the other components.

---

18. (iii) is it fair to compare cycles optimised based on efficiency in terms of specific cost? If an a economic comparison is desired, it would better to compare cycles that were optimised with this as the objective function.

Thanks for the comment, the reviewer is right however we would like to point out the following observations. This section aims at demonstrate that sCO_2 can be competitive not only for efficiency perspective but also from economic standpoint. Specific cost and LCOE results are suboptimal in this case and better figure can be obtained with a technoeconomic optimization using specific cost or LCOE as objective function. However, this involve an increase of numerical problem complexity and the risk of driving the solution far from the real technical optimum if the cost correlations are not precise enough.

---

19. -Section 4.2: again, this section does not provide sufficient detail for a reader to replicate the study.

Thanks for the comment, we tried to solve this issue providing a graphical explanation of the part load modelling methodology for the SRCB cycle configuration. We checked that all the needed information are reported regarding the turbomachinery off design performance and the corrective factors for pressure drops and heat transfer coefficients. We think that this information should be sufficient for a user of Aspen or Thermoflex, as well for a user implementing a code from the scratch. On the other hand, as already stated by the reviewer, it is pointless to report the all the equations employed in the numerical routines.

---

20. Can the authors comment on the validity of using non-dimensionalised performance maps for the compressor operation, particular considering the close proximity to the critical point where strong real-gas effects mean that conventional similarity laws breakdown?

Thanks for the comment. The compressor map has been realized for a different application but for the same compressor inlet conditions and for a very similar nominal pressure ratio.

---

21. The section on part load is interesting, and I believe a useful contribution to the field.

Thanks for the comment, we appreciate!

---

22. The conclusions are too long.

Thanks for the comment, we tried to reduce the length of this section in max one page. Please refer to the revised manuscript for further details.

sCO_2 POWER PLANTS FOR WASTE HEAT RECOVERY: DESIGN OPTIMIZATION AND PART-LOAD OPERATION STRATEGIES

Dario Alfani[1], Marco Binotti[1], Ennio Macchi[1], Paolo Silva[1], Marco Astolfi[1]*

[1]Politecnico di Milano, Energy Department,
Milano, Italy
*marco.astolfi@polimi.it

ABSTRACT

This paper focuses on the potential of supercritical carbon dioxide closed cycle for waste heat recovery applications. The valorization of waste heat released from glass, steel and cement production facilities is recognized as one of the most effective solutions for the reduction of carbon footprint of the industrial sector. Common solutions rely on steam Rankine cycles and organic Rankine cycles while only few sCO_2 power plants have been manufactured and operated so far as this technology has not yet reached the technical and commercial maturity. In spite of the large interest on sCO_2 power plant from industry, institutions and academia, the role of this solution in future waste heat recovery applications is still unclear, highlighting the need of research studies focused on the performance assessment of these novel systems in both design and off-design conditions.

This paper aims at bridging the gap between preliminary numerical studies and the design of real power systems by focusing on different aspects scarcely investigated in literature. The first section of this study deals with cycle design and provides a full description of the numerical complexity related to sCO_2 power plant optimization, with a detailed description of the assumptions and the models implemented for the design of cycle components. Five different cycle configurations for the exploitation of a heat source consisting of a 50 kg/s stream of flue gas at 550°C have been analyzed and optimized: results are presented with a set of sensitivity analyses and the most promising configurations are analyzed from both a thermodynamic and a techno-economic perspective. Simple recuperative cycle, simple recuperative cycle with recuperator bypass and turbine split flow configurations are compared in detail proving that sCO_2 technology can reach overall efficiencies up to 27.5%, a value higher than ORC for the same power output (around 6 MW_{el}), and with a similar specific cost (2000 $/kW). Simple recuperated cycle with recuperator bypass is selected as the most promising configuration and it is further studied in off design conditions in the second section of the paper. Five different part-load strategies have been implemented allowing to assess the part-load performance of the selected cycle, considering both variable CO_2 inventory and constant CO_2 inventory systems. Results highlight that sCO_2 recuperative cycles equipped with a CO_2 storage vessel present a very high and almost constant efficiency down to 50% of the normalized flue gases mass flow rate, while a lower efficiency is expected for constant inventory systems. Both solutions can be operated down to 30% load with no difficulties on system components and with a minimum plant efficiency still competitive against ORC technology.

KEYWORDS:

- Waste heat recovery
- Energy harvesting
- Supercritical carbon dioxide
- Part-load operation
- System optimization
- Techno-economic analysis

HIGHLIGHTS

- We optimized five sCO_2 cycle configurations for waste heat recovery application
- Optimal plants reach efficiency higher than ORC (>27%) with similar specific cost (2000$/kW)
- Simple recuperative cycle with bypass (SRBC) is selected as the optimal configuration
- We studied the different part-load strategies for this optimal configuration (SRBC)
- Variable inventory part load strategy is more efficient than constant inventory strategy

1. INTRODUCTION

In the imminent future, the global electricity production is expected to undergo drastic changes to meet the rising environmental concerns and to tackle the challenges of global warming and the growing electricity demand. Academia and industry are currently researching novel sustainable solutions to reach these targets and, apart from increasing the renewable energy penetration in the electricity generation mix, a crucial solution is represented by the energy efficiency improvement of the already existing facilities in the industrial and power generation sectors. In December 2018, the European Union (EU) reviewed upwards the target for the energy efficiency for 2030, passing from 27% to 32.5%, with a clause for a possible upwards revision by 2023 [1]. One of the most promising approaches to increase the industrial energy efficiency and to lower its greenhouse gases (GHG) emissions is represented by the recovery of the heat unexploited and lost after combustion or in heat transfer processes.

Several studies evaluated the quantity and quality of waste heat potential for the EU and US industrial sector, highlighting the vast potential of industrial waste heat recovery at high temperature.

Forman et al. [2] estimated the global waste heat recovery (WHR) potential of the electricity generation sector and of the main end-use sectors (transportation, industrial, commercial and residential) to be as high as 68.3 PWh_{th}/year. Using an approach based on the calculation of the Carnot potential, the authors highlighted that even if the largest part of the waste heat potential (63%) is at low temperature (<100°C), when passing to Carnot potential the main share (54.5%) is represented by high temperature (>300°C) sources.

Papapetrou et al. [3] focused on the industrial sector WHR technical potential in the EU: their analysis is based on waste heat fractions derived from a detailed study of the UK industry in the 2000-2003 period [4] updated for the year 2015 for each EU country and industrial sector, resulting in a new set of fractions sorted by temperature level. The analysis found out that the waste heat potential from exhaust streams at temperatures higher than 500°C amounts to 124 TWh_{th}/year (40.8% of the total) and it is mainly represented by the iron and steel (I&S) and non-metallic minerals (NMM) industries.

Bianchi et al. [5] highlighted how the EU industrial sector accounts for 26% of the total final energy consumption but nearly half of this energy (about 1534 TWh_{th}) is dissipated to the environment. More precisely, the authors estimated the energy wasted through exhausts/effluents to be 29% of the total industrial consumption, leading to an availability of 920 TWh_{th} from the EU industrial sector which correspond to a 279 TWh_{el} of Carnot potential. This figure demonstrates the large potential of WHR although, in the authors' opinion, the adopted methodology, based on the computation of the Carnot potential, is not conservative and may result in a non-negligible overestimation (+30%) of the actual electricity yield.

Vance et al. [6] investigated the potential and barriers for waste heat recovery at temperatures higher than 650 °C in five different industries (steel, aluminum, glass, cement, and lime). The authors estimated a potential for WHR from high temperature streams in the US to be equal to 113.6 TWh_{th}/year. The work also mentioned that the heat recovery process from these industries could be problematic due to the presence of several reactive constituents in the exhaust streams.

In the last decades, the most common technologies adopted for the conversion of waste heat into electricity have been the Steam (SRC) and Organic Rankine Cycles (ORC). These two technologies adopt the same thermodynamic cycle, i.e. the Rankine cycle, but are used in different size and temperature application ranges. In the WHR sector, subcritical superheated steam cycles without feedwater preheating represent a common option for applications characterized by medium-to-large size (from tens of MWs to hundreds of MWs) and high temperature levels (from 400°C to 700°C) thanks to the higher attainable efficiency and the use of standardized components which leads to a lower plant investment cost. On the other hand, steam Rankine cycles feature a low conversion efficiency when exploiting small available thermal powers (from few hundreds of kW up to tens of MW) or low-to-medium heat source temperatures (from 100°C to 400°C). In fact, the exploitation of such low temperature heat sources by means of steam cycles would lead to a strong cycle thermodynamic efficiency penalization due to the very low evaporation temperatures coupled with large superheating to guarantee a sufficiently high steam quality at turbine discharge. Furthermore, the exploitation of small available thermal powers would involve the miniaturization of the turbine blades, with penalization of the turbine adiabatic efficiency and higher specific cost [7].

ORC technology is generally based on the adoption of organic compounds (hydrocarbons, halogenated hydrocarbons, siloxanes) as working fluid and it currently represents the most common and reliable solution available on the market for the exploitation of low-to-medium temperature (from 100°C to 400°C) heat sources in a large range of power outputs (from few kW to tens of MW) [7]. The main advantages related to the adoption of an organic working fluid are associated to the reduction of the evaporation pressure and to the increase of the condensation one. These two aspects lead to a limited number of turbine stages and thus to a reduced turbine specific cost. Furthermore, the adoption of complex fluids with a completely overhanging saturation line always guarantee a dry expansion for saturated vapor conditions at turbine inlet. This feature solves the issues related to blade erosion, typical when using steam as working fluid, and makes possible a simple plant layout based on a subcritical saturated cycle. In fact, ORCs generally adopt less complex plant layouts than steam Rankine cycles,

typically with a single pressure level [7] and result in even higher efficiencies with respect to steam cycles when applied to low-to-medium temperature heat sources.

In the last decades, the ORC technology has penetrated the WHR market with more than 1700 installed plants corresponding to about 2.8 GW_{el} [8]. However, organic fluids cannot fully exploit the potential of heat source with temperatures higher than 400°C due to their low thermal stability limits [9].

Another technological solution that could be able to bridge the gap in industrial WHR applications and compete both with steam cycles and ORCs is the supercritical CO_2 (sCO_2) closed Brayton cycle. The sCO_2 power cycle has been originally proposed by Angelino [10] and Feher [11] and in recent years it has gained a large interest from both the industry and the academia, mainly after the publication of the Dostal doctoral thesis [12]. Supercritical CO_2 cycles have been mainly studied for concentrating solar power (mostly in the US by NREL [13][14] and SANDIA NL [15]), nuclear energy (for 4th generation nuclear plants, as small modular reactors [16] or sodium cooled reactors [17]) and fossil fuels fired applications as coal-fired power plants [18][19], natural gas oxy-fuel combustion [20][21] or bottoming cycles for gas turbines [22]. In these fields, sCO_2 power systems can compete against conventional steam Rankine cycles thanks to their more compact turbomachines, simpler plant arrangement, smaller footprint and investment cost, higher efficiency and flexibility [23][24].

The great interest in the adoption of sCO_2 power cycles in different power generation applications is also demonstrated by the large number of US and EU funded projects. An example is the STEP 10MW_{el} project [25], an US DOE funded project which aims to bring the technology readiness level (TRL) of natural gas indirectly fired sCO_2 power cycles from "proof of concept" (TRL3) to "system prototype" (TRL7). Supercritical carbon dioxide power cycles have been also investigated within the US DOE SunShot [26] and Gen3 [27] programs as the most promising technology for the power block of 3rd generation high-temperature CSP plants based on central receiver technology. Within the funding scheme of the EU H2020 research and innovation program, different projects have been financed, like the SOLARSCO2OL [28], which aims to build the first MW-scale sCO_2 power block operating in an actual CSP plant located in the European Union; or the sCO2-Flex project [29], which investigates the application of sCO_2 power cycles in order to enhance coal-fired power plants flexibility and ease the integration of non-dispatchable renewable energy sources in the electrical grid.

Apart from the aforementioned high-temperature applications, the sCO_2 power cycle is also considered as an alternative to ORCs for the exploitation of medium-temperature heat sources (from 250°C to 400°C) as CO_2 is an environmental friendly, widely available, safe and thermally stable working fluid [30][31].

In the US this technological solution has already been proposed to the market by Echogen [32], which manufactures and commercializes sCO_2-based WHR systems also in combined heat and power solutions (CHP). Echogen technology was initially based on a simple recuperated power cycle but now adopts a more complex design, called Dual Rail configuration, which is similar to the turbine split flow cycle and allows to obtain a higher power output and a better exploitation of exhaust gases sensible heat [33].

Table 1 reports the most interesting opportunities for waste heat recovery with sCO_2 power systems divided by sectors and processes.

Table 1. Industrial and power generation sector WHR opportunities and their respective temperature levels, rearranged from [2][30][34][35].

Industry	Process	Temperature	Comments	Competitor
Glass manufacturing	Melting furnace	1100-1300 °C	Very high particulate load which results in high fouling factors on heat transfer surfaces	SRC
	Oxyfuel melting furnace	1200-1400 °C		SRC
Iron and steel manufacturing	Electric arc furnace	1000-1300 °C	Dirty exhausts. Intermittency of the process. Temperature too low for good efficiency if recovery is already present.	SRC
	Electric arc furnace with recovery	200-300°C		ORC
	Blast and cupola furnace	450 °C		ORC
Aluminum manufacturing	Secondary melting	1000-1200 °C	Difficult to recover heat from the cell. Discontinuity of the process.	SRC
	Hall-Héroult cell	700 °C		SRC
Cement manufacturing	Wet kiln	300-350 °C	Generally, a good level of heat integration and recovery is already present.	ORC
	Dry kiln (no preheater or precalciner)	400-450 °C		ORC
	Dry kiln (recovered)	300-350 °C		ORC
Gas turbines	Exhausts	370-600 °C	Variable load	SRC, ORC
Reciprocating engines	Exhausts	230-600 °C	Variable load	ORC

Since 2012, several works have been published confirming the feasibility and convenience of the Echogen solution. Persichilli et al. [36] compared the levelized cost of electricity (LCOE) of several steam and sCO_2-based heat recovery system configurations exploiting the exhausts of a 22 MW_{el} LM2500 stationary gas turbine (GT).

The analysis showed how the sCO_2 technology may be able to reduce by up to 20% the LCOE with respect to steam-based solutions thanks to the higher attainable power output, the lower investment and operation and maintenance (O&M) costs. Kacludis et al. [37] resumed the analysis and investigated the adoption of sCO_2 power cycles for other two different WHR applications, namely the exhaust exploitation released by reciprocating engine gensets for remote power generation and a waste heat to power solution for a steel manufacturing facility. Regarding the first application, the authors showed that through the installation of two 300 kW_{el} sCO_2-based power systems it would be possible to increase by 10% the gensets power output without any additional fuel consumption. The second analysis focused on the possibility to recover waste heat from the exhaust gases of a steel mill which are usually discharged to the atmosphere at a temperature around 540°C, after the preheating of the furnace combustion air. Results showed that the adoption of a sCO_2 heat engine could cut down the effective furnace operating cost from 8.6 $/ton to 6.8 $/ton of steel manufactured thanks to the generation of 3.7 MW_{el}.

The simple recuperated sCO_2 power cycle adopted by the Echogen technology has been also supported by several studies thanks to its better exploitation of a heat source at variable temperature and its relatively low layout complexity.

Mohagheghi and Kapat [38] provided a comparison between the simple recuperated cycle and the recompression recuperated cycle exploiting a 100 kg/s mass flow rate of the exhaust gas considering a waste gas inlet temperature range between 225°C and 825°C. The authors showed that, even at high exhausts inlet temperatures, the more complex recompressed configuration does not outperform significantly the simpler recuperated cycle and that for low exhausts inlet temperature (lower than 425°C) the recompression does not provide any benefit due to poor heat source utilization.

Martinez et al. [39] assessed the potential of sCO_2 bottoming cycles coupled to a gas turbine releasing flue gases to the environment at a temperature of 600°C, expanding the configurations studied to the recuperated pre-compression cycle. The results of the analysis highlighted that, if the GT pressure ratio is not optimized, the simple recuperated cycle is able to reach a greater power output with respect to the recompression (+4%) and precompression cycle (+20%). On the other hand, the optimization of the GT pressure ratio leads to a shift in these trends resulting in a power output of the recompression cycle 20% greater than the one of the recuperated cycle and almost 34% higher than the fixed pressure ratio solution.

Moroz et al. [40] proposed a similar analysis considering a wide set of industrial gas turbine with power outputs up to 120 MW_{el}, flue gas mass flow rates between 100 and 700 kg/s and outlet temperatures ranging from 425 to 700°C. The analysis showed that the power output of the recuperated cycle is about 10% higher than outputs of recompression and pre-compression cycles for an exhaust stream of 100 kg/s at a temperature of 550°C. The analysis also highlights the presence of an optimal sCO_2 turbine inlet temperature, generally lower than the maximum allowable temperature, resulting from the tradeoff between heat source utilization and cycle thermodynamic efficiency.

Kimzey [41] has been the first to propose novel sCO_2 cycle architectures specifically developed for WHR applications by investigating the potential of a configuration with a single flow split and a dual expansion, which the author called Cascade I cycle. The author stated that this configuration is able to outperform the power output of a traditional two-pressure level steam Rankine cycle by 3%. On the other hand, its performances are still inferior to commonly employed triple pressure with reheat steam cycle when exploiting the flue gases discharged by a heavy-duty gas turbine. The cycle thermodynamic efficiency is in fact limited due to the large temperature differences in the low temperature recuperator (LTR), caused by the different heat capacities of the hot and cold streams.

Other two interesting and innovative cycle configurations for WHR applications are the recuperated cycle with recuperator bypass (also called preheating cycle) and the turbine split flow configuration (also called dual recuperated cycle), which have been studied by Wright et al. [42]. The authors proposed a preliminary techno-economic analysis comparing four different cycle configurations exploiting a 40.7 MW_{th} GT exhaust stream at 549°C. For each cycle configuration the turbine inlet temperature, the split fraction and all the heat exchangers approach temperatures have been optimized in order to maximize the net annual revenue. On the other hand, the compressor inlet and outlet pressure and the minimum cycle temperature have been considered as constant values in order to simplify the analysis. The analysis showed that, even if the innovative cycle configurations are able to produce up to 22.6% more power output than the benchmark simple recuperated cycle, the increased capital costs of these architectures (+41.7% for the recuperated cycle with recuperator bypass, +30.5% for the turbine split flow configuration) make them less favorable from an economic point of view.

The turbine split flow (called by the authors cascade recuperative) configuration has also been investigated by Astolfi et al. [31] for the recovery of 30 MW_{th} in a wide range of temperatures (from 200°C and 600°C) and cooling grades (from 0% to 100%). The analysis showed that a single optimal sCO_2 cycle configuration cannot be selected as this is highly dependent on the temperature and cooling grade of the heat source. The authors compared also the performance of sCO_2 cycles with the ORCs ones and highlighted that even if ORCs are the most efficient solution for heat source temperatures below 350°C, sCO_2 power systems represent a promising solution for higher temperatures.

Huck et al. [22] proposed an even more complex cycle configuration, the dual flow split with a dual expansion layout (also called Cascade III by Kimzey [41]). The configuration is similar to the Cascade I cycle but with the addition of an intercooling and the division of the primary heat exchanger in two separate components, between which the two CO_2 streams are mixed. The authors compared the performance attainable by this novel configuration against a three-pressure level steam Rankine bottoming cycle with reheat, showing that this innovative architecture can provide more electrical power. On the other hand, the analysis appears biased by the optimistic assumptions on the sCO_2 power cycle with maximum pressures of 400 bar, turbine inlet temperatures of 700°C and isentropic efficiencies for CO_2 turbomachinery equal to 95%.

Marchionni et al. [43] published a techno-economic analysis comparing four more conventional sCO_2 cycle configurations and four cycle architectures specifically developed for WHR applications. The second group included an innovative layout proposed by the authors, which consists in a recuperated cycle with recuperator bypass with the addition of a pre-compressor. The study investigates the exploitation of an exhausts stream at 650°C and highlights the potential of the innovative sCO_2 cycle configurations over the more conventional ones. However, the choice of the authors to fix the exhaust stack temperature to 350°C for the conventional configurations and to 150°C for the novel configurations could have led to an inaccurate comparison.

The same authors [44] investigated the off-design behavior and performances of a 50 KW_{el} simple recuperated cycle recovering heat from 1 kg/s stream of flue gases at 650°C. The analysis assessed the effect of both hot and cold sources inlet conditions by varying their mass flow rates and temperatures. The implementation of turbomachinery performance maps obtained through CFD simulations highlighted the impossibility to generate power when the heat source mass flow rate is lower than 0.9 kg/s and its temperature drops under 550°C.

Both these studies were performed in the context of the H2020 I-ThERM project [45] which aims at the development and demonstration of a packaged plug and play power system for high-temperature waste heat to power conversion based on a sCO_2 Brayton cycle.

Recently, Manente and Costa [46] discussed the optimization of several novel sCO_2 power cycle configurations for WHR applications analyzing the recuperated cycle with recuperator bypass, the turbine split flow and the Cascade I or dual expansion cycle. The authors showed that all these more complex configurations are obtained by the combination of two simpler sCO_2 Brayton cycles overlapped in the low temperature section and separated in the high temperature one. The authors optimized all the configurations by varying the turbine inlet temperature and the split fraction, retaining constant pressures and neglecting all the heat exchangers pressure drops. The analysis showed that the dual expansion cycle obtained the highest recovery efficiency with a value of 22.3% when employed to recover heat from exhausts at 600°C.

These aforementioned studies highlight the potential of sCO_2 power cycles for WHR applications and justify the academic and industrial interest in the development of this technology. However, the currently available scientific literature lacks in research studies dealing with both the cycle optimization and the evaluation of part load performance. The present work aims to investigate this topic of high relevance for WHR applications providing results that can be useful to guide studies on system dynamics or control for future sCO_2 power systems. First, a fair comparison of five cycle configurations in design conditions is presented, also including techno-economic and layout complexity considerations. Optimization of each cycle configuration has been implemented considering all the free design parameters instead of fixing some of them, in order to avoid suboptimal solutions and improve the accuracy and reliability of the results. Three cycles configurations are selected and discussed in detail and techno-economic analysis highlights that considering heat exchangers mass and cost is crucial when comparing different cycle architectures. Recuperative cycle with recuperator bypass has been selected as the most promising cycle configuration for this application and it has been eventually studied in part load conditions proposing and comparing different possible control strategy options based on both constant and variable inventory solutions.

2. CYCLE DESIGN AND OPTIMIZATION

This section focuses on the description of investigated cycle configurations, the set of assumptions adopted and the optimization procedure.

2.1 Investigated cycle architectures

In order to tackle the goal of this paper a dedicated numerical tool has been developed in MATLAB [47] for the optimization of the system design and the evaluation of part-load performance of sCO_2 power cycles. Carbon dioxide thermodynamic properties are computed through the REFPROP 9.1 database [48] using a high fidelity 42 terms reduced Helmholtz energy equation of state [49] allowing for an accurate evaluation of real gas effects close to the critical point of the working fluid. The developed numerical code is able to model several cycle configurations (more than 50 cycle schemes are proposed in literature [50]) that can be easily optimized and then simulated over a large range of off-design conditions.

In this work, five cycle configurations are investigated and optimized, identifying the most promising solutions for the exploitation of a variable temperature heat source, typical of WHR applications. Figure 1 depicts the five investigated cycle configurations: (i) the simple recuperated cycle (SRC), (ii) the recompressed recuperative cycle (RRC), (iii) the simple recuperated cycle with recuperator bypass (SRCB), (iv) the recompressed recuperative cycle with high temperature recuperator bypass (RRCB) and (v) the turbine split flow cycle (TSF).

The first configuration investigated is the simple recuperated cycle (SRC) (Figure 1.a) in which a single recuperative heat exchanger uses the heat available at the exit of the expander (point 5) to increase the temperature of high pressure CO_2 at compressor exit (point 2) up to Primary Heat Exchanger (PHE) inlet temperature (point 3). The recuperated sCO_2 cycle is the simplest configuration with internal heat recovery, which is anyhow characterized by a limited efficiency related to the high average temperature difference in the recuperator caused by the different heat capacities of the hot and cold streams. This penalization, due to the strong real gas effects on the cold high-pressure stream, entails a relatively low temperature at PHE inlet (point 3), which, on the other hand, allows to reduce the minimum temperature of the heat source thus increasing the heat recovered in WHR applications.

The second cycle configuration considered for the study is the recompressed recuperative cycle (RRC) (Figure 1.b), widely proposed in literature for solar [51][52][53] and nuclear applications [12][17]. In the RRC configuration, a fraction of the low pressure working fluid enters in the Heat Rejection Unit (HRU) (point 8a), it is cooled down to the minimum cycle temperature (point 1), compressed by the main compressor (point 2) and then heated up (point 3a) in the Low Temperature Recuperator (LTR). The remaining fraction (point 8b) is split just before the HRU and it is compressed to the cycle maximum pressure (point 3b) by a secondary compressor. The two flows are eventually mixed at HTR cold side inlet (point 3). The recompression allows enhancing the cycle efficiency by balancing the heat capacities of the hot and cold streams in the LTR, limiting the temperature differences in the heat exchanger and the irreversibilities related to the heat transfer process. The working fluid preheating is then completed (point 4) in the High Temperature Recuperator (HTR) which cools down the hot CO_2 exiting the turbine (point 6): temperature differences are minimized at HTR cold end and tend to increase moving towards the hot end since high pressure fluid always shows a slightly higher specific heat than the low pressure stream. As result, the thermodynamic cycle efficiency is increased, while the high effectiveness of the internal recuperative process may limit the exploitation of the variable temperature heat source thus limiting the thermal power input of the cycle and its power output.

For WHR applications, both simple recuperated (SRC) and recompressed recuperated (RRC) configurations may benefit from the adoption of a recuperator bypass: an additional heat exchanger in parallel to the recuperator which allows to reduce the temperature difference in the recuperator and at the same time allows to enhance heat source exploitation by a further cooling of the exhaust gas.

In the simple recuperated cycle with recuperator bypass (SRCB) (Figure 1.c), a fraction of the CO_2 exiting the compressor (point 2) is split before the recuperator (point 2b), heated in the recuperator bypass heat exchanger (BHE) (point 3b) further cooling the heat source and then mixed with the main flow at the recuperator outlet (point 3a). In the recompressed recuperative cycle with HTR bypass (RRCB), the bypass is performed only on the HTR as reported in Figure 1.d. This cycle configuration has been suggested for high temperature applications like fossil fuel power plants [29][54] since, thanks to the introduction of the bypass stream, it combines high heat recovery factors and high thermodynamic efficiency at the expense of an additional heat exchanger.

Last cycle configuration (Figure 1.e) is the so-called turbine split flow (TSF) or dual recuperated configuration [50][55]. This cycle configuration requires two turbines and a single compressor and, as the SRCB and the RRCB configurations aims at minimizing the temperature differences in the recuperators and improve the utilization of the available sensible heat from the heat source. After the compressor, the CO_2 flow is split in two different streams. The first stream exploits the heat provided by the primary source and expands from the cycle maximum temperature (point 4) in the main turbine. The residual sensible heat available from hot expanded CO_2 (point 5 – point 6a) is used to heat the second stream from compressor outlet (point 2) up to secondary turbine inlet temperature (point 4'). After the second stream is expanded in the secondary turbine, the hot low-pressure CO_2

released by the secondary turbine (point 5') is used to preheat the first stream up to PHE inlet temperature (point 3).

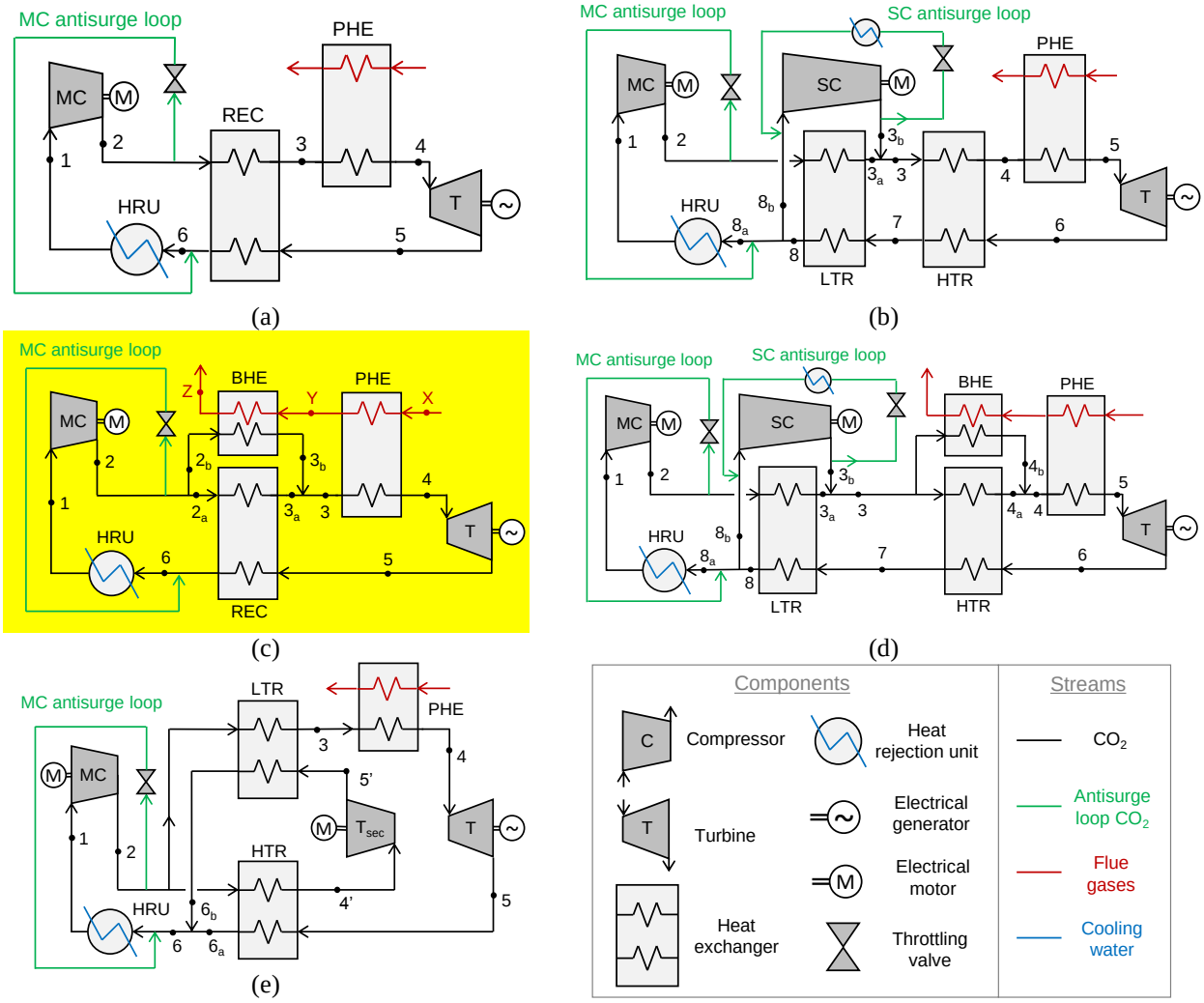

Figure 1. Schematic of the sCO_2 cycle layouts studied in this work: (a) SRC, (b) RRC, (c) SRCB, (d) RRCB and (e) TSF.

2.2 Design assumptions and system optimization

The design optimization routine evaluates the performance of the various cycle designs and selects the best combination of cycle design parameters in order to maximize a specific figure of merit.

The main figures of merit used to evaluate the system performance are the net cycle thermodynamic efficiency η_{cycle} (including HRU auxiliaries consumption, namely the cooling water circulation pump), the heat recovery factor χ and the overall plant efficiency η_{plant}. These parameters are defined in Eq. 1, Eq. 2 and Eq. 3 where the power consumption of the secondary compressor $\dot{W}_{sec\,comp}$ is equal to zero for both the SRC and SRCB and the power production from low temperature turbine ($\dot{W}_{sec\,turb}$) is null for all the configurations but the TSF. The optimization algorithm aims at maximizing the net power output and consequently the overall plant efficiency η_{plant} which takes into account not only the thermodynamic quality of the conversion from heat to electricity (through η_{cycle}), but also the fraction of heat exploited with respect to the total heat available from the heat source (through χ).

$$\eta_{cycle} = \frac{\dot{W}_{net}}{\dot{Q}_{in,cycle}} = \frac{\dot{W}_{turb} + \dot{W}_{sec\,turb} - \dot{W}_{main\,comp} - \dot{W}_{sec\,comp} - \dot{W}_{HRU,aux}}{\dot{Q}_{in,cycle}} \quad \text{Eq. 1}$$

$$\chi = \frac{\dot{Q}_{in,cycle}}{\dot{Q}_{hs,max}} = 1 - \frac{\dot{m}_{hs} c_{p,hs} (T_{stack} - T_{hs,min})}{\dot{m}_{hs} c_{p,hs} (T_{hs,max} - T_{hs,min})} \quad \text{Eq. 2}$$

$$\eta_{plant} = \chi_{rec}\,\eta_{cycle} = \frac{\dot{W}_{net}}{\dot{Q}_{hs,max}} \qquad \text{Eq. 3}$$

The heat source is modelled as a stream of gas with a mass flow rate $\dot{m}_{hs}$ of 50 kg/s, a maximum temperature $T_{hs,max}$ of 550°C, and a minimum allowable temperature of 150°C in order to avoid any formation of acid condenses and fouling on heat transfer surfaces. Gas specific heat capacity $c_{p,hs}$ is assumed constant and equal to 1.15 kJ/kgK. Heat source heat capacity can represent the flue gas of a combustion in an industrial process (steel, glass, cement industry) [35][37] or the exhausts of a small size gas turbine (i.e. in the 15-20 MW_{el} range [56]).
The numerical model relies on a set of assumptions adopted for cycle design reported in Table 2 and among them, the most relevant are the cycle minimum temperature and turbomachinery efficiency. The minimum cycle temperature is set equal to 33°C in order to operate the main compression process close to the CO_2 critical point, exploiting the real gas effects, thus increasing system efficiency [57]. A water-cooled HRU is adopted for all the cycles assuming the availability of a stream of water or the adoption of a cooling tower water loop which is often available in large industrial plants: the available cooling water temperature is assumed equal to 20°C.
Regarding compressors efficiency, preliminary performance analyses report values between 83% and 85% for a 50 MW_{el} plant [58]. In this work, due to the smaller scale of the system, a more conservative value equal to 80% is adopted.
Regarding the turbine efficiency, several works on sCO_2-based solar power applications [13][14][59] suggest values between 90% and 93% as the expander design should be less complex than the compressor one thanks to the ideal gas-like behavior of CO_2 along the expansion and the larger volumetric flow rates. A more conservative value equal to 85% is here considered, taking into account the stronger impact of secondary and leakage losses on the efficiency due to the smaller size of the investigated system. A comparison of the assumed values against those attainable with correlations from reference [60] is provided in the design result section.
An additional hypothesis generally adopted in literature is related to the imposition of isothermal mixing processes to minimize mixing irreversibilities. Isothermal mixing can be assumed at HTR cold side inlet (T_{3a}=T_{3b}) by varying the split ratio at HRU inlet and for the mixing processes downstream the bypass heat exchangers in the SRCB (T_{3a}=T_{3b}) and in the RRCB (T_{4a}=T_{4b}) configurations, by varying the recuperator bypass flowrates. A sensitivity analysis on this hypothesis is provided in the result section. On the contrary, isothermal mixing is never imposed at HRU inlet of TSF configuration allowing to investigate solutions with recuperators having different cold end temperature differences.

Table 2. Heat source data and cycle design assumptions.

Parameter	**Value**
Heat source mass flow rate $\dot{m}_{hs}$, kg/s	50
Heat source temperature $T_{hs,max}$, °C	550
Minimum heat source temperature $T_{hs,min}$, °C	150
Heat source specific heat $c_{p,hs}$, kJ/kgK	1.15
Minimum cycle temperature, °C	33
Minimum PHE pinch point $\Delta T_{pp,PHE}$, °C	25
Cooling water inlet temperature, °C	20
Cooling water temperature rise, °C	7
Cooling water Δp, bar	1.5
PHE CO_2 Δp, bar	2
HRU CO_2 $(\Delta p/p_{in})$	0.5%
Recuperators hot side $(\Delta p/p_{in})$ SRC/SRCB/TSF	1%
Recuperators hot side $(\Delta p/p_{in})$ RRC/RRCB	0.5%
Turbines isentropic efficiency, η_{turb}	85%
Compressors isentropic efficiency, η_{comp}	80%
Water pump efficiency, $\eta_{water\ pump}$	75%
Generator/motor efficiency $\eta_{me,t}$/ $\eta_{me,c}$	96.4%

The five cycle configurations are optimized by varying: (i) the working fluid minimum pressure, (ii) the cycle maximum pressure (iii) the turbine inlet temperature (iv) the recuperator(s) terminal cold and hot end temperature differences, (v) the recuperator(s) pinch point(s) temperature difference and (vi) the temperature difference between streams in the mixing process(es). In order to reduce the complexity of the numerical problem the parameters (i-iv) are optimized by a dedicated optimization algorithm while parameters (v-vi) are investigated with a sensitivity analysis and considered as a constraint to the optimization process. These last parameters should

be considered in order to catch the tradeoff between heat source heat recovery and cycle internal heat recovery effectiveness. Cycle minimum and maximum pressures are selected considering the trade-off between the need of having high cycle expansion ratio and the need to increase compressor fluid average density by exploiting the low compressibility factor of the CO_2 in the proximity of the critical point. An increase of cycle maximum temperature positively affects the cycle thermodynamic efficiency thanks to the increased turbine specific work but may negatively impact on the heat recovery factor for recuperative cycles.

The location of a selected pinch point temperature difference in sCO_2 cycle recuperator(s) is non-trivial since real gas effects on the cold and high-pressure CO_2 side involve a nonlinear trend of specific heat. Pinch point temperature difference can be located within the heat exchanger instead of being on the hot or cold end of the recuperator depending on the minimum and maximum pressure of the cycle. Moreover, for configurations provided by recuperator bypass (SRCB and RRCB) and for the TSF configuration it is possible to design the recuperator (HTR for RRCB and TSF) having the minimum temperature difference at cold end, at hot end, or at both extremities by tuning the bypass split ratio. For this reason, the terminal cold end and hot end temperature differences of recuperators are included as optimization variables while desired pinch point temperature differences are considered as constraints to the optimization algorithm and varied by an enumerative approach.

The optimization algorithm selected to maximize the net power output of the systems is the *patternsearch* algorithm available in the MATLAB optimization toolbox. *Patternsearch* is a direct search algorithm for constrained optimization problems which evaluates, at each iteration step, the objective function over an increasing/decreasing/rotating mesh of tentative solution and it does not require gradient calculation [61]. As result it can deal with non-continuous and non-differentiable functions and shows a good ability in avoiding local minimum/maximum. This algorithm has been preferred to simple *fmincon* and complex *genetic* or *particle swarm* algorithms because it shows a good compromise between computational time and accuracy of the solution. The number of free variables for each cycle configuration is reported in Table 3 and it increases with cycle complexity reaching six optimization variables plus four sensitivity analysis parameters for the RRCB configuration. Figure 2.a depicts the flow diagram at the base of the single simulation and the design optimization iterative procedure for the SRCB configuration. Scheme shows all the interconnections between the assumptions, the optimization variables and the calculation of the different thermodynamic points and quantities.

Table 3. Optimization variables for the different cycle layouts

	SRC	**SRCB**	**RRC**	**RRCB**	**TSF**	**Lower Bound**	**Upper Bound**
Parameters varied by sensitivity analysis and considered as constraints for the optimization algorithm							
$\Delta T_{pp,REC}$, °C	X	X				10	75
$\Delta T_{pp,LTR}$, °C			X	X	X	10	75
$\Delta T_{pp,HTR}$, °C			X	X	X	10	75
$\Delta T_{mix,REC,outlet}$ or $\Delta T_{mix,LTR,outlet}$, °C		X	X	X		-30	+30
$\Delta T_{mix,HTR,outlet}$, °C				X		-30	+30
Optimization variables varied by *patternsearch* optimization algorithm to maximize η_{plant} and respect recuperator(s) pinch point temperature difference and mixing process temperature difference constraints							
p_{min}, bar	X	X	X	X	X	75	150
p_{max}, bar	X	X	X	X	X	150	250
T_{max}, °C	X	X	X	X	X	200	525
$\Delta T_{cold-end,REC}$, °C	X	X				10	75
$\Delta T_{hot-end,REC}$, °C		X				10	75
$\Delta T_{cold-end,LTR}$, °C			X	X	X	10	75
$\Delta T_{hot-end,LTR}$			X	X		10	75
$\Delta T_{cold-end,HTR}$, °C					X	10	75
$\Delta T_{hot-end,HTR}$, °C				X	X	10	75

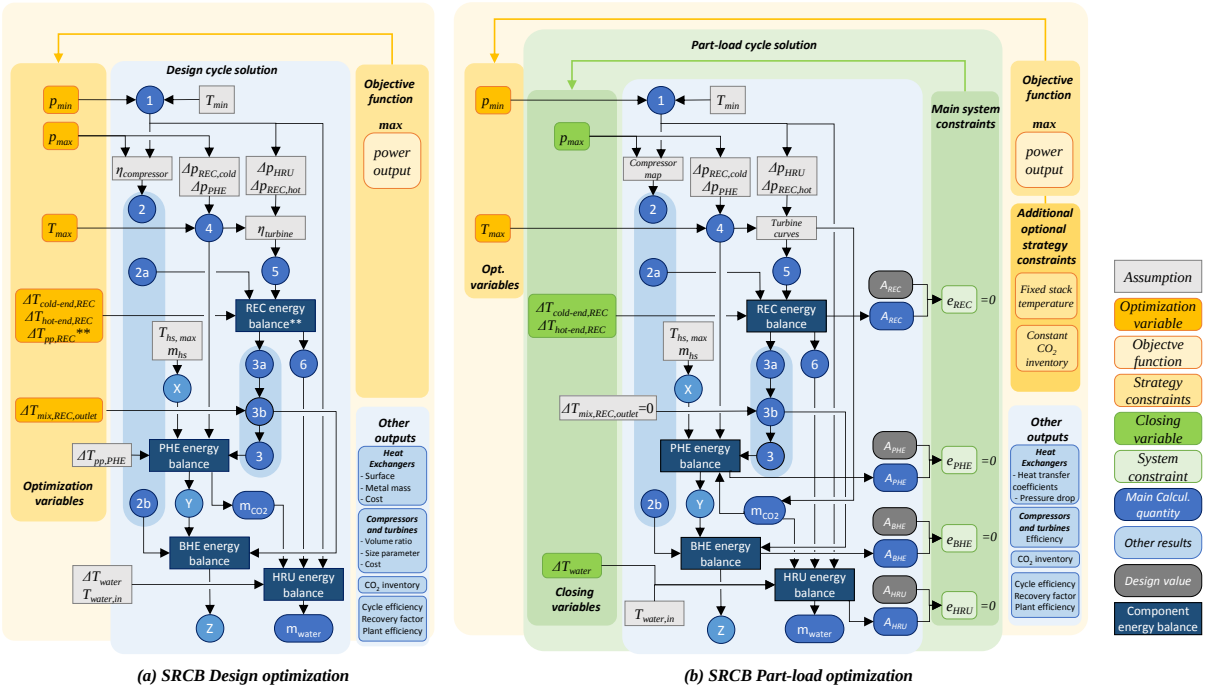

(a) SRCB Design optimization *(b) SRCB Part-load optimization*

Figure 2. Flow diagrams representing all the interconnections between assumptions, optimization variables and calculated quantities for the design optimization routine (a) and the part-load routine (b) referred to SRCB configuration.

Heat exchanger design is carried out with a dedicated set of numerical routines for the calculation of the heat transfer coefficients, the volume of fluid and the mass of the heat exchangers. The recuperators are modelled as printed circuit heat exchangers (PCHE) according to the model suggested in [62] integrated with manufacturer data already presented in [19] and reported in Table 4. The minimum temperature difference in each recuperator directly affects the thermal duty while the assumed hot side allowable pressure drop directly affects the CO_2 velocity in the heat exchanger, the heat transfer coefficients and the channels length. The numerical code assumes perfect counter-current flow arrangement and the same number of channel flows on both hot and cold side. Hot fluid velocity is varied in order to match the desired pressure drop and eventually, the global heat transfer coefficient referred to the internal surface (U_{int}) (Eq. 5), the actual heat transfer area (Eq. 6) and metal mass of the heat exchanger as well as the pressure drops on the cold side are computed. Each heat exchanger is discretized in 30 sections in order to catch local variations of fluid thermophysical properties and calculate the needed heat transfer area with higher accuracy The PHE and the BHE (if present) are modelled as finned tube heat exchangers with CO_2 inside the tubes and flue gas flowing outside the tubes bundles. The HRU is modelled as a shell and tubes (S&T) heat exchanger with the CO_2 flowing into the tubes while cold water flows in the shell. CO_2 pressure drop side in BHE is set equal to the cold side pressure drop of the bypassed recuperator, in order to limit the mixing irreversibilities at the end of the two components. In the HRU, the cooling water pressure drops are considered fixed and assumed equal to 1.5 bar, while in the PHE and BHE the hot gas side pressure drops are neglected. The HRU, PHE and BHE tubes thicknesses have been computed through Eq. 4 starting from the internal diameters reported in Table 4, adopting ASME allowable stress value (σ_{max}) [63] and considering a safety factor of 1.15.

$$t = 1.15 \left[\frac{p \cdot d_{ext}}{2\sigma_{max}(T) + p} + 0.005 d_{ext} \right] \qquad \text{Eq. 4}$$

From the design of each heat exchanger, and assuming a connecting piping length value between the different cycle components, the nominal CO_2 plant inventory is calculated. The piping length is assumed equal to 15 m for each pipe connected to the PHE and the HRU while all other pipes are assumed to be 2 m long. The internal piping diameter has been computed considering a maximum CO_2 velocity equal to half the erosional one [64], while the external diameter and piping thickness has been computed through Eq. 4. For simplicity, the piping thermal losses and their pressure drops are neglected. Table 4 reports the main assumptions related to the heat exchangers design adopted in this work.

$$U_{int} = \left(\frac{1}{htc_{int}} + \frac{d_{int} \cdot \ln\left(\frac{d_{ext}}{d_{int}}\right)}{2k_{metal}} + \frac{1}{\frac{A_{ext,finned}}{A_{ext,plain}} \cdot \frac{A_{ext,plain}}{A_{int}} \cdot htc_{ext}} \right)^{-1} \quad \text{Eq. 5}$$

$$A_i^{des} = \sum_{n=1}^{30} \frac{Q_{i,n}}{U_{i,n}\Delta T_{i,n}}, \text{ with } i = [HRU, REC, LTR, HTR, BHE, PHE] \quad \text{Eq. 6}$$

Table 4. Main assumptions for the heat exchangers design.

REC/LTR/HTR	
HX type	PCHE
Thickness of plate, mm	1.5
Diameter of semi-circular channel, mm	2
Thickness of wall between channels, mm	0.4
Heat exchanger material	SS316L
Heat transfer correlation hot side	Gnielinski
Heat transfer correlation cold side	Gnielinski
PHE/BHE	
HX type	Finned tube HX
Tube internal diameter, mm	20
Ratio of tube pitch to external diameter	1.25
Ratio of finned to plain external area	12
Tube material	Inconel 617
Heat transfer coefficient flue gas side	125 W/m^{2}K
Heat transfer correlation CO_2 side	Dittus-Boelter
HRU	
HX type	S&T
Tube internal diameter, mm	20
Ratio of tube pitch to external diameter	1.25
Ratio of finned to plain external area	12
Tube/fin material	Copper/Aluminum
Heat transfer coefficient water side	7500 W/m^{2}K
Heat transfer correlation CO_2 side	Gnielinski

.

3. DESIGN RESULTS

In this section the results for the optimal design of the five investigated cycles configurations are presented and discussed. Not all the free variables reported in Table 3 have the same impact on cycle performance and for this reason their role is first discussed with separate sensitivity analyses on maximum cycle temperature, pinch point temperature difference in recuperators and streams temperature difference before mixing processes while minimum and maximum cycle pressures and recuperators terminal hot and cold end temperature differences are optimized at all times. Final optimal results are discussed at the end of this section.

3.1 Effect of maximum cycle temperature

In order to evaluate the effect of the maximum cycle temperature on plant performance, a sensitivity analysis is carried out optimizing both minimum and maximum cycle pressures for every considered maximum cycle temperature while considering fixed minimum temperature differences in the recuperators at the lower bound (10°C) and isothermal mixing. Figure 3 depicts the results of the sensitivity analysis on cycle maximum temperature for the simplest cycle configuration (SRC), for the most complex one (RRCB) and for the TSF configuration, to highlight the importance of optimizing this parameter independently of the cycle architecture.
The cycle maximum temperature affects both the cycle thermodynamic efficiency and the heat recovery factor: a tradeoff between these two figures is evident for both the SRC configuration (Figure 3.a1) and the RRCB configuration (Figure 3.a2). Cycle efficiency is positively affected by the increase of turbine inlet temperature as typical of gas cycles because of the increase of turbine specific work with respect to compressors specific consumption (Figure 3.b1 and b2). On the contrary, the heat recovery factor is penalized due to the higher CO_2 temperature at PHE inlet when maximum cycle temperature increases (Figure 3.c1 and c2) which entails a poor utilization of the available heat and eventually a lower CO_2 mass flow rate (Figure 3.b1 and b2). For both SRC and RRCB architectures, the turbine inlet temperature that maximizes the overall plant efficiency is fairly below the maximum limit (525°C) defined as the heat source inlet temperature minus the pinch point temperature difference at PHE (25°C). Optimal values are 391.8°C and 335.6°C for SRC and RRCB configurations respectively, giving the possibility to increase the plant efficiency by more than 3.05 and 6.94 points of efficiency with respect to the case with the highest possible value of turbine inlet temperature.
Different considerations can be stated for the TSF configuration: for this cycle architecture, the adoption of the maximum allowable turbine inlet temperature (525°C) does not imply a poor utilization of the available heat: χ is equal to 91.9% while the same figure is around 57.5% and 40% for the SRC and RRCB configurations respectively at the same maximum cycle temperature. This implies that the range of turbine inlet temperature to be investigated is narrower than for the other cycles and with a maximum temperature of 450°C a complete utilization of the available thermal power is obtained. In this temperature range (450°C-525°C) the cycle efficiency change is more marked than for the other two configurations because of the adoption of two turbines and larger than the relative increase of heat recovery factor χ, thus reducing the main turbine inlet temperature is not convenient from thermodynamic perspective.

3.2 Effect of recuperator temperature difference

The effect on the plant efficiency of assuming different recuperators pinch point temperature differences is not trivial: enhancing the effectiveness of the internal heat recovery process certainly allows to reduce the irreversibility of the compressed CO_2 heating process but, on the other hand, involves an increase of the PHE inlet temperature with a consequent limitation of heat source exploitation. In literature generally the recuperators pinch point temperature difference is always assumed equal to a fixed value (ranging generally from 5°C to 15°C) and rarely is subject to optimization. An exception is represented by the work of Held [33] where the heat exchangers UA value (overall heat transfer coefficient, *U*, multiplied by the heat transfer surface, *A*) is selected as an optimization variable rather than pinch point temperature differences. Figure 4 depicts the trend of the three figures of merit (η_{cycle}, χ and η_{plant}) as function of ΔT_{pp} of recuperator for non-recompressed cycle configurations (SRC and SRCB): turbine inlet temperature, minimum and maximum pressures are optimized at all times and isothermal mixing assumption at the exit of SRCB recuperator is adopted. For SRC plant (Figure 4.a), pinch point temperature difference can be located at recuperator cold end or within the heat exchanger depending on the cycle minimum and maximum pressure which changes from case to case. Adopting the minimum investigated ΔT_{pp} (i.e.10°C) the cycle efficiency is maximized while the heat recovery factor is around 83%. A better heat exploitation can be obtained by increasing the ΔT_{pp} but the overall effect on the plant efficiency is penalized by the contextual, and more marked reduction of cycle thermodynamic efficiency. All the optimal solutions have the pinch point temperature difference located at recuperator cold end because of the higher specific heat of cold high-pressure fluid with respect to the hot low pressure one. For SRCB plant the minimum temperature difference can be located within the recuperator, at cold end, at hot end or at both depending on the bypass mass flow rate and fluid pressures. For this configuration (Figure 4.c), the adoption of the recuperator bypass allows to totally exploit the heat source (which minimum allowable temperature is 150°C) even at minimum recuperator temperature differences, so any increase of this parameter simply contributes to a penalization of the net power output. From thermodynamic perspective, the solution with pinch point at both cold and hot ends is particularly attractive since

it allows to reach the highest internal heat recovery effectiveness without penalizing the heat recovery but, on the other hand, it entails a larger heat transfer area and investment cost.

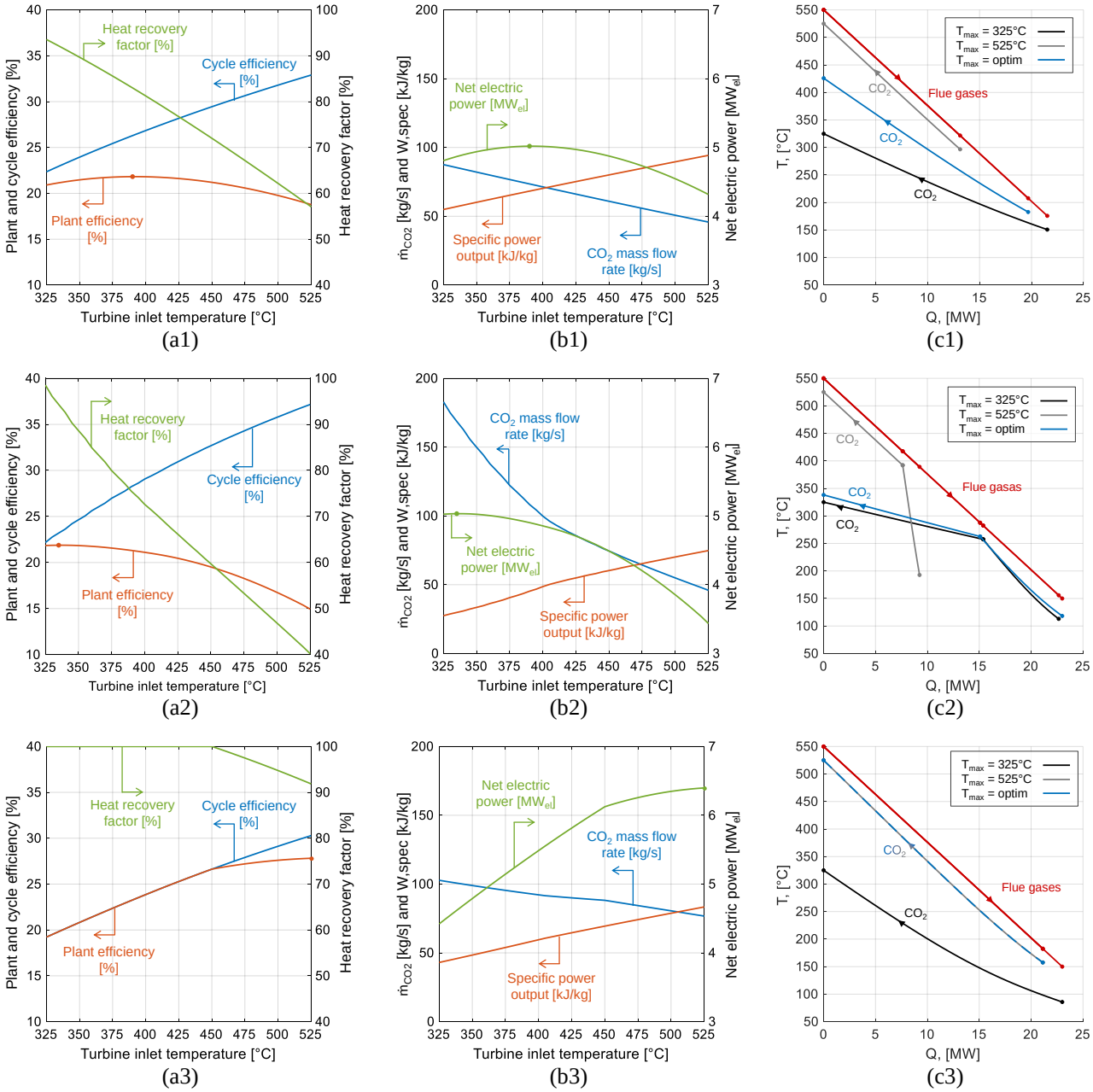

Figure 3. (a) Trends of the main system efficiencies and (b) of the net power output, of the CO_2 mass flow rate, of the specific power output as function of the maximum turbine inlet temperature. (c) T-Q diagrams of the CO_2-flue gas heat exchangers for two extreme cycles maximum temperatures and for the optimal one (blue line). The cycle configurations considered are (1) the simple recuperated cycle (SRC), (2) the recompressed recuperative cycle with HTR bypass (RRCB) and (3) the turbine split flow (TSF).

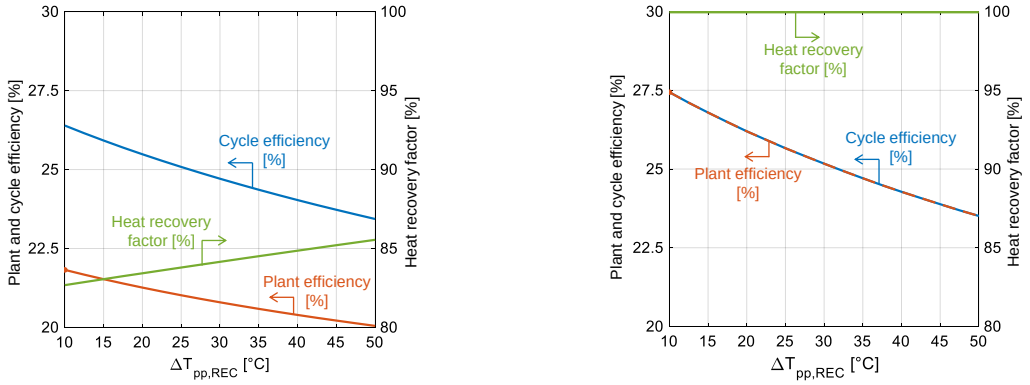

Figure 4. Trend of the three figures of merit (η_{cycle}, χ and η_{plant}) as function of ΔT_{pp} of recuperator for SRC (a) and SRCB (b) configurations.

The same analysis, applied to recompressed cycles configurations (RRC and RRCB), is less trivial because of the presence of two recuperators (LTR and HTR) and the possibility of varying both components minimum temperature differences. For the RRC cycle the heat capacity of the cold stream of the LTR is modulated by varying the split ratio at the entrance of the HRU towards the secondary compressor while the HTR works with the same mass flow rate on both sides. As result the pinch point temperature difference of the LTR may be located at cold end, at hot end or within the component while for the HTR the pinch point temperature difference is always at cold end because the high pressure cold fluid always has an average specific heat higher than the low pressure hot fluid. Considering the constraint of isothermal mixing it results that it is only possible to investigate designs with $\Delta T_{pp,HTR} \geq \Delta T_{pp,LTR}$ and the two temperature differences coincide when the pinch point is located at hot end of LTR and at cold end of HTR. Figure 5.a depicts the cycle thermodynamic efficiency, the heat recovery factor and the plant efficiency for the RRC configuration as function of HTR pinch point temperature difference while optimal $\Delta T_{pp,LTR}$ is always equal to the minimum value (10°C) because higher values lead to an increase of the thermal power released to the HRU with penalizing effects on cycle thermodynamic efficiency. For each point the performance is maximized by varying the cycle minimum and maximum pressure, the turbine inlet temperature, the $\Delta T_{cold,end,LTR}$ and the $\Delta T_{hot,end,LTR}$ (also equal to $\Delta T_{cold,end,HTR}$ because of the constraint of isothermal mixing at LTR outlet). Adopting the minimum value of ΔT_{pp} for both LTR and HTR results in a very high thermodynamic efficiency (27.9%) but in a poor utilization of the heat source (69.2%) finally resulting in a plant efficiency of 19.3%. Increasing the $\Delta T_{pp,HTR}$ the HTR duty progressively decreases (Figure 5.b), reducing the boiler inlet temperature and increasing the heat exploitation. Results clearly show that the optimal RRC configuration collapses on the SRC configuration substantially eliminating both the HTR (by employing a very high ΔT_{pp}) and the secondary compressor (using split fraction close to 1) as reported in both Figure 6.b and in the Ts diagram in Figure 5.c.

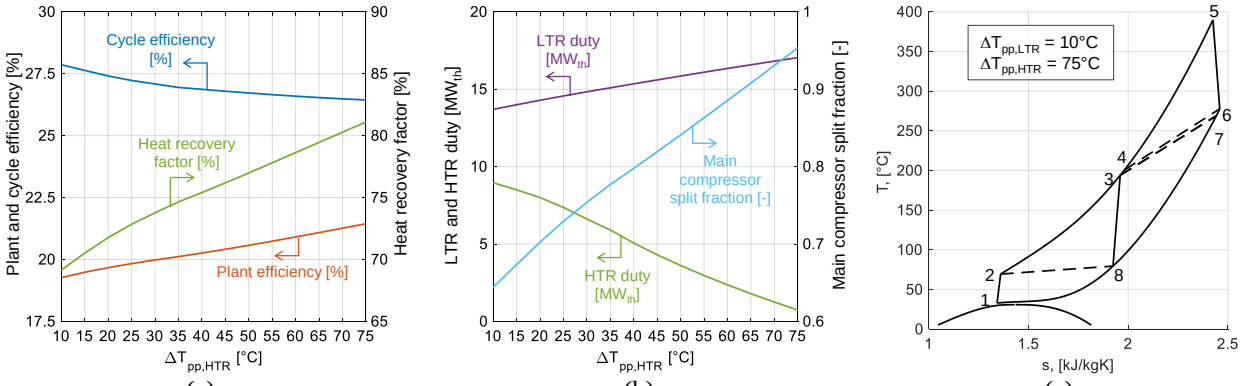

Figure 5. Results for the RRC configuration: (a) trend of η_{cycle}, χ and η_{plant} as function of ΔT_{pp} of HTR, (b) trend of recuperators duty and main compressor split fraction as function of ΔT_{pp} of HTR, (c) T-s diagram of optimal RRC configuration. Dashed lines in (c) represent the cold and hot extremities of the recuperators

For the RRCB configuration thanks to the HTR bypass it is possible to consider cases where the $\Delta T_{pp,HTR}$ is located at the hot end of the heat exchanger thus enabling the possibility to investigate solutions with HTR minimum temperature difference lower than the LTR value. Sensitivity analysis is carried out varying the pinch

point temperature difference of LTR and HTR and by optimizing the performance by varying the cycle maximum temperature, the cycle maximum and minimum pressures, the $\Delta T_{cold\text{-}end,LTR}$, the $\Delta T_{hot\text{-}end,LTR}$ and the $\Delta T_{hot\text{-}end,HTR}$ while always considering a isothermal mixing a both LTR and HTR recuperators. Best result is obtained adopting the minimum temperature difference (10°C) at LTR and HTR but adopting a larger value (15.6°C) for the $\Delta T_{cold\text{-}end,HTR}$. Maximum efficiency is 23.2% that is almost 1.3 points of efficiency higher than the performance attainable by adopting 10°C for all the three temperature differences.
On the contrary, the TSF configuration thanks to the very high heat recovery factor, benefits from adopting the low pinch point temperature difference in the recuperators and optimal solution is obtained considering 10°C for $\Delta T_{cold\text{-}end}$ of both recuperators and for $\Delta T_{hot\text{-}end,HTR}$.

3.3 Effect of imposing isothermal rather than non-isothermal mixing processes

General assumption in literature is to impose isothermal mixing for the recompressed cycle configuration (RRC and RRCB) at secondary compressor/LTR cold stream outlet and for the cycles with recuperator bypass (SRCB and RRCB) at recuperator/BHE outlet. This constraint involves the adoption of a specific value for the split or bypass ratio (depending on the cycle configuration) which may lead to suboptimal solutions. A sensitivity analysis is carried out in order to highlight the correctness of this assumption by varying the ΔT_{mix} (namely T_{3a}-T_{3b} and T_{4a}-T_{4b}) in a range of -30°C/+30°C thus investigating the effect of a non-isothermal mixing process. The results show that it is always beneficial to have ΔT_{mix} equal to zero at the outlet of high temperature recuperator bypass (namely at the outlet of REC in SRCB and HTR in RRCB configurations) while for the RRCB configuration optimal ΔT_{mix} at LTR recuperator outlet (T_{3a}-T_{3b}) is pushed towards negative values in order to reduce the duty in the LTR. This results in a final RRCB design that collapses on the SRCB configuration which has a higher efficiency. This numerical test shows also the stability of the numerical algorithm that, independently of the selected cycle configuration, when provided by a sufficient number of optimization variables, is able to optimize the system by excluding some components and to numerically converge to the optimal configuration.

3.4 Optimal selected cycles

Table 5 reports the overall results and the power balance of SRC, SRCB and TSF configurations optimal design while both recuperative RRC and RRCB configurations are discarded since their numerical optimization converge towards the simple cycles SRC and SRCB configurations respectively, as discussed in the previous sensitivity analysis. Figure 6 depicts the Ts diagram and the T-Q charts for heat introduction, internal heat recovery and heat rejection processes in the three selected cycle configurations. Finally, Table 6 reports the main results related to component preliminary sizing with a quantification of overall heat exchangers metal mass.
The two cycle configurations with the highest performance are the TSF and the SRCB with very similar plant efficiency equal to 27.8% and 27.4% respectively.
The TSF configuration reaches a higher cycle thermodynamic efficiency (30.3%) than the SRCB configuration (27.4%) with an almost total exploitation of the available thermal power (91.9%) while the SRCB configuration thanks to the use of the recuperator bypass can reach a total heat recovery factor confirming the crucial role of recuperator bypass for WHR systems exploiting a variable temperature heat source. Both TSF and SRCB configurations show a recuperator with ΔT_{pp} on both heat exchanger hot and cold ends thus maximizing the effectiveness of the internal heat recovery process.
TSF configuration can benefit from a more compact design of some heat exchangers: in particular, metal mass of the HRU and the recuperators (LTR+HTR) is 11.6% and 31.2% lower with respect to the SRCB. However, the metal mass of the PHE in TSF configuration is nearly twice than the sum of PHE and BHE in SRCB configuration, leading to an overall heat exchangers metal mass which is 30% higher in the TSF configuration. This implies a higher investment cost and a higher system footprint.
Results can be confirmed by verifying the correctness of turbomachinery efficiency assumptions against the results attainable with correlations developed for sCO_2 components as function of pressure ratio and size parameter [60]. Considering single-stage and multi-stage turbomachinery the efficiency for SRCB configuration ranges between 80.74% and 81.42% for the compressor and 84.32% and 87.68% for the turbine confirming that the calculated SRCB performance is realistic though a little conservative. On the contrary, TSF configuration adopts two turbines which size parameter is smaller than for the SRCB configuration because of the high pressure flow split: considering data from reference an efficiency below 85% for the primary turbine (below 82% considering a single-stage expander) and below 82% for the secondary turbine (below 79% considering a single-stage expander) is expected meaning that the calculated performance are not conservative and a realistic system efficiency is expected to be lower than the efficiency of the SRCB configuration. Considering the high performance, the lower overall metal mass and the need of a single expander the SRCB configuration looks the more promising one among the two.
With respect to RRC and SRCB configuration the SRC can reach a lower plant efficiency (21.8%) due to both lower thermodynamic efficiency (26.4%) and heat recovery factor (82.7%) but dramatically differ in required heat exchanger surface and metal mass. The recuperator metal mass in SRC is 4.7 times smaller than for the SRCB configuration because the lack of recuperator bypass does not allow to balance the heat capacity of cold and hot

side of the recuperator causing large temperature differences in the heat transfer process. Also heat introduction process of SRC configuration requires a lower heat transfer area and metal mass which is around 60% of the sum of PHE and BHE for the SRCB configuration. As result the overall metal mass of SRC configuration is less than half the metal mass required for the optimized SRCB. In conclusion, the SRC can be certainly considered as a possible solution when a low complexity, low capital cost and low footprint power plant is required by the end user or when the minimum exhaust temperature is high (e.g. 250°C-300°C) allowing to reach a plant performance of at least 28.6% and making this configuration an attractive solution against other WHR systems like ORC which efficiency generally ranges between 15-25% [31].

Considering the result of the optimization procedure for the three selected cycle configurations it is possible to highlight that the maximum pressure is pushed to the upper bound (250 bar) while minimum pressure is close to the CO_2 critical point (80 bar) for all cases in order to exploit real gas effects and high density during compression. Cycle pressure ratio results around 3 confirming the possibility to adopt compact turbomachinery with a limited number of stages. As final consideration, the results also highlight that the choice of sCO_2 cycle configuration must be always tailored to the considered application and that the adoption of configurations suggested for other applications (i.e. RRC and RRCB for high temperature cases like fossil fuel combustion or solar tower technology) may lead to questionable system design characterized by poor efficiency and very expensive equipment.

Table 5. Overall results and power balance for SRC, SRCB and TSF configurations optimal design.

	SRC	**SRCB**	**TSF**
Optimization variables optimal values			
Maximum cycle pressure p_2, bar	250	250	250
Minimum cycle pressure p_1, bar	79.19	79.88	79.18
Turbine inlet temperature, °C	391.78	411.17	525
$\Delta T_{pp,REC}$, °C	10	10	-
$\Delta T_{pp,LTR}$, °C	-	-	10
$\Delta T_{hot\ end,REC}$, °C	-	10	-
$\Delta T_{cold\ end\ HTR}$, °C	-	-	10
$\Delta T_{hot\ end\ HTR}$, °C	-	-	10
System performance			
Cycle thermodynamic efficiency, %	26.39	27.44	30.28
Heat recovery factor, %	82.68	100	91.86
Plant efficiency, %	21.82	27.44	27.82
Second law efficiency %	42.60	53.55	54.31
Power balance			
Thermal power recovered, MW_{th}	19.02	23.00	21.13
Main turbine electric power, MW_{el}	7.48	9.19	5.58
Secondary turbine electric power, MW_{el}	-	-	3.40
Main compressor electric power, MW_{el}	2.37	2.77	2.48
Heat rejection auxiliaries consumption, kW_{el}	95.28	113.55	100.00
Net electric power, MW_{el}	5.02	6.31	6.40
Mass flow rates			
CO_2 mass flow at turbine inlet, kg/s	73.13	87.18	76.75
CO_2 mass flow at bypass, kg/s	-	25.53	-
CO_2 mass flow at secondary turbine, kg/s	-	-	33.11
Cooling water mass flow rate, kg/s	462.12	550.71	484.94

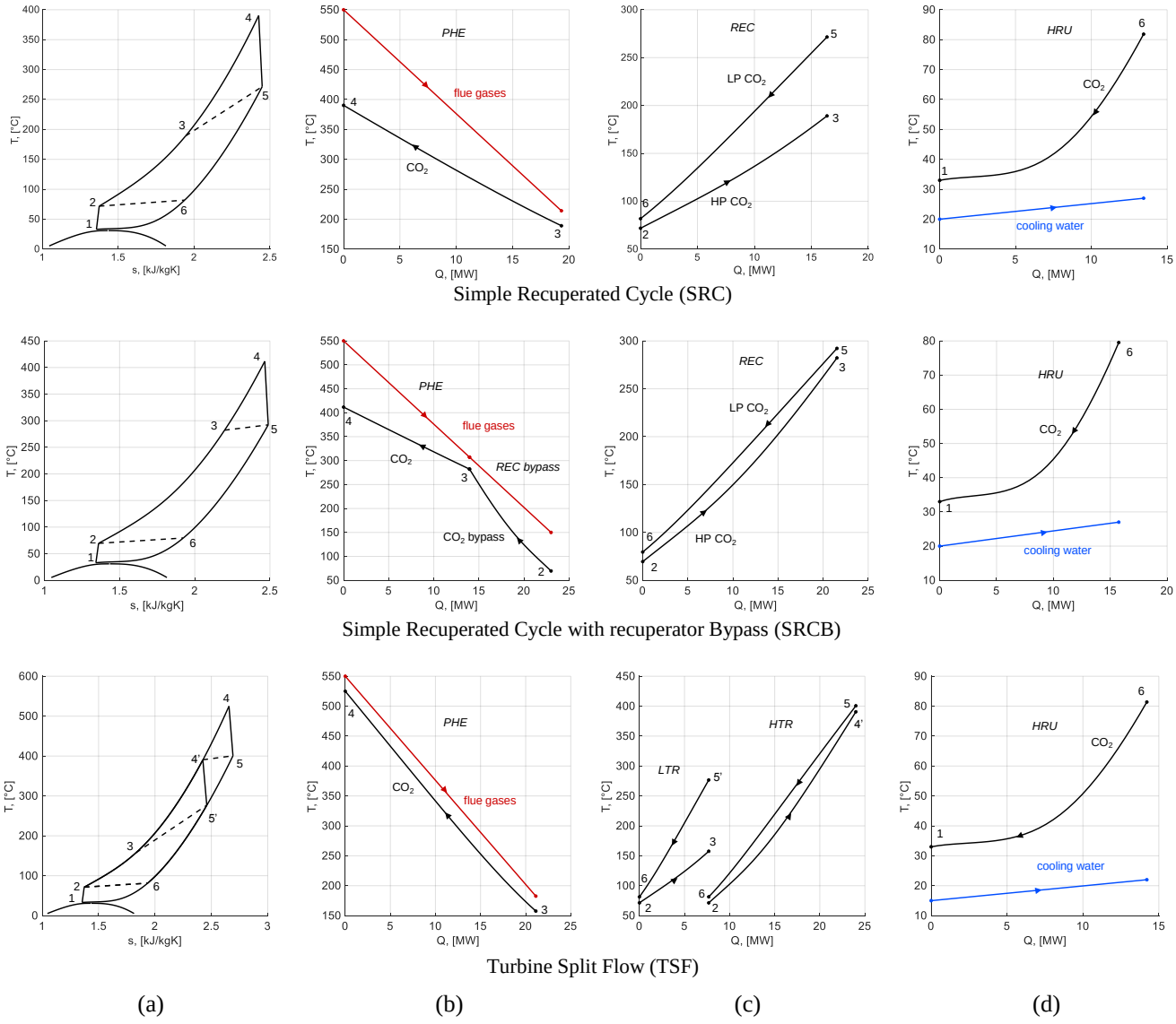

Figure 6. (a) T-s diagram of the best cycle design and corresponding T-Q diagrams of the heat source/CO2 heat exchangers (b), of the cycle recuperators (c) and of the heat rejection unit (d). Dashed lines in (a) represent the cold and hot extremities of the recuperators.

Table 6. Main results related to component preliminary sizing for SRC, SRCB and TSF configurations optimal design.

	SRC	**SRCB**	**TSF**
Total metal mass (piping excluded), kg	11455.41	24040.41	31018.84
Total metal mass (piping included) kg	17434.47	33570.24	35854.46
Total CO_2 inventory (piping excluded), kg	673.33	1224.14	1304.80
Total CO_2 inventory (piping included), kg	1338.68	2170.25	1929.89
HRU			
Duty, MW_{th}	13.54	16.14	14.21
ΔTmln, °C	27.32	27.00	27.33
U (int), W/m^2K	3752.51	3790.16	3748.78
A_{int}, m^2	153.28	180.39	161.02
A_{ext}, m^2	171.47	202.00	180.14
Metal mass, kg	1727.24	2052.59	1814.32

CO_2 mass, kg	245.93	297.47	257.83
REC (SRC, SRCB) or LTR (TSF)			
Duty, MW_{th}	17.13	22.52	7.69
ΔTmln, °C	48.69	18.38	63.45
U, W/m^2K	1446.24	845.44	1615.06
A, m^2	334.05	1557.92	112.18
Metal mass, kg	2083.02	9714.72	699.52
CO_2 mass, kg (hot/cold)	12.43/58.46	51.98/209.80	4.25/21.05
HTR (TSF)			
Duty, MW_{th}	-	-	16.31
ΔTmln, °C	-	-	24.66
U, W/m^2K	-	-	779.25
A, m^2	-	-	959.37
Metal mass, kg	-	-	5982.34
CO_2 mass, kg (hot/cold)	-	-	28.20/112.85
BHE (SRCB)			
Duty, MW_{th}	-	9.33	-
ΔTmln, °C	-	64.76	-
U (int), W/m^2K	-	718.47	-
A_{int}, m^2	-	224.31	-
A_{ext}, m^2	-	288.71	-
Metal mass, kg	-	6155.97	-
CO_2 mass, kg	-	432.21	-
PHE			
Duty, MW_{th}	19.02	13.67	21.13
ΔTmln, °C	94.25	82.30	32.00
U (int), W/m^2K	964.72	981.29	899.19
A_{int}, m^2	262.39	208.76	743.59
A_{ext}, m^2	341.82	272.27	976.52
Metal mass, kg	7645.15	6117.13	22522.66
CO_2 mass, kg	356.51	232.67	880.62
Turbine			
V_{in}, m^3/s	0.375	0.463	0.276
V_{out}, m^3/s	0.919	1.130	0.689
Z_{in}	1.011	1.017	1.042
Z_{out}	0.969	0.975	0.997
Vr	2.45	2.44	2.49
Δh, kJ/kg	106.06	109.32	132.62
PR	3.08	3.06	3.08
SP	0.050	0.055	0.041
Secondary turbine (TSF)			
V_{in}, m^3/s	-	-	0.168
V_{out}, m^3/s	-	-	0.415
Z_{in}	-	-	1.011
Z_{out}	-	-	0.969
Vr	-	-	2.47
Δh, kJ/kg	-	-	106.50
PR	-	-	3.11
SP	-	-	0.034
Compressor			
V_{in}, m^3/s	0.123	0.143	0.129
V_{out}, m^3/s	0.100	0.118	0.105
Z_{in}	0.230	0.226	0.230
Z_{out}	0.526	0.523	0.526
Vr	1.22	1.21	1.23
Δh, kJ/kg	31.19	30.60	31.20
PR	3.16	3.13	3.16
SP	0.028	0.030	0.022

3.5 Economic analysis

Finally, an evaluation of the capital investment cost for the three selected cycle configurations is carried out. Each component is described by a specific cost correlation obtained from literature, however for some components different references are available leading to a different evaluation of equipment cost and thus plant specific cost. Two main sets of cost correlations, the first one from Weiland [65] and the second from Carlson [66], are adopted in this analysis and integrated with cost correlation for sCO_2/exhaust heat exchanger (BHE and PHE) from [42][43]. Main differences between the two sets rely in the cost of turbomachinery: for the same turbine (e.g. 10 MW) Carlson correlations estimates a specific cost which is around 30% higher than the specific cost of Weiland radial turbine and around triple with respect to Weiland axial turbine (including gearbox and generator cost). Similarly, Carlson compressor cost (e.g. 5 MW) is almost two times the Weiland estimation (including motor). On the contrary, heat exchangers cost calculated with Carlson reference is 40% lower with respect to the Weiland one for the HRU and 24% lower for the recuperator. It is important to highlight that the turbine size of this paper is below the minimum size of cost correlations from literature (10 MW for axial turbine and 8 MW for radial turbine) and thus the cost of this piece of equipment is extrapolated with possible inaccuracy in economic evaluation. However, minimum turbine size is 3.4 MW for the TSF configuration while for the SRCB the turbine power output (9.19 MW) is very close to the correlation range of validity and so the economic results reported in Table 7 can be considered reliable taking into account the ±30% accuracy suggested by the authors for the cost correlations. Table 7 reports the cost breakdown of the capital investment cost of the three selected configurations carried out considering Weiland and Carlson set of correlations and using both axial and radial correlation in case of Weiland reference. Despite the different cost share obtained with the different correlations, the range of calculated specific cost is relatively narrow and comparable among the three selected configurations. Specific cost is lower for SRC configuration that benefits from very compact heat exchangers which low cost is not totally balanced by the reduction of power output, on the contrary TSF configuration shows the highest specific cost because of the larger heat transfer area and the smaller turbine size. SRCB specific cost ranges between 1617 $\$/kW_{el}$ (Weiland with axial turbine) and 2223 $\$/kW_{el}$ (Carlson): values of waste heat recovery ORC for the same range of power output are around 2000 $€/kW_{el}$ [67].

Table 7. Cost breakdown of the capital investment cost of SRC, SRCB and TSF configurations optimal design.

	SRC			SRCB			TSF		
	Weiland (axial)	Weiland (radial)	Carlson	Weiland (axial)	Weiland (radial)	Carlson	Weiland (axial)	Weiland (radial)	Carlson
PHE	1.27	1.27	1.27	1.02	1.02	1.02	3.34	3.34	3.34
BHE	-	-	-	0.80	0.80	0.80			
Turb1	0.57	2.09	3.57	0.64	2.47	4.11	0.48	1.65	2.92
GB Turb 1	0.29	0.29	-	0.31	0.31	-	0.27	0.27	-
Turb 2	-	-	-	-	-	-	0.37	1.11	2.08
GB Turb 2	-	-	-	-	-	-	0.24	0.24	-
Generator	0.33	0.33	-	0.37	0.37	-	0.36	0.36	-
Compressor	1.71	1.71	3.02	1.82	1.82	3.41	1.74	1.74	3.14
Motor comp	0.36	0.36	-	0.40	0.40	-	0.37	0.37	-
Recuperator	0.98	0.98	0.66	2.05	2.05	1.65	-	-	-
LTR	-	-	-	-	-	-	0.47	0.47	0.28
HTR	-	-	-	-	-	-	1.34	1.34	0.97
HRU	1.09	1.09	0.76	1.25	1.25	0.89	1.13	1.13	0.80
Contingency	0.46	0.57	0.65	0.61	0.73	0.83	0.71	0.84	0.95
Engineering	0.73	0.89	1.02	0.95	1.15	1.31	1.11	1.32	1.49
Total IC [M$]	7.78	9.58	10.95	10.20	12.36	14.03	11.95	14.21	15.97
Specific cost [$/KW]	1550.86	1908.45	2181.98	1616.89	1958.39	2223.29	1867.75	2220.94	2496.75

4 PART-LOAD METHODOLOGY

The part load operation of a sCO_2 system strongly depends on the cycle configuration and on the type of components installed. The part-load strategy usually aims at maximizing the plant performance while respecting a set of constraints on the components and on the sub-systems connected to the power block like the main industrial process upstream or possible thermal users downstream the WHR system. Real part-load operation inevitably refers to the direct control of some physical quantities of the system while the thermodynamic of the cycle spontaneously follows and adapts to the new operating condition. The numerical approach to part-load operation acts on different variables by imposing quantities that usually result from real plant operation (like components efficiency and temperature differences in heat exchangers) and by calculating quantities that are usually imposed in real plant (like the fluid inventory) but inevitably the final results must coincide.
The power plant part-load strategy is briefly proposed below, then the numerical approach adopted in this work is presented to provide a full explanation of the methodology and of the algorithms employed.

4.1 Real power plant part-load operation

In a real power plant, the off-design operation strategy is strongly linked to system dynamic and control. When a variation of the boundary conditions occurs, the system goes through a controlled transient to ensure proper operation of the different components and to maximize the performance in the new steady-state operative condition. The study of the dynamic and the control of sCO_2 power plants is beyond the scope of this paper, but the actions that can be reasonably done to control the system are listed below. This list of actions shall not be considered as a sequence of operation since all of them must be taken simultaneously.

- Cooling water pump rotational speed is varied to control the inlet temperature at the main compressor. Considering the very low nominal minimum temperature of the cycle (2°C above the critical point) it is seems reasonable to control the cooling medium mass flow rate to keep the minimum cycle temperature equal to the nominal one[1]. Increasing this temperature, (i.e. reducing the cooling water mass flow rate) is generally detrimental from an efficiency perspective since it involves an increase of main compressor specific work due to the CO_2 density reduction. On the other hand, reducing the main compressor inlet temperature (i.e. increasing the cooling water mass flow rate) may improve the efficiency of the system but it could possibly involve issues related to cavitation in the compressor due to vapor bubbles formation during fluid acceleration in the compressor distributor and stator [68].
- Turbine is not controlled with rotational speed, Inlet Guide Vanes (IGV) or variable degree of admission, but it is its sliding pressure operative curve (i.e. corrected mass flow vs pressure ratio) which determines the cycle maximum pressure as function of turbine inlet temperature and mass flow rate. The use of a more complex turbine design provided with features that allow to vary the machine operative curve may help to reach higher efficiencies in part load but are not strictly recommended for sCO_2 power plants. For TSF configuration the mass flow rate repartition between main and secondary turbine in part load can be different from the nominal value possibly resulting in different inlet pressures to the expanders. In this case the compressor outlet pressure is set equal to the highest value and control valves are required to guarantee a correct fluid repartition.
- Main compressor volumetric mass flow rate is varied in order to obtain the desired turbine inlet temperature while for RRC and RRCB configurations the secondary compressor mass flow rate is varied in order to ensure a desired ΔT_{mix} between the temperature of the streams at LTR and secondary compressor exit (T_{3a}-T_{3b}).
- Both main and secondary compressor operating points are set acting on available control strategies (IGV aperture and/or rotational speed variation) in order to provide the desired mass flow rate at the correct pressure while maximizing compressor adiabatic efficiency within the component operative map. These features look particularly effective for WHR sCO_2 power plants where the expected operative range is relatively wide [69]. Compressor operability is ensured by an anti-surge bypass loop which activates if the compressor operative point falls too close to the surge line.
- Recuperator bypass and HTR bypass split ratio, for SRCB and RRCB respectively, are varied to ensure a desired ΔT_{mix} between the streams at recuperator (REC or HTR) and BHE outlets (T_{3a}-T_{3b} for SRCB and T_{4a}-T_{4b} for RRCB).
- Fluid inventory is varied in order to achieve a specific objective. Considering sliding pressure turbines, when CO_2 mass flow rate is reduced also cycle maximum pressure decrease and, without an active control on fluid inventory, the minimum cycle pressure would increase to compensate the density reduction of gas in high pressure side of the cycle. The adoption of a pressurized CO_2 storage vessel may allow to

[1] Controlling the HRU operation measuring main compressor inlet temperature may lead to difficulties and system instability as small variations of temperature around the critical point, due to delay in response or measurements errors, result in dramatic variations of fluid density and thus in volumetric flow at compressor inlet. For this reason, a HRU control based on the direct measure of density at main compressor inlet with Coriolis mass flow and density meter looks more reliable [74].

vary the CO_2 mass in the system, freely vary the minimum pressure of the cycle. Fluid inventory can be varied in order to maximize plant performance or to satisfy a specific constraint like the need to control the flue gas minimum temperature due to downstream process specifications or because the need of avoiding acid condensation or fouling deposition on heat transfer surface. The CO_2 inventory storage can be constituted by a system of small vessels in parallel in order to limit the safety risk and to maintain the storage pressure nearly constant independently of stored mass. The storage system can be designed to operate with a pressure between the actual cycle maximum and minimum pressure. In this manner it is possible to depressurize the system and store fluid opening a throttling valve on the high-pressure side of the plant towards the storage and increase the fluid inventory by opening a throttling valve towards the low-pressure side of the plant. Another option is to design the inventory storage with a pressure between saturation pressure at ambient temperature and critical pressure (57 bar-73.8 bar) in order to condensate the fluid mass removed from the cycle and store it in liquid phase with less issues regarding leakages, however in this case a pump is required to fill again the system.

4.2 Numerical approach to part load operation

The numerical part load analysis is carried out varying the flue gas mass flow rate coming from the main upstream process between 30-100% of the nominal value and by imposing a set of cycle parameters: some of them are kept constant for the whole part-load operation while others are varied in order to maximize plant performance or to satisfy a specific constraint.

- Heat source maximum temperature (*fixed*): always equal to the design value thus neglecting variation of upstream main process gas cooling at part load condition. This assumption can be valid for a generic industrial or chemical process while it may not be accurate for gas turbine WHR since turbine outlet temperature can sensibly increase at part load as result of pressure ratio reduction and turbine efficiency decay, unless the gas turbine is controlled keeping the Turbine Outlet Temperature (TOT) constant [70][71].
- Cooling water minimum temperature (*fixed*): always equal to the design value according to the focus of this work on the part load analysis. Variation of minimum temperature of the cooling medium on nigh-day and seasonal base can clearly affect system performance but the penalizing effect on annual energy yield can be rather limited when water cooled or wet and dry HRU solutions are adopted [57].
- Main compressor inlet temperature (*fixed*): always equal to the design value according to the need of exploiting real gas effects in main compressor without issues related to cavitation.
- Temperature difference at mixing processes (*fixed*): always equal to zero in order to limit the irreversibility of the mixing process in SRCB, RRC and RRCB configurations.
- Main compressor inlet pressure (*varied*): this parameter affects the cycle pressure ratio with consequent effect on turbine and compressors operating point and it can be varied in order to maximize the cycle efficiency or to match a specific constraint. An example can be the need of keeping the minimum flue gas temperature at PHE/BHE outlet above a certain threshold.
- Turbine inlet temperature (*varied*): this parameter can be set constant or varied in part load in order to maximize plant performance. For example, a reduction of the TIT at part load could lead to an increase in the power output if the benefit related to the increase of CO_2 mass flow rate outweighs the detrimental effect related to the reduction of the turbine specific power.

Once the aforementioned parameters are set, the steady-state part load operating condition is obtained by solving a system of nonlinear equations each one representing the part load behavior of a component in the system (system constraints in Table 8). Table 8 also reports the selected closing variables of the off-design problem, namely those quantities, unknown a priori, that are varied by the solving algorithm in order to verify system constraints. Once the off-design problem is solved, the power output is computed and the fluid inventory variation within the system is calculated knowing the internal volume of each component, the connecting piping volume and the thermodynamic conditions of sCO_2. Table 8 only refers to the SRCB configuration which is the one selected for part load operation detailed analysis. Figure 2.b depicts the flow diagram for the SRCB part load analysis: only the first four closing variables and system constraints (referred to heat exchangers constant area) are reported in the diagram while the other ones (referred to pressure drops and turbomachinery efficiency) are omitted for sake of clarity.

Table 8. Numerical constraints and closing variable for the system of non-linear equations representing the part load (*pl*) numerical problem for the SRCB configuration. * labels closing variables directly handled by the solving numerical algorithm.

SRCB	
System constraint	**Closing variable**
$A_{HRU}^{pl} = A_{HRU}^{des}$	$\Delta T_{cooling\ water}^{pl-(*)}$
$A_{REC}^{pl} = A_{REC}^{des}$	$\Delta T_{cold\ end\ REC}^{pl-(*)}$
$A_{BHE}^{pl} = A_{BHE}^{des}$	$\Delta T_{hot\ end\ REC}^{pl-(*)}$
$A_{PHE}^{pl} = A_{PHE}^{des}$	$p_{max}^{pl-(*)}$
$\Delta p_{REC,cold}^{pl-(*)} = \Delta p_{REC,cold}^{pl-calc}$	$\Delta p_{REC,cold}^{pl-(*)}$
$\Delta p_{REC,hot}^{pl-(*)} = \Delta p_{REC,hot}^{pl-calc}$	$\Delta p_{REC,hot}^{pl-(*)}$
$\Delta p_{BHE,cold}^{pl-(*)} = \Delta p_{BHE,cold}^{pl-calc}$	$\Delta p_{BHE,cold}^{pl-(*)}$
$\Delta p_{PHE,cold}^{pl-(*)} = \Delta p_{PHE,cold}^{pl-calc}$	$\Delta p_{PHE,cold}^{pl-(*)}$
$\Delta p_{HRU,hot}^{pl-(*)} = \Delta p_{HRU,hot}^{pl-calc}$	$\Delta p_{HRU,hot}^{pl-(*)}$
$\eta_{main\ comp}^{pl-(*)} = \eta_{main\ comp}^{pl-calc}$	$\eta_{main\ comp}^{pl-(*)}$
$\eta_{turbine}^{pl-(*)} = \eta_{turbine}^{pl-calc}$	$\eta_{turbine}^{pl-(*)}$

As reported in Table 8, main closing variables are the temperature differences in the recuperators that are varied in order to match the calculated heat transfer area in part load (*pl*) operation with the design value (*des*). Off design heat transfer area of each heat exchanger is imposed equal to the design value and calculated considering the same discretization of the component in order to catch local variations of thermodynamic properties as reported in Eq. 5 and Eq. 6.

Pressure drops and heat transfer coefficients on the CO_2 side are computed by adopting the same correlations used for the cycle design using the average stream properties in each heat exchanger subsection; for flue gas and cooling water, Eq. 7 and Eq. 8 are used for pressure drops and heat transfer coefficients respectively [72]. As CO_2 side pressure drops directly affect fluid thermodynamic and transport properties, thus influencing both the heat exchanger duty and the heat transfer coefficients, from the numerical stability point of view it is preferable to include them as closing variables and constraints in the system of equations representative of the off-design problem as reported in Table 8.

$$\Delta p_{pl} = \Delta p_{des} \left(\frac{\rho_{des}}{\rho_{pl}}\right) \left(\frac{\dot{m}_{pl}}{\dot{m}_{des}}\right)^2 \qquad \text{Eq. 7}$$

$$htc_{X,pl} = htc_{X,des} \left(\frac{\dot{m}_{X,pl}}{\dot{m}_{X,des}}\right)^{\alpha} \quad \text{with} \begin{cases} X = gas & \alpha = 0.6 \\ X = water & \alpha = 0.8 \end{cases} \qquad \text{Eq. 8}$$

Turbomachinery design can be assumed coherent with the design proposed by Baker Hughes General Electric (BHGE) in the framework of sCO2-Flex project [29] adopting the following design criteria and off design performances.

Both main and secondary compressor are designed as multistage centrifugal compressors, each one mounted on a dedicated high-speed shaft driven by a variable speed electrical motor. In addition, compressors are provided by Inlet Guide Vanes (IGV) which are close to fully open position in nominal condition. Compressors efficiency variation at part-load is evaluated as function of normalized volumetric flow rate and normalized enthalpy rise ratios with respect to the nominal values, adopting dimensionless operative maps provided by BHGE [73].

Compressors maps have been developed considering the possibility to act on both shaft rotational speed and IGV aperture in order to maximize the compressor efficiency for any operating condition. Main compressor map is reported in Figure 7 highlighting the iso-efficiency levels.

In part load conditions the compressor can be operated in a high efficiency region down to low volumetric flow rates by contextually reducing the cycle pressure ratio and controlling the compressor mainly through speed variation and adjusting the IGV aperture only when rotational speed is close to lower or upper limit. However, if the variation of enthalpy head is too high, the operative point moves towards the choked flow region characterized by low turbomachinery performance (path A). On the contrary, if the enthalpy head remains fairly constant at part load, the compressor operative point approaches the surge line and the surge safety limit computed considering a 10% margin with respect to the volumetric flow rate that causes an incipient surge condition for a given enthalpy head. If the volumetric flow rate falls below this limit, the anti-surge loop is activated to maintain a proper compressor inlet volumetric flow rate and avoid instability issues (path B). When compressor anti-surge bypass

is activated, a fraction of CO_2 mass flow rate is recirculated from the outlet of the compressor, throttled down to cycle minimum pressure and cooled in order to keep compressor inlet conditions unchanged.
The power plant HRU is used to cool down the main compressor bypass while an additional gas cooler is employed for the secondary compressor bypass for both RRC and RRCB cases. As result, the compressor elaborates a mass flow rate higher than the one required by the system, leading to an increase of the power plant internal consumption, HRU auxiliary consumptions and eventually involving a penalization of the plant overall efficiency. The compressors antisurge loops are depicted in green in Figure 1.
The expander is designed as a full admission axial turbine, mounted on a high-speed shaft according to the very high machine power density and the small turbine diameter. High speed shaft is eventually connected through a gearbox to the 3000 RPM generator shaft.
Turbine part load operative curve and off design performance is derived from BHGE calculations carried out in the frame of sCO2-Flex project [29]. Raw data on corrected mass flow rate and efficiency as function of the turbine pressure ratio (at fixed outlet pressure) have been normalized with respect to nominal quantities. Then the turbine off-design behavior has been implemented as the normalized corrected mass flow rate and the normalized efficiency (Figure 7.b) against the normalized load coefficient (Eq. 9) which is proportional to the normalized enthalpy drop for a fixed rotational speed turbine. Part load isentropic turbine efficiency remains fairly constant until the pressure ratio is above half of the critical value. Compressors and the turbine efficiencies affect the thermodynamic of the cycle and, as for the heat exchanger pressure drops, it is preferable to include them as unknown quantities in the system of equations representing the off-design problem as reported in Table 8.

$$k_{is*} = \frac{\Delta h_{is}^{pl}}{\Delta h_{is}^{des}} \left(\frac{u_{is}^{des}}{u_{is}^{pl}} \right)^2 \qquad \text{Eq. 9}$$

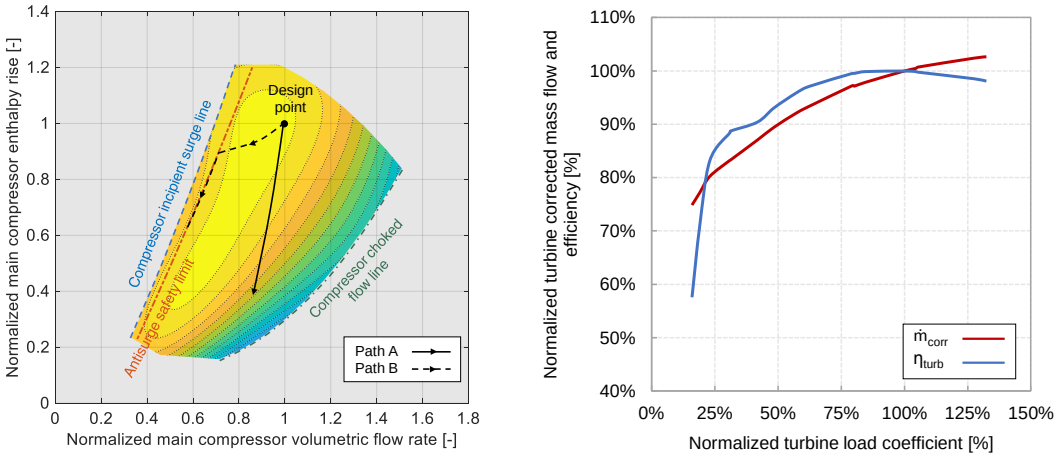

(a) (b)

Figure 7. Normalized operative map of main compressor (a) and normalized operative curve of the turbine (b) (normalized corrected mass flow rate (red) and the normalized efficiency (blue) vs. the normalized load coefficient).

5. PART-LOAD RESULTS

Part load analysis is carried out only for the SRCB configuration which represents a good compromise between design efficiency, system complexity and specific cost. Different part-load cycle operation strategies can be implemented in order to optimize the power production and/or to meet specific operational constraints. Two main parameters have been identified as optimization variables in part-load strategy definition namely the compressor inlet pressure, i.e. the cycle minimum pressure, and the turbine inlet temperature, i.e. the cycle maximum temperature. In addition, two main part-load operation constraints can be identified: the first one is related to the minimum stack temperature to be respected in order to avoid acid condenses while the second one is related to the inventory variation that can be imposed equal to zero to simulate a totally sealed cycle without the need of CO_2 storage vessel. No additional constraint is introduced to limit the maximum cycle pressure to the design value (250 bar), anyhow, the maximum value obtained in all the investigated cases is 256 bar which should not entail any safety issue.

Table 9 summarizes the different investigated strategies: strategies from S1 to S3 are obtained through CO_2 inventory change while strategies S4 and S5 with fixed CO_2 mass within the cycle. The activation of a specific strategy constraint involves an additional closing variable: as result one strategy control variable must be calculated to satisfy the additional constraint instead of being varied with the aim at maximizing power output. Maximum flue gas temperature, minimum coolant temperature and compressor inlet temperature are constant and equal to the nominal value while performance are calculated by varying the flue gas mass flow rate from 100% down to 30%.

Table 9. Summary of the different investigated part-load operation strategies.

Strategy	**Strategy control variables**		**Strategy constraints**	
	Turbine inlet temperature	*Compressor inlet pressure*	*Minimum stack temperature*	*Constant inventory*
S1	Equal to nominal	Equal to nominal	Not active	Not active
S2	optimized	optimized	Not active	Not active
S3	optimized	calculated	Active	Not active
S4	optimized	calculated	Not active	Active
S5	calculated	calculated	Active	Active

5.1 Part-load of cycles with CO_2 storage vessel

With reference to Table 9, three different strategies (S1-S2-S3) can be identified for plants that can implement inventory variation. Figure 8 reports the trends of the most relevant quantities as function of the flue gas mass flow rate: cycle maximum pressure and cycle minimum pressure (Figure 8.a), turbine inlet temperature and stack temperature (Figure 8.b), heat recovery factor and difference against S1 strategy (Figure 8.c), cycle thermodynamic efficiency and difference against S1 strategy (Figure 8.d), net power output and difference against S1 strategy (Figure 8.e), cycle pressure ratio and fluid inventory variation (Figure 8.f).

- Strategy S1 is the simplest one, it does not include any optimization in order to maximize power output and it is reported here as term of comparison: both maximum temperature and cycle minimum pressure are not varied from nominal condition with the aim of not penalizing turbine power output and keeping the main compressor inlet condition in a region with marked real gas effects. Reducing the flue gas mass flow rate, the cycle maximum pressure decreases (from 250 bar to slightly below 135 bar at minimum load, Figure 8.a) because of the sliding pressure operation of the turbine leading to a reduction of the cycle pressure ratio (Figure 8.f) from 3.13 to 1.67 with a consequent penalization of the thermodynamic cycle efficiency (Figure 8.d). Moreover, main compressor outlet temperature decreases while turbine outlet temperature increases enhancing the internal heat recovery process. Recuperator is oversized at part-load operation as it features a thermal duty lower than the nominal one leading to an increase in heat transfer effectiveness, partially balancing the detrimental effect caused by the reduction of pressure ratio on the cycle thermodynamic efficiency. For this reason, cycle thermodynamic efficiency (Figure 8.d) is above the nominal value for flue gas mass flow rates between 85% and 100% and below the nominal one for normalized flue gas mass flow rate values below 85%: at minimum load thermodynamic cycle efficiency loss is around 6.2 points. The reduced flue gas and working fluid mass flow rates involve also a higher effectiveness of PHE and BHE which operate with lower average temperature differences, involving a reduction of stack temperature (Figure 8.b) and thus a heat recovery factor higher than 100% (Figure 8.c). Minimum stack temperature is around 139°C for a flue gas mass flow rate equal to 43% of the nominal one. This aspect must be carefully considered in case of the presence of a minimum stack temperature limit due to acid condenses formation or requirements of downstream processes (other industrial heat use or flue gas treatment section). Power output (Figure 8.e) always decreases with a trend which is determined by both heat recovery factor and cycle thermodynamic efficiency trends in part load. Fluid inventory (Figure 8.f) is progressively reduced because of the lower cycle maximum pressure with

a minimum value at the minimum flue gas mass flow rate corresponding to -21% (-470 kg_{CO2}) of fluid inventory with respect to the inventory in nominal conditions.

- Strategy S2 aims at optimizing cycle power output by varying both minimum pressure (compressor inlet) and maximum cycle temperature (turbine inlet). Figure 9.a depicts the trend of power output variation against strategy S1 attainable by the adoption of different cycle maximum temperatures and by optimizing the cycle minimum pressure (Figure 9.b) at all times. Results show that in part-load it is always convenient to reduce both the cycle minimum pressure and maximum temperature in order to increase the main compressor volume flow rate and to limit the reduction of cycle pressure ratio. Only the optimal results of strategy S2, namely the envelope of iso-maximum temperature lines of Figure 9, are reported in Figure 8. By optimizing both the cycle maximum temperature and minimum pressure it is possible to increase the plant power output with respect to S1 strategy for any value of flue gas mass flow rate. For nominal flue gas mass flow rate, it is possible to increase the power output of 25 kW_{el} (Figure 8.e) thanks to the adoption of a slightly higher maximum pressure (255.8 bar vs. 250 bar) (Figure 8.a), a higher minimum pressure (81.7 bar vs. 79.9 bar) (Figure 8.a) and a lower cycle maximum temperature (400.3°C vs. 411.2°C) (Figure 8.b) while keeping nearly the same pressure ratio (Figure 8.b). As result, the cycle thermodynamic efficiency decreases (-0.4%) (Figure 8.d) while the heat recovery factor increases at 101.9% with a consequent slightly positive effect on power output. For a flue gas mass flow rate lower than the nominal one, it is convenient to reduce both cycle minimum pressure (Figure 8.a) and cycle maximum temperature (Figure 8.b) which are 77.0 bar and 378.1°C respectively at minimum load. In this manner it is possible to operate the compressor in a region of high efficiency and to further reduce the stack temperature with a minimum value of 125.9°C (Figure 8.b). At minimum load the power output is around 93 kW_{el} higher with respect to S1 strategy. Plant CO_2 inventory is higher than strategy S1 for flue gas mass flow rates above 50% of the nominal one and lower (-692 kg_{CO2} with respect to nominal baseline fluid inventory) at minimum load.
- Strategy S3 aims at optimizing the power output at any load also respecting the constraint of a minimum stack temperature equal to the nominal value (Figure 8.a). Only cycle maximum temperature is optimized while cycle minimum pressure is calculated in order to respect the stack temperature constraint[2]. Heat recovery factor (Figure 8.c) is always equal to the nominal value (100%) and the overall plant efficiency is thus equal to the cycle thermodynamic efficiency (Figure 8.d). Since the algorithm cannot further reduce the flue gas stack temperature, it pushes the cycle thermodynamic efficiency at the maximum attainable with values that are always higher than the ones found both with S1 and S2 strategies. It should be mentioned that for a nominal flue gas mass flow rate the cycle operation differs from design point because the optimization algorithm slightly increases both the maximum cycle temperature (413.0°C vs. 411.2°C) (Figure 8.b) and the cycle minimum pressure (81.3 bar vs. 79.9 bar) (Figure 8.a) with respect to the nominal values in order to get a power output increment lower than 1 kW_{el} thanks to a slightly higher compressor efficiency: this solution proves the capability of the optimization procedure but also highlights that very similar values of net power output can be obtained with different combinations of cycle maximum temperature and minimum pressure. Cycle maximum pressure (Figure 8.a) decreases at lower flue gas mass flow rates with a trend similar to both strategies S1 and S2 while cycle minimum pressure is always below the one of case S2 and higher than the nominal one only for flue gas mass flow rates above 91% of the nominal one. Power output (Figure 8.e) is lower than the nominal for flue gas mass flow rates between 48% and 100% of the nominal one (with a maximum difference of -28 kW_{el}) but reaches similar values of S2 strategy at minimum load, performing better than S1 strategy (+85 kW_{el}).

[2] The same result can be obtained by optimizing cycle minimum pressure and calculating the cycle maximum temperature.

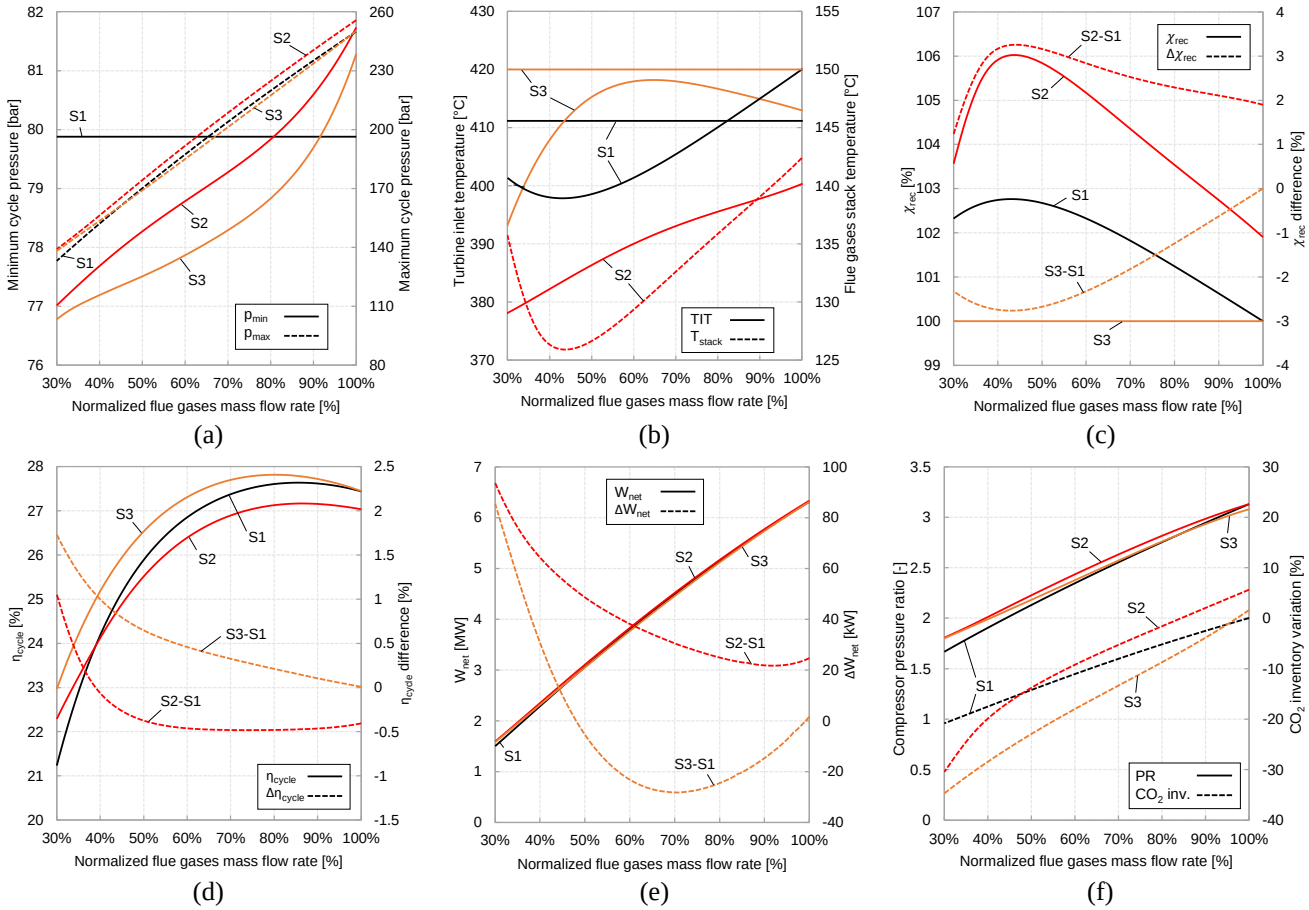

Figure 8. Trend of cycle maximum pressure and cycle minimum pressure (a), turbine inlet temperature and stack temperature (b), heat recovery factor (c), cycle thermodynamic efficiency (d), net power output (e), cycle pressure ratio and fluid inventory variation (f) against normalized flue gas mass flow rate for the strategy S1, S2 and S3.

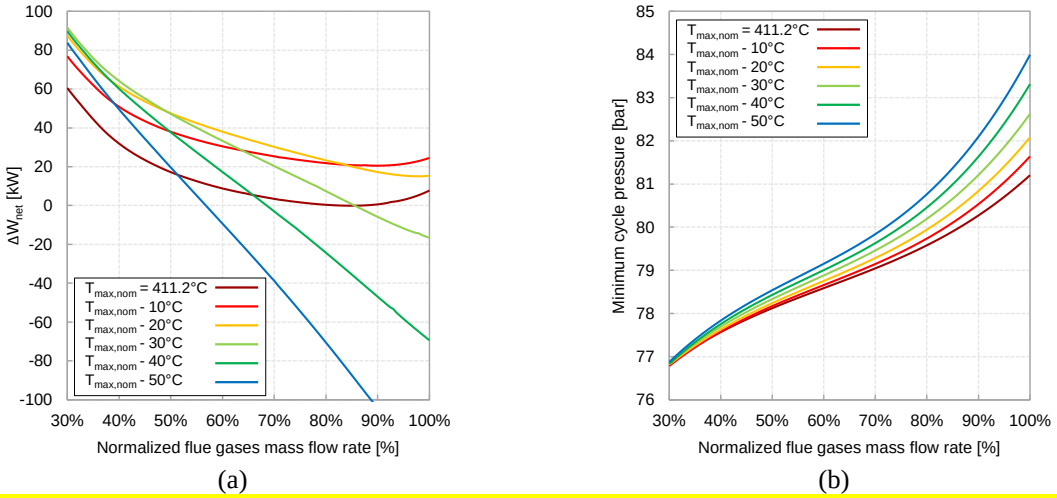

Figure 9. (a) Net power output variation with respect to S1 strategy attainable by varying cycle maximum temperatures and optimizing cycle minimum pressure at all times, (b) corresponding optimal compressor inlet pressure for the different cycle maximum temperatures.

Figure 10.a reports the main compressor operative points path on the compressor map for strategies S1, S2 and S3: each marker represents a 10% reduction of normalized flue gas mass flow rate, ranging from 100% to 30%. It is possible to highlight that the main compressor operative points for the three operating strategies are almost overlapped in the 100%-60% range, while, for further reductions of flue gas mass flow rates, S1 path drifts away from S2 and S3 paths approaching the lower limit of the compressor operative map and getting close to anti-surge limit. S2 and S3 strategies, tuning the cycle minimum pressure, allow to increase the cycle pressure ratio keeping

the main compressor operative point closer to nominal one, leading to a lower turbine efficiency penalization (Figure 10.b).

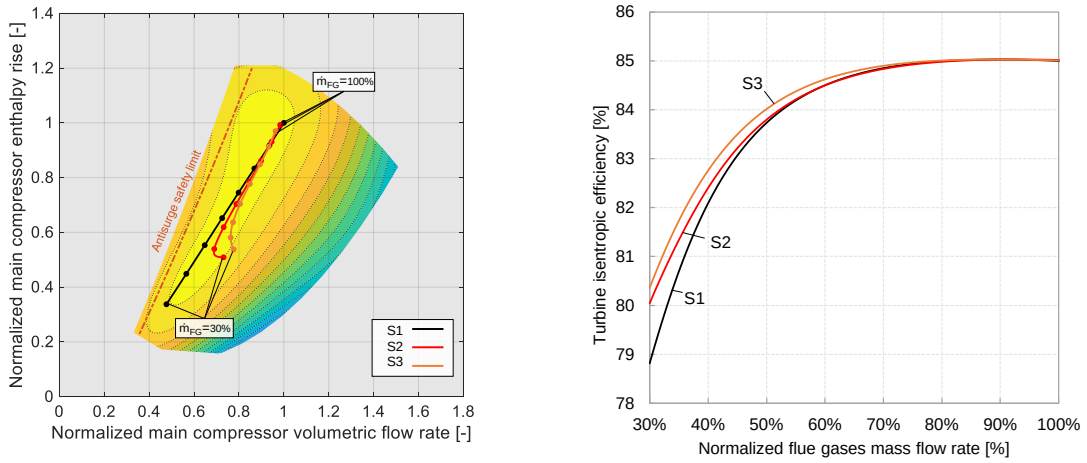

(a) (b)

Figure 10. a) S1, S2 and S3 strategies main compressor operative points and b) turbine efficiency in the range 100%-30% normalized flue gas mass flow rate.

5.2 Part-load of cycles without CO_2 storage vessel

Inventory variation involves an inevitable increase of system complexity and its control represents a non-trivial challenge because of the transients related to charging and discharging operation of the carbon dioxide vessels. Moreover, considering the relatively small size of WHR applications in industrial facilities and the need of ease installation and simplicity of operation, the possibility to design a totally sealed system that does not require inventory variation during part load looks particularly attractive. Results are shown in Figure 11 comparing the results of the two proposed constant inventory strategies (S4 and S5) against the corresponding variable CO_2 inventory strategy: namely S4 against S2 (both without active constraint on minimum stack temperature) and S5 against S3 (both with active constraint on minimum stack temperature). Strategy S4 aims at maximizing plant power output through optimization of cycle maximum temperature while keeping constant the fluid inventory by variation of cycle minimum pressure. On the contrary, strategy S5 aims at keeping the inventory constant and the stack minimum temperature above the nominal value: as a consequence, both cycle maximum temperature and cycle minimum pressure are computed to satisfy these constraints and power output cannot be maximized. Main compressor operative points and turbine efficiency values as function of normalized flue gas mass flow rate are reported in Figure 12. Considerations common to both strategies regard the trend of cycle minimum pressure (Figure 11.a) which increases at part load given the need to compensate the fluid density reduction on high pressure side of the cycle due to the sliding pressure operation of the turbine. As result, cycle pressure ratio (Figure 11.f) decreases more than in variable inventory strategies (S1-S3) leading to main compressor operative point very close to map lower bound with a penalization of compressor efficiency (Figure 12.a) and a larger drop of turbine efficiency (Figure 12.b) with respect to strategies S1-S3. The effect is more marked for S5 strategy due to the need of limiting the stack temperature variation (Figure 11.b) which involves a higher cycle maximum temperature (Figure 11.b) and consequently a higher cycle minimum pressure. On the contrary, S4 strategy is optimized by decreasing the cycle maximum temperature and the stack temperature, thus leading to a heat recovery factor greater than 100% (Figure 11.c). Imposing a constant CO_2 inventory strongly penalizes cycle thermodynamic efficiency[3] (Figure 11.d) because of the stronger reduction of pressure ratio and turbomachinery efficiencies: performance are fairly constant down to 75% of normalized flue gas mass flow rate while at minimum load the plant efficiency results to be 18.3%, equivalent to a drop of around 9.1 percentage points with respect to the nominal case (-33% on relative base). From the point of view of net electric power output (figure 11.e) both S4 and S5 strategies are penalized with a maximum loss of net power output equal to 124 kW_{el} (-7.8%) and 347 kW_{el} (-15.2%) for S4 and S5 strategies respectively when compared to S2 and S3 strategies.

[3] For S5 strategy, this parameter is proportional to system efficiency because of constant heat recovery factor.

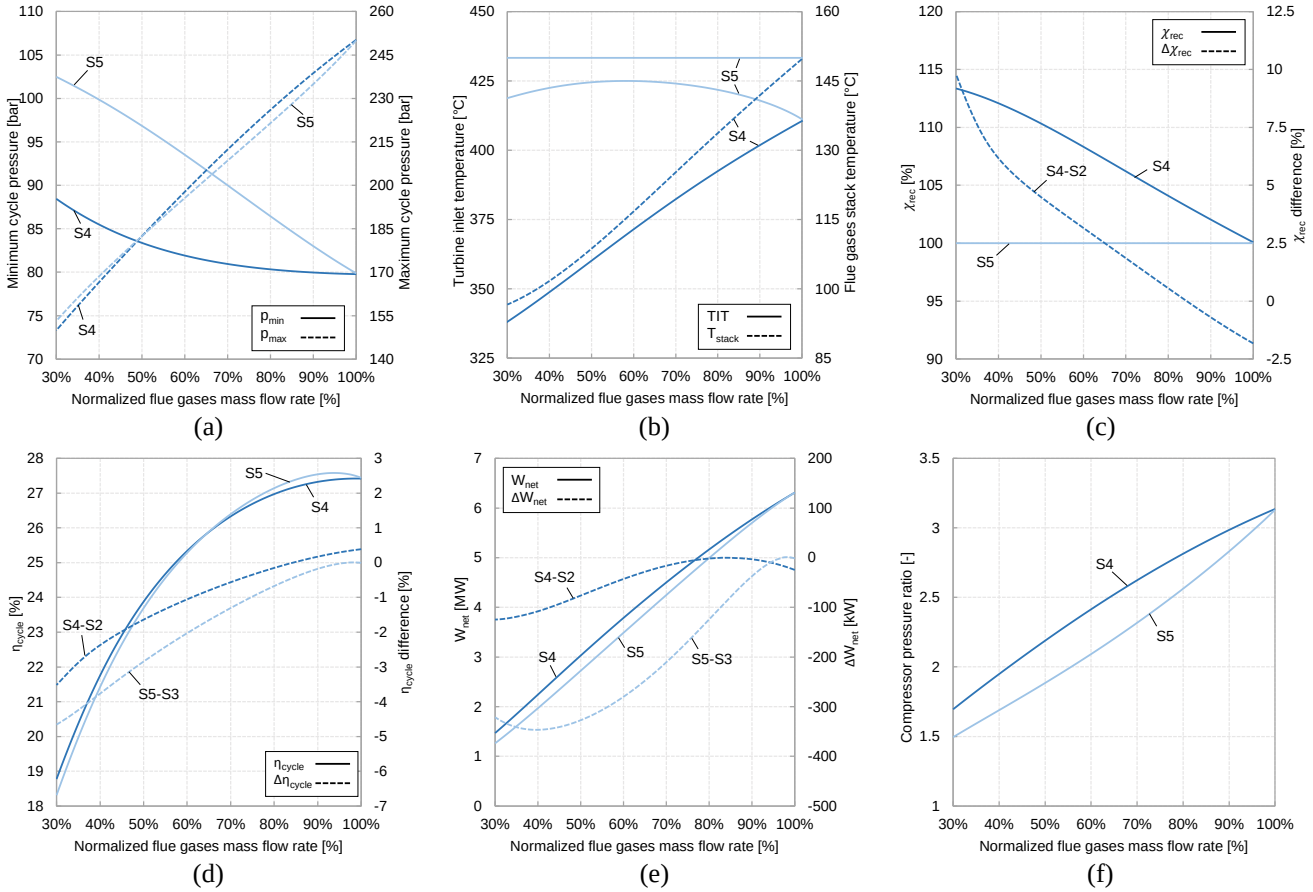

Figure 11. Trend of cycle maximum pressure and cycle minimum pressure (a), turbine inlet temperature and stack temperature (b), heat recovery factor (c), cycle thermodynamic efficiency (d), net power output (e), cycle pressure ratio (f) against normalized flue gas mass flow rate for the strategy S4 and S5.

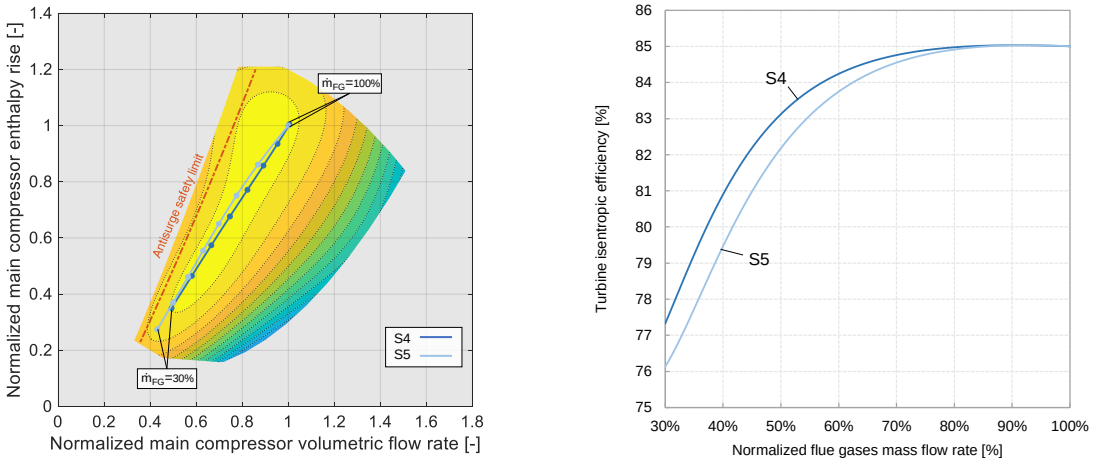

Figure 12. S4 and S5 strategies main compressor operative points (a) and turbine efficiency (b) in the range 100%-30% normalized flue gas mass flow rate.

5.3 Final comparison

Among the five proposed part load strategies, S3 and S5 have been selected as the most relevant ones as they respect the minimum stack temperature limit, avoiding an excessive cooling of the flue gases at part load. Figure 13 depicts the temperature-specific entropy diagrams for S3 and S5 strategies at 70%, 50% and 30% of normalized flue gas mass flow rate. It is possible to appreciate the fact that both strategies keep the cycle maximum temperature close to the nominal one while cycle minimum pressure is higher for S5 strategy pushing main compressor inlet condition to the left of the critical point. Finally, Table 10 reports the main results for S3 and S5 strategies at different normalized flue gas mass flow rates: it is possible to appreciate that, even if plant efficiency is fairly similar for both strategies ($\Delta\eta_{plant}$=1.3%) down to 70% normalized flue gas mass flow rate, at minimum

load the adoption of a constant CO_2 inventory strongly penalizes the plant efficiency which for S5 strategy results 4.7% points lower than for S3 strategy (-20% on relative base).
Figure 14 reports the breakdown of CO_2 inventory variation within the plant components against normalized flue gas mass flow rate for strategies S3 and S5. It is possible to highlight that for strategy S3 both maximum and minimum pressures decrease leading to a homogeneous reduction of fluid inventory in all the plant components. At minimum load about one-third of the overall CO_2 inventory needs to be stored in an external CO_2 vessel.
On the contrary, in strategy S5, as no external CO_2 vessel is considered, the cycle maximum pressure reduction due to the turbine sliding pressure operation involves a shift of the CO_2 from the high-pressure side components (cold side REC, BHE, PHE, and piping to/from PHE) to the low-pressure side components (hot side REC, HRU and piping to/from HRU) of the plant. The higher amount of CO_2 can fit in the low-pressure side of the system thanks to the reduced average temperature of the HRU and thanks to the increase of the minimum cycle pressure.

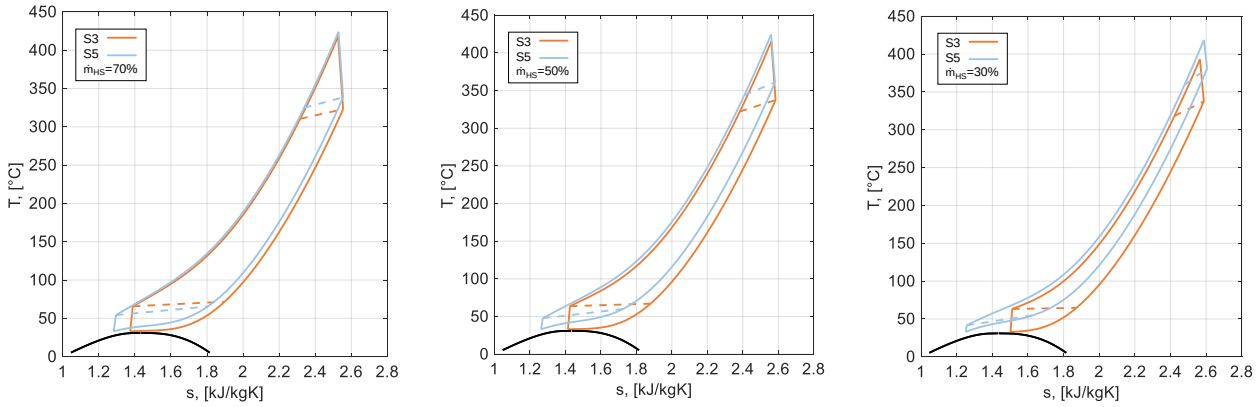

Figure 13. Comparison between optimized Ts diagrams of constant stack temperature S3 (variable inventory) and S5 (constant inventory) strategies for 70% (a), 50% (b), and 30% (c) normalized flue gas mass flow rate.

Table 10. main results for S3 and S5 strategies at different normalized flue gas mass flow rates.

	S3 strategy				S5 strategy			
Normalized flue gas mass flue rate [%]	90.0%	70.0%	50.0%	30.0%	90.0%	70.0%	50.0%	30.0%
Normalized electric power output [%]	90.9%	70.7%	48.4%	25.1%	90.3%	67.3%	43.2%	20.0%
Plant efficiency [%]	27.7%	27.7%	26.5%	23.0%	27.5%	26.4%	23.7%	18.3%
Gross power output [MW]	5.81	4.49	3.06	1.59	5.76	4.26	2.73	1.26
HRU consumption [MW]	0.07	0.03	0.01	0.00	0.06	0.01	0.00	0.00
Net power output [MW]	5.74	4.46	3.05	1.58	5.70	4.25	2.72	1.26
Turbine inlet temperature [°C]	414.93	417.96	415.24	393.18	417.90	424.02	424.48	418.77
Maximum cycle pressure [bar]	233.64	201.20	169.04	138.16	234.94	208.52	182.48	153.16
Minimum cycle pressure [bar]	79.69	78.29	77.51	76.78	83.00	90.00	96.85	102.50
Compressor pressure ratio [-]	2.93	2.57	2.18	1.80	2.83	2.32	1.88	1.49
Turbine isentropic efficiency [%]	85.0%	84.9%	84.0%	80.4%	85.0%	84.5%	82.2%	76.1%
Compressor isentropic efficiency [%]	80.2%	80.1%	80.0%	79.5%	80.2%	80.0%	80.0%	79.1%
Inventory variation [kg]	-87.05	-303.03	-521.29	-788.99	0.00	0.00	0.00	0.00
Inventory variation [%]	-3.8%	-13.3%	-22.9%	-34.7%	0.0%	0.0%	0.0%	0.0%

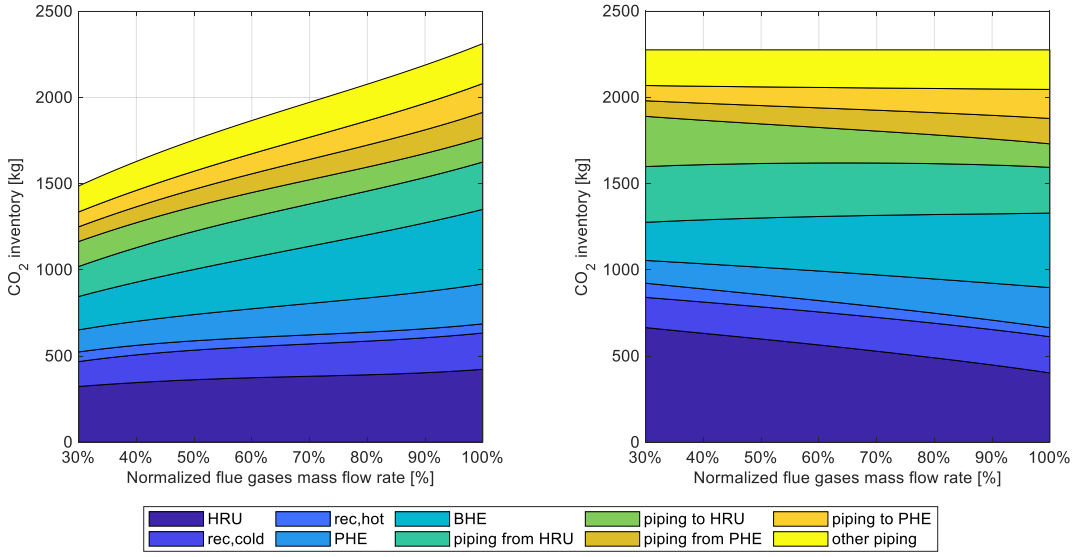

(a) (b)

Figure 14. Breakdown of CO_2 inventory variation within the plant components against normalized flue gas mass flow rate for strategy S3 (a) and S5 (b). For S3 strategy (a) the difference between actual CO_2 inventory and nominal fluid inventory correspond to the CO_2 mass sent to the storage.

6. CONCLUSIONS

In this work the numerical optimization of sCO_2 power plants for a WHR application has been performed and the best control strategies in part load operation have been identified. Assuming as heat source a flue gas stream of 50 kg/s at 550°C with a minimum stack temperature of 150°C, a preliminary sizing heat exchanger and the definition of turbomachinery main parameters has been also carried out, as well as an analysis on the system investment cost. The main outcome of the study is that sCO_2 cycles are a viable technical solution for industrial waste heat recovery applications showing nominal efficiencies higher than ORC, comparable plant specific costs and nearly stable part-load performance down to 50% of the thermal input. More detailed conclusions can be listed referring to design and part-load results.

Conclusions on cycle design optimization

- Not all the cycle configurations are appropriate for WHR applications. In particular, recompressed cycles, due to their effective internal heat recovery, show a poor utilization of the heat source and thus a lower overall plant efficiency.
- Cycle minimum pressure needs to be optimized for any operating conditions according to the assumptions on all the other cycle parameters. As a general observation, the variation of the optimal cycle minimum pressure between the different configurations is rather limited in order to allow the operation of the main compressor in the proximity of the CO_2 critical point in order to benefit from the consequent marked real gas effects.
- Sensitivity analysis demonstrates that optimal turbine inlet temperature can be significantly lower than the maximum allowable cycle temperature: in most of the cycles it is convenient to reduce this parameter in order to improve waste heat utilization, while for the TSF configuration the cycle maximum temperature is pushed to the upper bound as this does not limit the heat recovery factor.
- Adopting the minimum allowable pinch point temperature difference in the recuperators and minimizing the temperature difference at mixing processes is generally correct unless it leads to a poor exploitation of the heat source. This is the case for the recompressed RRC and the RRCB configurations which optimization collapse towards SRC and SRCB configurations respectively when those quantities are optimized.
- The three best cycle configurations are the SRC, the SRCB and TSF. Overall plant efficiency of SRCB and TSF is relatively similar (around 27.5%) but the first one can benefit from the adoption of a single turbine, a more compact heat exchangers design and eventually a lower system specific cost. The plant efficiency of the SRC configuration (22%) is significantly lower than the one of SRCB but also allow for lower Capex investment.
- At a similar plant specific cost, sCO_2 power plants can reach a higher overall conversion efficiency with respect to ORCs, as organic compounds feature a limited maximum allowable temperature due to thermal stability and decomposition issues.

Conclusions on cycle part load analysis

- Different part load strategies can be implemented depending on the equipment installed in the system and on the choice of part-load active constraints. In particular both variable and constant inventory systems are analyzed.
- Best result is obtained by optimizing at each part-load condition both the cycle minimum pressure and the cycle maximum temperature by actively controlling the cycle inventory. Imposing a limit in heat source minimum temperature (in order to avoid condensed formation or because specific needs of downstream processes) involves a very little penalization of the power output and thus is a viable option in industrial field.
- The use of an external CO_2 storage vessel and thus the possibility of varying the CO_2 inventory in the cycle components has a positive impact on part-load system performance. In particular at low flue gas mass flow rates (30% of nominal one), an increase of power output equal to 20% can be attained with respect to constant inventory strategies.
- Totally sealed cycles with constant inventory can be attractive thanks to their easiness of installation and operation but are more penalized in part-load due to the increase of cycle minimum pressure and the marked reduction of cycle pressure ratio. However, they can operate with nearly constant efficiency for industrial processes characterized by rather high minimum load (>75%)

Future works

Future steps of the present research will focus on the techno-economic optimization of different cycle configurations and fixed Capex comparison among different cycle architectures. Moreover, the analysis will be extended to different type of waste heat recovery applications, as well as on a deeper comparison with state-of-art technologies for the conversion of these sources.

NOMENCLATURE

Symbols

A	Area (m^2)
cp	Specific heat capacity (J/kgK)
d	Diameter (m)
h	Specific enthalpy (kJ/kg)
htc	Heat transfer coefficient (W/m^2K)
k	Thermal conductivity (W/mK)
$\dot{m}$	Mass flow rate (kg/s)
mln	Logarithmic mean
p	Pressure (bar)
PR	Pressure ratio
$\dot{Q}$	Thermal power (W)
s	Specific entropy (kJ/kgK)
SP	Size parameter (m)
T	Temperature (°C)
U	Overall heat transfer coefficient (W/m^2K)
V	Volumetric flow rate (m^3/s)
Vr	Volumetric ratio
u	peripheral blade speed (m/s)
$\dot{W}$	Power (W)
Z	Compressibility factor
η	Efficiency (%)
χ	Heat recovery factor (%)

Acronyms

APH	Air Preheater
BHE	Bypass Heat Exchanger
CSP	Concentrating Solar Power
GB	Gearbox
HRU	Heat Rejection Unit
HTR	High Temperature Recuperator
HTRB	High Temperature Recuperator Bypass
HX	Heat Exchanger
IGV	Inlet Guide Vanes
LTR	Low Temperature Recuperator
ORC	Organic Rankine Cycle
PCHE	Printed Circuit Heat Exchanger
PHE	Primary Heat Exchanger
REC	Recuperator
RRC	Recompressed Recuperated Cycle
RRCB	Recompressed Recuperated Cycle with HTR bypass
sCO_2	Supercritical CO_2
S&T	Shell &Tube
SR	Split Ratio
SRC	Simple Recuperated Cycle
SRCB	Simple Recuperated Cycle with Recuperator Bypass
TIT	Turbine Inlet Temperature
TOT	Turbine Outlet Temperature
TSF	Turbine Split Flow Cycle
WHR	Waste Heat Recovery

AKNOWLEDGEMENTS

The sCO2-Flex project has received funding from the European Union's Horizon 2020 research and innovation programme under grant agreement N° 764690.

REFERENCES

[1] European Parliament, "Directive 2018/2002/EU amending Directive 2012/27/EU on Energy Efficiency," *Off. J. Eur. Union*, vol. 328, no. November, pp. 210–230, 2018.

[2] C. Forman, I. K. Muritala, R. Pardemann, and B. Meyer, "Estimating the global waste heat potential," *Renew. Sustain. Energy Rev.*, vol. 57, pp. 1568–1579, 2016.

[3] M. Papapetrou, G. Kosmadakis, A. Cipollina, U. La Commare, and G. Micale, "Industrial waste heat: Estimation of the technically available resource in the EU per industrial sector, temperature level and country," *Appl. Therm. Eng.*, vol. 138, no. July 2017, pp. 207–216, 2018.

[4] G. P. Hammond and J. B. Norman, "Heat recovery opportunities in UK industry," *Appl. Energy*, vol. 116, pp. 387–397, 2014.

[5] G. Bianchi *et al.*, "Estimating the waste heat recovery in the European Union Industry," *Energy, Ecol. Environ.*, vol. 4, no. 5, pp. 211–221, 2019.

[6] D. Vance *et al.*, "Estimation of and barriers to waste heat recovery from harsh environments in industrial processes," *J. Clean. Prod.*, vol. 222, pp. 539–549, 2019.

[7] E. Macchi and M. Astolfi, *Organic Rankine Cycle (ORC) Power Systems*. Elsevier Science, 2016.

[8] T. Tartière and M. Astolfi, "A World Overview of the Organic Rankine Cycle Market," *Energy Procedia*, vol. 129, pp. 2–9, 2017.

[9] C. M. Invernizzi and D. Bonalumi, "Thermal stability of organic fluids for Organic Rankine Cycle systems," in *Organic Rankine Cycle (ORC) Power Systems: Technologies and Applications*, 2017.

[10] G. Angelino, "Carbon Dioxide Condensation Cycles For Power Production," *J. Eng. Power*, vol. 90, no. 3, pp. 287–295, Jul. 1968.

[11] E. G. Feher, "The supercritical thermodynamic power cycle," *Energy Convers.*, vol. 8, no. 2, pp. 85–90, 1968.

[12] V. Dostal, "A supercritical carbon dioxide cycle for next generation nuclear reactors," Massachusetts Institute of Technology, 2004.

[13] T. Neises and C. Turchi, "A comparison of supercritical carbon dioxide power cycle configurations with

an emphasis on CSP applications," *Energy Procedia*, vol. 49, pp. 1187–1196, 2014.
[14] T. Neises and C. Turchi, "Supercritical carbon dioxide power cycle design and configuration optimization to minimize levelized cost of energy of molten salt power towers operating at 650 °C," *Sol. Energy*, vol. 181, no. November 2018, pp. 27–36, 2019.
[15] M. D. Carlson, B. M. Middleton, and C. K. Ho, "Techno-Economic Comparison of Solar-Driven SCO2 Brayton Cycles Using Component Cost Models Baselined With Vendor Data and Estimates," in *ASME 2017 11th International Conference on Energy Sustainability*, 2017, pp. 1–5.
[16] S. P. Kao, "Application of supercritical CO2 Brayton cycle for small modular light water reactors," *Int. Congr. Adv. Nucl. Power Plants, ICAPP 2016*, vol. 3, no. September, pp. 1647–1656, 2016.
[17] J. Floyd *et al.*, "A numerical investigation of the sCO2 recompression cycle off-design behaviour, coupled to a sodium cooled fast reactor, for seasonal variation in the heat sink temperature," *Nucl. Eng. Des.*, vol. 260, no. March, pp. 78–92, 2013.
[18] M. Mecheri and Y. Le Moullec, "Supercritical CO2 Brayton cycles for coal-fired power plants," *Energy*, vol. 103, pp. 758–771, 2016.
[19] D. Alfani, M. Astolfi, M. Binotti, S. Campanari, F. Casella, and P. Silva, "Multi Objective Optimization of Flexible Supercritical CO2 Coal-Fired Power Plants," in *Volume 3: Coal, Biomass, Hydrogen, and Alternative Fuels; Cycle Innovations; Electric Power; Industrial and Cogeneration; Organic Rankine Cycle Power Systems*, 2019, vol. 3, pp. 1–11.
[20] R. Allam *et al.*, "Demonstration of the Allam Cycle: An Update on the Development Status of a High Efficiency Supercritical Carbon Dioxide Power Process Employing Full Carbon Capture," *Energy Procedia*, vol. 114, no. November 2016, pp. 5948–5966, 2017.
[21] R. Scaccabarozzi, M. Gatti, and E. Martelli, "Thermodynamic Optimization and Part-load Analysis of the NET Power Cycle," *Energy Procedia*, vol. 114, no. November 2016, pp. 551–560, 2017.
[22] P. Huck, S. Freund, M. Lehar, and P. Maxwell, "Performance comparison of supercritical CO2 versus steam bottoming cycles for gas turbine combined cycle applications," *5th Int. Symp. - Supercrit. CO2 Power Cycles*, pp. 1–14, 2016.
[23] V. T. Cheang, R. A. Hedderwick, and C. McGregor, "Benchmarking supercritical carbon dioxide cycles against steam Rankine cycles for Concentrated Solar Power," *Sol. Energy*, vol. 113, pp. 199–211, 2015.
[24] J. D. Miller *et al.*, "Comparison of Supercritical CO2 Power Cycles to Steam Rankine Cycles in Coal-Fired Applications," in *Volume 9: Oil and Gas Applications; Supercritical CO2 Power Cycles; Wind Energy*, 2017, pp. 1–12.
[25] J. Marion, M. Kutin, A. McClung, J. Mortzheim, and R. Ames, "The STEP 10 MWe SCO2 pilot plant demonstration," in *Proceedings of the ASME Turbo Expo*, 2019.
[26] J. Gary, C. Turchi, and N. Siegel, "CSP and the DOE SunShot Initiative," *System*, 2011.
[27] M. Mehos *et al.*, "Concentrating Solar Power Gen3 Demonstration Roadmap," *Nrel/Tp-5500-67464*, 2017.
[28] "SOLARSCO2OL: Unlocking the potential of integrating sCO2 in all kinds of CSP plants. Available online at: https://www.rina.org/en/media/casestudies/solarsco2ol." .
[29] "sCO2-Flex: Supporting the electricity system By making fossil fuel based electricity production more flexible. Available online at: http://www.sco2-flex.eu." .
[30] K. Brun, P. Friedman, and R. Dennis, *Fundamentals and Applications of Supercritical Carbon Dioxide (SCO2) Based Power Cycles*. 2017.
[31] M. Astolfi, D. Alfani, S. Lasala, and E. Macchi, "Comparison between ORC and CO2 power systems for the exploitation of low-medium temperature heat sources," *Energy*, vol. 161, pp. 1250–1261, Oct. 2018.
[32] "Echogen Power Systems: Waste Heat Recovery Power Generation. Available online at: https://www.echogen.com/." .
[33] T. J. Held, "Supercritical CO2 cycles for gas turbine combined cycle power plants," in *Power Gen International*, 2015.
[34] U.S. Department of Energy, "Waste Heat Recovery: Technology Opportunities in the US Industry," 2008.
[35] B. Egilegor *et al.*, "ETEKINA: Analysis of the potential for waste heat recovery in three sectors: Aluminium low pressure die casting, steel sector and ceramic tiles manufacturing sector," *Int. J. Thermofluids*, vol. 1–2, p. 100002, 2020.
[36] M. Persichilli, A. Kacludis, E. Zdankiewicz, and T. Held, "Supercritical CO2 Power Cycle Developments and Commercialization: Why sCO2 can Displace Steam Ste am," *Power-Gen India Cent. Asia*, pp. 1–15, 2012.
[37] A. Kacludis, S. Lyons, D. Nadav, and E. Zdankiewicz, "Waste Heat to Power (WH2P) Applications Using a Supercritical CO 2 -Based Power Cycle," *Power-Gen Int.*, vol. 2, no. December, pp. 1–10, 2012.

[38] M. Mohagheghi and J. Kapat, "Thermodynamic Optimization of Recuperated S-Co2 Brayton Cycles for Waste Heat Recovery Applications," *4th Int. Symp. - Supercrit. CO2 Power Cycles*, vol. 53, no. 9, pp. 1689–1699, 2013.
[39] G. S. Martínez, D. Sánchez, F. Crespi, and G. Gavagnin, "A global approach to assessing the potential of combined cycles using supercritical technology," *1st Glob. Power Propuls. Forum*, pp. 1–8, 2017.
[40] L. Moroz, P. Pagur, O. Rudenko, M. Burlaka, and C. Joly, "Evaluation for Scalability of a Combined Cycle Using Gas and Bottoming SCO2 Turbines," pp. 1–10, 2015.
[41] G. Kimzey, "Development of a Brayton bottoming cycle using supercritical carbon dioxide as the working fluid," *Electr. Power Res. Institute, Univ. Turbine Syst. Res. Program, Gas Turbine Ind. Fellowship, Palo Alto, CA*, 2012.
[42] S. A. Wright, C. S. Davidson, and W. O. Scammell, "Thermo-Economic Analysis of Four sCO2 Waste Heat Recovery Power Systems," *5th Int. Symp. - Supercrit. CO2 Power Cycles*, pp. 1–16, 2016.
[43] M. Marchionni, G. Bianchi, and S. A. Tassou, "Techno-economic assessment of Joule-Brayton cycle architectures for heat to power conversion from high-grade heat sources using CO2 in the supercritical state," *Energy*, vol. 148, pp. 1140–1152, 2018.
[44] M. Marchionni, G. Bianchi, S. S. Saravi, and S. A. Tassou, "Modelling and performance analysis of a supercritical CO2 system for high temperature industrial heat to power conversion at off-design conditions," in *Proceedings of the 3rd European supercritical CO2 Conference*, 2019, pp. 1–10.
[45] "I-ThERM: Industrial Thermal Energy Recovery Conversion and Management. Available online at: http://www.itherm-project.eu/." .
[46] G. Manente and M. Costa, "On the conceptual design of novel supercritical CO2 power cycles for waste heat recovery," *ECOS 2019 - Proc. 32nd Int. Conf. Effic. Cost, Optim. Simul. Environ. Impact Energy Syst.*, pp. 2219–2231, 2019.
[47] The MathWorks Inc., "MATLAB version R2019b." 2019.
[48] E. W. Lemmon, M. L. Huber, and M. O. McLinden, "NIST Standard Reference Database 23: Reference Fluid Thermodynamic and Transport Properties (REFPROP), Version 9.0," *Phys. Chem. Prop. ...*, 2010.
[49] R. Span and W. Wagner, "A new equation of state for carbon dioxide covering the fluid region from the triple-point temperature to 1100 K at pressures up to 800 MPa," *J. Phys. Chem. Ref. Data*, 1996.
[50] F. Crespi, G. Gavagnin, D. Sánchez, and G. S. Martínez, "Supercritical carbon dioxide cycles for power generation: A review," *Appl. Energy*, vol. 195, pp. 152–183, 2017.
[51] D. Alfani, M. Astolfi, M. Binotti, P. Silva, and E. Macchi, "Off-design Performance of CSP Plant Based on Supercritical CO2 Cycles," in *AIP Conference Proceedings*, 2020, vol. 2303, no. i.
[52] M. Binotti, M. Astolfi, S. Campanari, G. Manzolini, and P. Silva, "Preliminary assessment of sCO2 cycles for power generation in CSP solar tower plants," *Appl. Energy*, vol. 204, pp. 1007–1017, 2017.
[53] C. S. Turchi, Z. Ma, T. W. Neises, and M. J. Wagner, "Thermodynamic study of advanced supercritical carbon dioxide power cycles for concentrating solar power systems," *J. Sol. Energy Eng. Trans. ASME*, vol. 135, no. 4, pp. 1–7, 2013.
[54] D. Alfani, M. Astolfi, M. Binotti, and P. Silva, "Part Load Strategy Definition and Annual Simulation for Small Size sCO2 Based Pulverized Coal Power Plant," in *Proceedings of ASME Turbo Expo 2020 Turbomachinery Technical Conference and Exposition GT2020 June 22-26, 2020, London, England*, 2020, pp. 1–10.
[55] Y. Ahn *et al.*, "Cycle layout studies of S-CO 2 cycle for the next generation nuclear system application," *Trans. Korean Nucl. Soc. Autumn Meet. Pyeongchang*, pp. 2–5, 2014.
[56] T. Koji, "Kawasaki L20A Gas Turbine," 2004.
[57] D. Alfani, M. Astolfi, M. Binotti, and P. Silva, "Effect of the ambient temperature on the performance of small size sCO2 based pulverized coal power plants," in *The 4th European sCO2 Conference for Energy Systems March 23-24, 2021, Online Conference*, 2021, pp. 1–10.
[58] J. S. Noall and J. J. Pasch, "Achievable Efficiency and Stability of Supercritical CO2 Compression Systems," *Supercrit. CO 2 Power Cycle Symp.*, 2014.
[59] C. K. Ho, M. Carlson, P. Garg, and P. Kumar, "Technoeconomic Analysis of Alternative Solarized s-CO2 Brayton Cycle Configurations," *J. Sol. Energy Eng. Trans. ASME*, vol. 138, no. 5, 2016.
[60] A. Romei, P. Gaetani, A. Giostri, and G. Persico, "The Role of Turbomachinery Performance in the Optimization of Supercritical Carbon Dioxide Power Systems," *J. Turbomach.*, 2020.
[61] C. Audet and J. E. Dennis, "Analysis of generalized pattern searches," *SIAM J. Optim.*, 2003.
[62] V. Dostal, P. Hejzlar, and M. J. Driscoll, "The supercritical carbon dioxide power cycle: Comparison to other advanced power cycles," *Nucl. Technol.*, vol. 154, no. 3, pp. 283–301, 2006.
[63] ASME, "An International Code - ASME Boiler and Pressure Vessel Code," *Am. Soc. Mechnical Eng.*, 2015.
[64] American Petroleum Institute, "Recommended Practice for Design and Installation of Offshore Production Platform Piping Systems," *Am. Pet. Inst. Recomm. Pract. 14E*, 1991.

[65] N. T. Weiland, B. W. Lance, and S. R. Pidaparti, “SCO2 power cycle component cost correlations from DOE data spanning multiple scales and applications,” *Proc. ASME Turbo Expo*, vol. 9, pp. 1–17, 2019.
[66] M. D. Carlson, B. M. Middleton, and C. K. Ho, “Techno-economic Comparison of Solar-Driven sCO2 Brayton Cycles Using Component Cost Models Baselined With Vendor Data,” *Proc. ASME 2017 Power Energy Conf.*, pp. 1–7, 2017.
[67] S. Lemmens, “A perspective on costs and cost estimation techniques for organic Rankine cycle systems,” *Proc. 3rd Int. Semin. ORC Power Syst.*, no. 2010, pp. 1–10, 2015.
[68] G. Persico, P. Gaetani, A. Romei, L. Toni, E. F. Bellobuono, and R. Valente, “Implications of Phase Change On the Aerodynamics of Centrifugal Compressors for Supercritical Carbon Dioxide Applications,” *J. Eng. Gas Turbines Power*, 2021.
[69] D. Alfani, M. Astolfi, M. Binotti, E. Macchi, and P. Silva, “Optimization of the Part-load Operation Strategy of sCO2 Power Plants,” in *5th International Seminar on ORC Power Systems*, 2019, no. i, pp. 1–10.
[70] J. M. Muñoz De Escalona, D. Sánchez, R. Chacartegui, and T. Sánchez, “Part-load analysis of gas turbine & ORC combined cycles,” *Appl. Therm. Eng.*, vol. 36, no. 1, pp. 63–72, 2012.
[71] M. P. Boyce, *Gas Turbine Engineering Handbook*. 2006.
[72] F. Crespi, D. Sánchez, K. Hoopes, B. Choi, and N. Kuek, “The conductance ratio method for off-design heat exchanger modeling and its impact on an SCO2 recompression cycle,” *Proc. ASME Turbo Expo*, vol. 9, pp. 1–11, 2017.
[73] A. M. Bigi *et al.*, “sCO2-Flex D3.13 – First turbomachinery models and report,” 2020.
[74] F. Casella, G. Mangola, and D. Alfani, “Density-Based Control of Air Coolers in Supercritical CO 2 Power Cycles,” in *21st IFAC World Congress, Germany, July 12-17, 2020*, 2020.

HIGHLIGHTS

- We optimized five sCO_2 cycle configurations for waste heat recovery application
- Optimal plants reach efficiency higher than ORC (>27%) with similar specific cost (2000$/kW)
- Simple recuperative cycle with bypass (SRBC) is selected as the optimal configuration
- We studied the different part-load strategies for this optimal configuration (SRBC)
- Variable inventory part load strategy is more efficient than constant inventory strategy

Declaration of interests

☒ The authors declare that they have no known competing financial interests or personal relationships that could have appeared to influence the work reported in this paper.

☐The authors declare the following financial interests/personal relationships which may be considered as potential competing interests:

sCO_2 POWER PLANTS FOR WASTE HEAT RECOVERY: DESIGN OPTIMIZATION AND PART-LOAD OPERATION STRATEGIES

Dario Alfani[1], Marco Binotti[1], Ennio Macchi[1], Paolo Silva[1], Marco Astolfi[1]*

[1]Politecnico di Milano, Energy Department,
Milano, Italy
*marco.astolfi@polimi.it

ABSTRACT

This paper focuses on the potential of supercritical carbon dioxide closed cycle for waste heat recovery applications. The valorization of waste heat released from glass, steel and cement production facilities is recognized as one of the most effective solutions for the reduction of carbon footprint of the industrial sector. Common solutions rely on steam Rankine cycles and organic Rankine cycles while only few sCO_2 power plants have been manufactured and operated so far as this technology has not yet reached the technical and commercial maturity. In spite of the large interest on sCO_2 power plant from industry, institutions and academia, the role of this solution in future waste heat recovery applications is still unclear, highlighting the need of research studies focused on the performance assessment of these novel systems in both design and off-design conditions.

This paper aims at bridging the gap between preliminary numerical studies and the design of real power systems by focusing on different aspects scarcely investigated in literature. The first section of this study deals with cycle design and provides a full description of the numerical complexity related to sCO_2 power plant optimization, with a detailed description of the assumptions and the models implemented for the design of cycle components. Five different cycle configurations for the exploitation of a heat source consisting of a 50 kg/s stream of flue gas at 550°C have been analyzed and optimized: results are presented with a set of sensitivity analyses and the most promising configurations are analyzed from both a thermodynamic and a techno-economic perspective. Simple recuperative cycle, simple recuperative cycle with recuperator bypass and turbine split flow configurations are compared in detail proving that sCO_2 technology can reach overall efficiencies up to 27.5%, a value higher than ORC for the same power output (around 6 MW_{el}), and with a similar specific cost (2000 $/kW). Simple recuperated cycle with recuperator bypass is selected as the most promising configuration and it is further studied in off design conditions in the second section of the paper. Five different part-load strategies have been implemented allowing to assess the part-load performance of the selected cycle, considering both variable CO_2 inventory and constant CO_2 inventory systems. Results highlight that sCO_2 recuperative cycles equipped with a CO_2 storage vessel present a very high and almost constant efficiency down to 50% of the normalized flue gases mass flow rate, while a lower efficiency is expected for constant inventory systems. Both solutions can be operated down to 30% load with no difficulties on system components and with a minimum plant efficiency still competitive against ORC technology.

KEYWORDS:

- Waste heat recovery
- Energy harvesting
- Supercritical carbon dioxide
- Part-load operation
- System optimization
- Techno-economic analysis

HIGHLIGHTS

- We optimized five sCO_2 cycle configurations for waste heat recovery application
- Optimal plants reach efficiency higher than ORC (>27%) with similar specific cost (2000$/kW)
- Simple recuperative cycle with bypass (SRBC) is selected as the optimal configuration
- We studied the different part-load strategies for this optimal configuration (SRBC)
- Variable inventory part load strategy is more efficient than constant inventory strategy

1. INTRODUCTION

In the imminent future, the global electricity production is expected to undergo drastic changes to meet the rising environmental concerns and to tackle the challenges of global warming and the growing electricity demand. Academia and industry are currently researching novel sustainable solutions to reach these targets and, apart from increasing the renewable energy penetration in the electricity generation mix, a crucial solution is represented by the energy efficiency improvement of the already existing facilities in the industrial and power generation sectors. In December 2018, the European Union (EU) reviewed upwards the target for the energy efficiency for 2030, passing from 27% to 32.5%, with a clause for a possible upwards revision by 2023 [1]. One of the most promising approaches to increase the industrial energy efficiency and to lower its greenhouse gases (GHG) emissions is represented by the recovery of the heat unexploited and lost after combustion or in heat transfer processes.

Several studies evaluated the quantity and quality of waste heat potential for the EU and US industrial sector, highlighting the vast potential of industrial waste heat recovery at high temperature.

Forman et al. [2] estimated the global waste heat recovery (WHR) potential of the electricity generation sector and of the main end-use sectors (transportation, industrial, commercial and residential) to be as high as 68.3 PWh_{th}/year. Using an approach based on the calculation of the Carnot potential, the authors highlighted that even if the largest part of the waste heat potential (63%) is at low temperature (<100°C), when passing to Carnot potential the main share (54.5%) is represented by high temperature (>300°C) sources.

Papapetrou et al. [3] focused on the industrial sector WHR technical potential in the EU: their analysis is based on waste heat fractions derived from a detailed study of the UK industry in the 2000-2003 period [4] updated for the year 2015 for each EU country and industrial sector, resulting in a new set of fractions sorted by temperature level. The analysis found out that the waste heat potential from exhaust streams at temperatures higher than 500°C amounts to 124 TWh_{th}/year (40.8% of the total) and it is mainly represented by the iron and steel (I&S) and non-metallic minerals (NMM) industries.

Bianchi et al. [5] highlighted how the EU industrial sector accounts for 26% of the total final energy consumption but nearly half of this energy (about 1534 TWh_{th}) is dissipated to the environment. More precisely, the authors estimated the energy wasted through exhausts/effluents to be 29% of the total industrial consumption, leading to an availability of 920 TWh_{th} from the EU industrial sector which correspond to a 279 TWh_{el} of Carnot potential. This figure demonstrates the large potential of WHR although, in the authors' opinion, the adopted methodology, based on the computation of the Carnot potential, is not conservative and may result in a non-negligible overestimation (+30%) of the actual electricity yield.

Vance et al. [6] investigated the potential and barriers for waste heat recovery at temperatures higher than 650 °C in five different industries (steel, aluminum, glass, cement, and lime). The authors estimated a potential for WHR from high temperature streams in the US to be equal to 113.6 TWh_{th}/year. The work also mentioned that the heat recovery process from these industries could be problematic due to the presence of several reactive constituents in the exhaust streams.

In the last decades, the most common technologies adopted for the conversion of waste heat into electricity have been the Steam (SRC) and Organic Rankine Cycles (ORC). These two technologies adopt the same thermodynamic cycle, i.e. the Rankine cycle, but are used in different size and temperature application ranges. In the WHR sector, subcritical superheated steam cycles without feedwater preheating represent a common option for applications characterized by medium-to-large size (from tens of MWs to hundreds of MWs) and high temperature levels (from 400°C to 700°C) thanks to the higher attainable efficiency and the use of standardized components which leads to a lower plant investment cost. On the other hand, steam Rankine cycles feature a low conversion efficiency when exploiting small available thermal powers (from few hundreds of kW up to tens of MW) or low-to-medium heat source temperatures (from 100°C to 400°C). In fact, the exploitation of such low temperature heat sources by means of steam cycles would lead to a strong cycle thermodynamic efficiency penalization due to the very low evaporation temperatures coupled with large superheating to guarantee a sufficiently high steam quality at turbine discharge. Furthermore, the exploitation of small available thermal powers would involve the miniaturization of the turbine blades, with penalization of the turbine adiabatic efficiency and higher specific cost [7].

ORC technology is generally based on the adoption of organic compounds (hydrocarbons, halogenated hydrocarbons, siloxanes) as working fluid and it currently represents the most common and reliable solution available on the market for the exploitation of low-to-medium temperature (from 100°C to 400°C) heat sources in a large range of power outputs (from few kW to tens of MW) [7]. The main advantages related to the adoption of an organic working fluid are associated to the reduction of the evaporation pressure and to the increase of the condensation one. These two aspects lead to a limited number of turbine stages and thus to a reduced turbine specific cost. Furthermore, the adoption of complex fluids with a completely overhanging saturation line always guarantee a dry expansion for saturated vapor conditions at turbine inlet. This feature solves the issues related to blade erosion, typical when using steam as working fluid, and makes possible a simple plant layout based on a subcritical saturated cycle. In fact, ORCs generally adopt less complex plant layouts than steam Rankine cycles,

typically with a single pressure level [7] and result in even higher efficiencies with respect to steam cycles when applied to low-to-medium temperature heat sources.

In the last decades, the ORC technology has penetrated the WHR market with more than 1700 installed plants corresponding to about 2.8 GW_{el} [8]. However, organic fluids cannot fully exploit the potential of heat source with temperatures higher than 400°C due to their low thermal stability limits [9].

Another technological solution that could be able to bridge the gap in industrial WHR applications and compete both with steam cycles and ORCs is the supercritical CO_2 (sCO_2) closed Brayton cycle. The sCO_2 power cycle has been originally proposed by Angelino [10] and Feher [11] and in recent years it has gained a large interest from both the industry and the academia, mainly after the publication of the Dostal doctoral thesis [12]. Supercritical CO_2 cycles have been mainly studied for concentrating solar power (mostly in the US by NREL [13][14] and SANDIA NL [15]), nuclear energy (for 4th generation nuclear plants, as small modular reactors [16] or sodium cooled reactors [17]) and fossil fuels fired applications as coal-fired power plants [18][19], natural gas oxy-fuel combustion [20][21] or bottoming cycles for gas turbines [22]. In these fields, sCO_2 power systems can compete against conventional steam Rankine cycles thanks to their more compact turbomachines, simpler plant arrangement, smaller footprint and investment cost, higher efficiency and flexibility [23][24].

The great interest in the adoption of sCO_2 power cycles in different power generation applications is also demonstrated by the large number of US and EU funded projects. An example is the STEP 10MW_{el} project [25], an US DOE funded project which aims to bring the technology readiness level (TRL) of natural gas indirectly fired sCO_2 power cycles from "proof of concept" (TRL3) to "system prototype" (TRL7). Supercritical carbon dioxide power cycles have been also investigated within the US DOE SunShot [26] and Gen3 [27] programs as the most promising technology for the power block of 3rd generation high-temperature CSP plants based on central receiver technology. Within the funding scheme of the EU H2020 research and innovation program, different projects have been financed, like the SOLARSCO2OL [28], which aims to build the first MW-scale sCO_2 power block operating in an actual CSP plant located in the European Union; or the sCO2-Flex project [29], which investigates the application of sCO_2 power cycles in order to enhance coal-fired power plants flexibility and ease the integration of non-dispatchable renewable energy sources in the electrical grid.

Apart from the aforementioned high-temperature applications, the sCO_2 power cycle is also considered as an alternative to ORCs for the exploitation of medium-temperature heat sources (from 250°C to 400°C) as CO_2 is an environmental friendly, widely available, safe and thermally stable working fluid [30][31].

In the US this technological solution has already been proposed to the market by Echogen [32], which manufactures and commercializes sCO_2-based WHR systems also in combined heat and power solutions (CHP). Echogen technology was initially based on a simple recuperated power cycle but now adopts a more complex design, called Dual Rail configuration, which is similar to the turbine split flow cycle and allows to obtain a higher power output and a better exploitation of exhaust gases sensible heat [33].

Table 1 reports the most interesting opportunities for waste heat recovery with sCO_2 power systems divided by sectors and processes.

Table 1. Industrial and power generation sector WHR opportunities and their respective temperature levels, rearranged from [2][30][34][35].

Industry	Process	Temperature	Comments	Competitor
Glass manufacturing	Melting furnace	1100-1300 °C	Very high particulate load which results in high fouling factors on heat transfer surfaces	SRC
	Oxyfuel melting furnace	1200-1400 °C		SRC
Iron and steel manufacturing	Electric arc furnace	1000-1300 °C	Dirty exhausts. Intermittency of the process. Temperature too low for good efficiency if recovery is already present.	SRC
	Electric arc furnace with recovery	200-300°C		ORC
	Blast and cupola furnace	450 °C		ORC
Aluminum manufacturing	Secondary melting	1000-1200 °C	Difficult to recover heat from the cell. Discontinuity of the process.	SRC
	Hall-Héroult cell	700 °C		SRC
Cement manufacturing	Wet kiln	300-350 °C	Generally, a good level of heat integration and recovery is already present.	ORC
	Dry kiln (no preheater or precalciner)	400-450 °C		ORC
	Dry kiln (recovered)	300-350 °C		ORC
Gas turbines	Exhausts	370-600 °C	Variable load	SRC, ORC
Reciprocating engines	Exhausts	230-600 °C	Variable load	ORC

Since 2012, several works have been published confirming the feasibility and convenience of the Echogen solution. Persichilli et al. [36] compared the levelized cost of electricity (LCOE) of several steam and sCO_2-based heat recovery system configurations exploiting the exhausts of a 22 MW_{el} LM2500 stationary gas turbine (GT).

The analysis showed how the sCO_2 technology may be able to reduce by up to 20% the LCOE with respect to steam-based solutions thanks to the higher attainable power output, the lower investment and operation and maintenance (O&M) costs. Kacludis et al. [37] resumed the analysis and investigated the adoption of sCO_2 power cycles for other two different WHR applications, namely the exhaust exploitation released by reciprocating engine gensets for remote power generation and a waste heat to power solution for a steel manufacturing facility. Regarding the first application, the authors showed that through the installation of two 300 kW_{el} sCO_2-based power systems it would be possible to increase by 10% the gensets power output without any additional fuel consumption. The second analysis focused on the possibility to recover waste heat from the exhaust gases of a steel mill which are usually discharged to the atmosphere at a temperature around 540°C, after the preheating of the furnace combustion air. Results showed that the adoption of a sCO_2 heat engine could cut down the effective furnace operating cost from 8.6 $/ton to 6.8 $/ton of steel manufactured thanks to the generation of 3.7 MW_{el}.

The simple recuperated sCO_2 power cycle adopted by the Echogen technology has been also supported by several studies thanks to its better exploitation of a heat source at variable temperature and its relatively low layout complexity.

Mohagheghi and Kapat [38] provided a comparison between the simple recuperated cycle and the recompression recuperated cycle exploiting a 100 kg/s mass flow rate of the exhaust gas considering a waste gas inlet temperature range between 225°C and 825°C. The authors showed that, even at high exhausts inlet temperatures, the more complex recompressed configuration does not outperform significantly the simpler recuperated cycle and that for low exhausts inlet temperature (lower than 425°C) the recompression does not provide any benefit due to poor heat source utilization.

Martinez et al. [39] assessed the potential of sCO_2 bottoming cycles coupled to a gas turbine releasing flue gases to the environment at a temperature of 600°C, expanding the configurations studied to the recuperated pre-compression cycle. The results of the analysis highlighted that, if the GT pressure ratio is not optimized, the simple recuperated cycle is able to reach a greater power output with respect to the recompression (+4%) and precompression cycle (+20%). On the other hand, the optimization of the GT pressure ratio leads to a shift in these trends resulting in a power output of the recompression cycle 20% greater than the one of the recuperated cycle and almost 34% higher than the fixed pressure ratio solution.

Moroz et al. [40] proposed a similar analysis considering a wide set of industrial gas turbine with power outputs up to 120 MW_{el}, flue gas mass flow rates between 100 and 700 kg/s and outlet temperatures ranging from 425 to 700°C. The analysis showed that the power output of the recuperated cycle is about 10% higher than outputs of recompression and pre-compression cycles for an exhaust stream of 100 kg/s at a temperature of 550°C. The analysis also highlights the presence of an optimal sCO_2 turbine inlet temperature, generally lower than the maximum allowable temperature, resulting from the tradeoff between heat source utilization and cycle thermodynamic efficiency.

Kimzey [41] has been the first to propose novel sCO_2 cycle architectures specifically developed for WHR applications by investigating the potential of a configuration with a single flow split and a dual expansion, which the author called Cascade I cycle. The author stated that this configuration is able to outperform the power output of a traditional two-pressure level steam Rankine cycle by 3%. On the other hand, its performances are still inferior to commonly employed triple pressure with reheat steam cycle when exploiting the flue gases discharged by a heavy-duty gas turbine. The cycle thermodynamic efficiency is in fact limited due to the large temperature differences in the low temperature recuperator (LTR), caused by the different heat capacities of the hot and cold streams.

Other two interesting and innovative cycle configurations for WHR applications are the recuperated cycle with recuperator bypass (also called preheating cycle) and the turbine split flow configuration (also called dual recuperated cycle), which have been studied by Wright et al. [42]. The authors proposed a preliminary techno-economic analysis comparing four different cycle configurations exploiting a 40.7 MW_{th} GT exhaust stream at 549°C. For each cycle configuration the turbine inlet temperature, the split fraction and all the heat exchangers approach temperatures have been optimized in order to maximize the net annual revenue. On the other hand, the compressor inlet and outlet pressure and the minimum cycle temperature have been considered as constant values in order to simplify the analysis. The analysis showed that, even if the innovative cycle configurations are able to produce up to 22.6% more power output than the benchmark simple recuperated cycle, the increased capital costs of these architectures (+41.7% for the recuperated cycle with recuperator bypass, +30.5% for the turbine split flow configuration) make them less favorable from an economic point of view.

The turbine split flow (called by the authors cascade recuperative) configuration has also been investigated by Astolfi et al. [31] for the recovery of 30 MW_{th} in a wide range of temperatures (from 200°C and 600°C) and cooling grades (from 0% to 100%). The analysis showed that a single optimal sCO_2 cycle configuration cannot be selected as this is highly dependent on the temperature and cooling grade of the heat source. The authors compared also the performance of sCO_2 cycles with the ORCs ones and highlighted that even if ORCs are the most efficient solution for heat source temperatures below 350°C, sCO_2 power systems represent a promising solution for higher temperatures.

Huck et al. [22] proposed an even more complex cycle configuration, the dual flow split with a dual expansion layout (also called Cascade III by Kimzey [41]). The configuration is similar to the Cascade I cycle but with the addition of an intercooling and the division of the primary heat exchanger in two separate components, between which the two CO_2 streams are mixed. The authors compared the performance attainable by this novel configuration against a three-pressure level steam Rankine bottoming cycle with reheat, showing that this innovative architecture can provide more electrical power. On the other hand, the analysis appears biased by the optimistic assumptions on the sCO_2 power cycle with maximum pressures of 400 bar, turbine inlet temperatures of 700°C and isentropic efficiencies for CO_2 turbomachinery equal to 95%.

Marchionni et al. [43] published a techno-economic analysis comparing four more conventional sCO_2 cycle configurations and four cycle architectures specifically developed for WHR applications. The second group included an innovative layout proposed by the authors, which consists in a recuperated cycle with recuperator bypass with the addition of a pre-compressor. The study investigates the exploitation of an exhausts stream at 650°C and highlights the potential of the innovative sCO_2 cycle configurations over the more conventional ones. However, the choice of the authors to fix the exhaust stack temperature to 350°C for the conventional configurations and to 150°C for the novel configurations could have led to an inaccurate comparison.

The same authors [44] investigated the off-design behavior and performances of a 50 KW_{el} simple recuperated cycle recovering heat from 1 kg/s stream of flue gases at 650°C. The analysis assessed the effect of both hot and cold sources inlet conditions by varying their mass flow rates and temperatures. The implementation of turbomachinery performance maps obtained through CFD simulations highlighted the impossibility to generate power when the heat source mass flow rate is lower than 0.9 kg/s and its temperature drops under 550°C.

Both these studies were performed in the context of the H2020 I-ThERM project [45] which aims at the development and demonstration of a packaged plug and play power system for high-temperature waste heat to power conversion based on a sCO_2 Brayton cycle.

Recently, Manente and Costa [46] discussed the optimization of several novel sCO_2 power cycle configurations for WHR applications analyzing the recuperated cycle with recuperator bypass, the turbine split flow and the Cascade I or dual expansion cycle. The authors showed that all these more complex configurations are obtained by the combination of two simpler sCO_2 Brayton cycles overlapped in the low temperature section and separated in the high temperature one. The authors optimized all the configurations by varying the turbine inlet temperature and the split fraction, retaining constant pressures and neglecting all the heat exchangers pressure drops. The analysis showed that the dual expansion cycle obtained the highest recovery efficiency with a value of 22.3% when employed to recover heat from exhausts at 600°C.

These aforementioned studies highlight the potential of sCO_2 power cycles for WHR applications and justify the academic and industrial interest in the development of this technology. However, the currently available scientific literature lacks in research studies dealing with both the cycle optimization and the evaluation of part load performance. The present work aims to investigate this topic of high relevance for WHR applications providing results that can be useful to guide studies on system dynamics or control for future sCO_2 power systems. First, a fair comparison of five cycle configurations in design conditions is presented, also including techno-economic and layout complexity considerations. Optimization of each cycle configuration has been implemented considering all the free design parameters instead of fixing some of them, in order to avoid suboptimal solutions and improve the accuracy and reliability of the results. Three cycles configurations are selected and discussed in detail and techno-economic analysis highlights that considering heat exchangers mass and cost is crucial when comparing different cycle architectures. Recuperative cycle with recuperator bypass has been selected as the most promising cycle configuration for this application and it has been eventually studied in part load conditions proposing and comparing different possible control strategy options based on both constant and variable inventory solutions.

2. CYCLE DESIGN AND OPTIMIZATION

This section focuses on the description of investigated cycle configurations, the set of assumptions adopted and the optimization procedure.

2.1 Investigated cycle architectures

In order to tackle the goal of this paper a dedicated numerical tool has been developed in MATLAB [47] for the optimization of the system design and the evaluation of part-load performance of sCO_2 power cycles. Carbon dioxide thermodynamic properties are computed through the REFPROP 9.1 database [48] using a high fidelity 42 terms reduced Helmholtz energy equation of state [49] allowing for an accurate evaluation of real gas effects close to the critical point of the working fluid. The developed numerical code is able to model several cycle configurations (more than 50 cycle schemes are proposed in literature [50]) that can be easily optimized and then simulated over a large range of off-design conditions.

In this work, five cycle configurations are investigated and optimized, identifying the most promising solutions for the exploitation of a variable temperature heat source, typical of WHR applications. Figure 1 depicts the five investigated cycle configurations: (i) the simple recuperated cycle (SRC), (ii) the recompressed recuperative cycle (RRC), (iii) the simple recuperated cycle with recuperator bypass (SRCB), (iv) the recompressed recuperative cycle with high temperature recuperator bypass (RRCB) and (v) the turbine split flow cycle (TSF).

The first configuration investigated is the simple recuperated cycle (SRC) (Figure 1.a) in which a single recuperative heat exchanger uses the heat available at the exit of the expander (point 5) to increase the temperature of high pressure CO_2 at compressor exit (point 2) up to Primary Heat Exchanger (PHE) inlet temperature (point 3). The recuperated sCO_2 cycle is the simplest configuration with internal heat recovery, which is anyhow characterized by a limited efficiency related to the high average temperature difference in the recuperator caused by the different heat capacities of the hot and cold streams. This penalization, due to the strong real gas effects on the cold high-pressure stream, entails a relatively low temperature at PHE inlet (point 3), which, on the other hand, allows to reduce the minimum temperature of the heat source thus increasing the heat recovered in WHR applications.

The second cycle configuration considered for the study is the recompressed recuperative cycle (RRC) (Figure 1.b), widely proposed in literature for solar [51][52][53] and nuclear applications [12][17]. In the RRC configuration, a fraction of the low pressure working fluid enters in the Heat Rejection Unit (HRU) (point 8a), it is cooled down to the minimum cycle temperature (point 1), compressed by the main compressor (point 2) and then heated up (point 3a) in the Low Temperature Recuperator (LTR). The remaining fraction (point 8b) is split just before the HRU and it is compressed to the cycle maximum pressure (point 3b) by a secondary compressor. The two flows are eventually mixed at HTR cold side inlet (point 3). The recompression allows enhancing the cycle efficiency by balancing the heat capacities of the hot and cold streams in the LTR, limiting the temperature differences in the heat exchanger and the irreversibilities related to the heat transfer process. The working fluid preheating is then completed (point 4) in the High Temperature Recuperator (HTR) which cools down the hot CO_2 exiting the turbine (point 6): temperature differences are minimized at HTR cold end and tend to increase moving towards the hot end since high pressure fluid always shows a slightly higher specific heat than the low pressure stream. As result, the thermodynamic cycle efficiency is increased, while the high effectiveness of the internal recuperative process may limit the exploitation of the variable temperature heat source thus limiting the thermal power input of the cycle and its power output.

For WHR applications, both simple recuperated (SRC) and recompressed recuperated (RRC) configurations may benefit from the adoption of a recuperator bypass: an additional heat exchanger in parallel to the recuperator which allows to reduce the temperature difference in the recuperator and at the same time allows to enhance heat source exploitation by a further cooling of the exhaust gas.

In the simple recuperated cycle with recuperator bypass (SRCB) (Figure 1.c), a fraction of the CO_2 exiting the compressor (point 2) is split before the recuperator (point 2b), heated in the recuperator bypass heat exchanger (BHE) (point 3b) further cooling the heat source and then mixed with the main flow at the recuperator outlet (point 3a). In the recompressed recuperative cycle with HTR bypass (RRCB), the bypass is performed only on the HTR as reported in Figure 1.d. This cycle configuration has been suggested for high temperature applications like fossil fuel power plants [29][54] since, thanks to the introduction of the bypass stream, it combines high heat recovery factors and high thermodynamic efficiency at the expense of an additional heat exchanger.

Last cycle configuration (Figure 1.e) is the so-called turbine split flow (TSF) or dual recuperated configuration [50][55]. This cycle configuration requires two turbines and a single compressor and, as the SRCB and the RRCB configurations aims at minimizing the temperature differences in the recuperators and improve the utilization of the available sensible heat from the heat source. After the compressor, the CO_2 flow is split in two different streams. The first stream exploits the heat provided by the primary source and expands from the cycle maximum temperature (point 4) in the main turbine. The residual sensible heat available from hot expanded CO_2 (point 5 – point 6a) is used to heat the second stream from compressor outlet (point 2) up to secondary turbine inlet temperature (point 4'). After the second stream is expanded in the secondary turbine, the hot low-pressure CO_2

released by the secondary turbine (point 5') is used to preheat the first stream up to PHE inlet temperature (point 3).

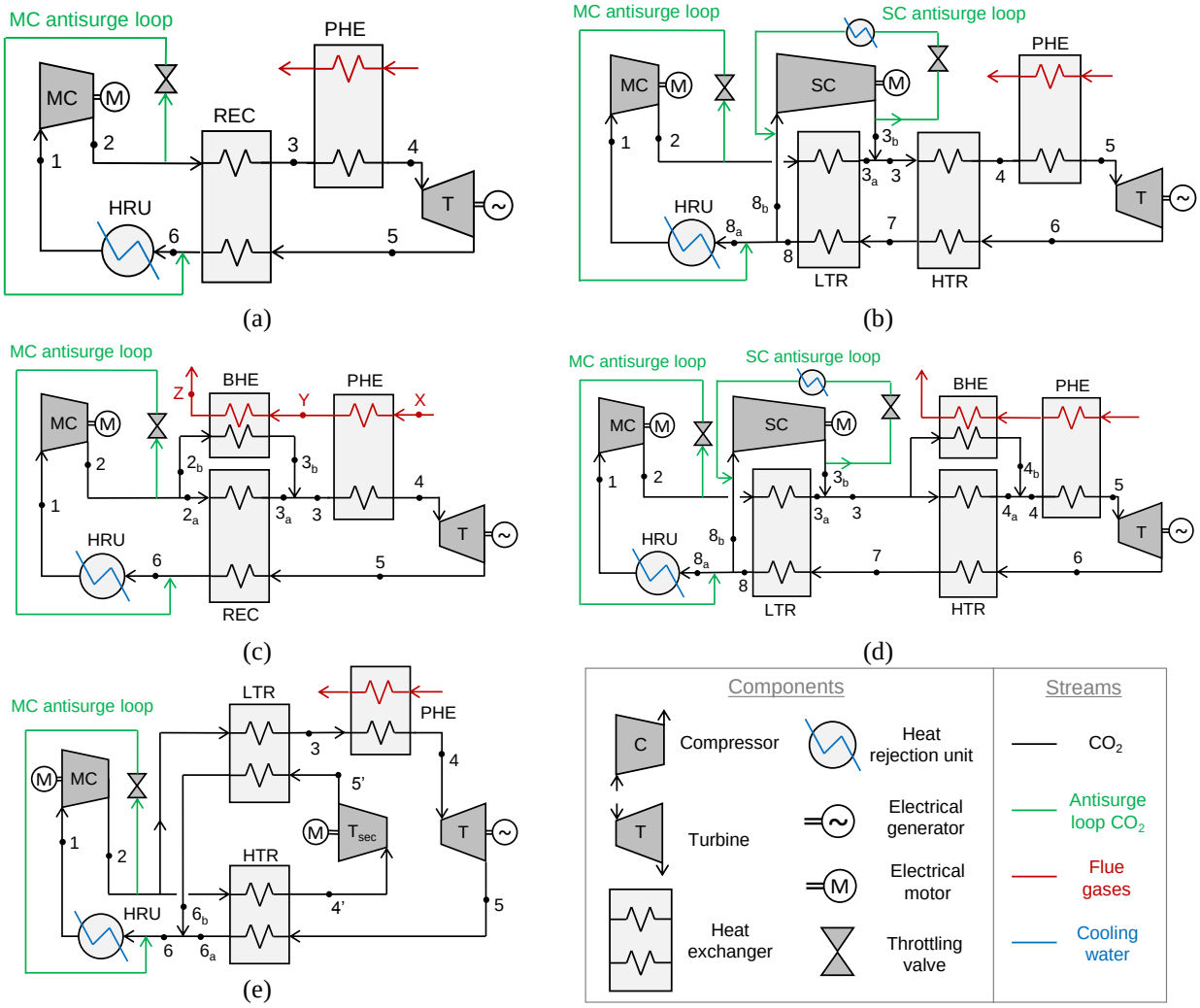

Figure 1. Schematic of the sCO_2 cycle layouts studied in this work: (a) SRC, (b) RRC, (c) SRCB, (d) RRCB and (e) TSF.

2.2 Design assumptions and system optimization

The design optimization routine evaluates the performance of the various cycle designs and selects the best combination of cycle design parameters in order to maximize a specific figure of merit.

The main figures of merit used to evaluate the system performance are the net cycle thermodynamic efficiency η_{cycle} (including HRU auxiliaries consumption, namely the cooling water circulation pump), the heat recovery factor χ and the overall plant efficiency η_{plant}. These parameters are defined in Eq. 1, Eq. 2 and Eq. 3 where the power consumption of the secondary compressor $\dot{W}_{sec\,comp}$ is equal to zero for both the SRC and SRCB and the power production from low temperature turbine ($\dot{W}_{sec\,turb}$) is null for all the configurations but the TSF. The optimization algorithm aims at maximizing the net power output and consequently the overall plant efficiency η_{plant} which takes into account not only the thermodynamic quality of the conversion from heat to electricity (through η_{cycle}), but also the fraction of heat exploited with respect to the total heat available from the heat source (through χ).

$$\eta_{cycle} = \frac{\dot{W}_{net}}{\dot{Q}_{in,cycle}} = \frac{\dot{W}_{turb} + \dot{W}_{sec\,turb} - \dot{W}_{main\,comp} - \dot{W}_{sec\,comp} - \dot{W}_{HRU,aux}}{\dot{Q}_{in,cycle}} \quad \text{Eq. 1}$$

$$\chi = \frac{\dot{Q}_{in,cycle}}{\dot{Q}_{hs,max}} = 1 - \frac{\dot{m}_{hs} c_{p,hs} (T_{stack} - T_{hs,min})}{\dot{m}_{hs} c_{p,hs} (T_{hs,max} - T_{hs,min})} \quad \text{Eq. 2}$$

$$\eta_{plant} = \chi_{rec}\,\eta_{cycle} = \frac{\dot{W}_{net}}{\dot{Q}_{hs,max}} \qquad \text{Eq. 3}$$

The heat source is modelled as a stream of gas with a mass flow rate $\dot{m}_{hs}$ of 50 kg/s, a maximum temperature $T_{hs,max}$ of 550°C, and a minimum allowable temperature of 150°C in order to avoid any formation of acid condenses and fouling on heat transfer surfaces. Gas specific heat capacity $c_{p,hs}$ is assumed constant and equal to 1.15 kJ/kgK. Heat source heat capacity can represent the flue gas of a combustion in an industrial process (steel, glass, cement industry) [35][37] or the exhausts of a small size gas turbine (i.e. in the 15-20 MW_{el} range [56]). The numerical model relies on a set of assumptions adopted for cycle design reported in Table 2 and among them, the most relevant are the cycle minimum temperature and turbomachinery efficiency. The minimum cycle temperature is set equal to 33°C in order to operate the main compression process close to the CO_2 critical point, exploiting the real gas effects, thus increasing system efficiency [57]. A water-cooled HRU is adopted for all the cycles assuming the availability of a stream of water or the adoption of a cooling tower water loop which is often available in large industrial plants: the available cooling water temperature is assumed equal to 20°C.
Regarding compressors efficiency, preliminary performance analyses report values between 83% and 85% for a 50 MW_{el} plant [58]. In this work, due to the smaller scale of the system, a more conservative value equal to 80% is adopted.
Regarding the turbine efficiency, several works on sCO_2-based solar power applications [13][14][59] suggest values between 90% and 93% as the expander design should be less complex than the compressor one thanks to the ideal gas-like behavior of CO_2 along the expansion and the larger volumetric flow rates. A more conservative value equal to 85% is here considered, taking into account the stronger impact of secondary and leakage losses on the efficiency due to the smaller size of the investigated system. A comparison of the assumed values against those attainable with correlations from reference [60] is provided in the design result section.
An additional hypothesis generally adopted in literature is related to the imposition of isothermal mixing processes to minimize mixing irreversibilities. Isothermal mixing can be assumed at HTR cold side inlet (T_{3a}=T_{3b}) by varying the split ratio at HRU inlet and for the mixing processes downstream the bypass heat exchangers in the SRCB (T_{3a}=T_{3b}) and in the RRCB (T_{4a}=T_{4b}) configurations, by varying the recuperator bypass flowrates. A sensitivity analysis on this hypothesis is provided in the result section. On the contrary, isothermal mixing is never imposed at HRU inlet of TSF configuration allowing to investigate solutions with recuperators having different cold end temperature differences.

Table 2. Heat source data and cycle design assumptions.

Parameter	**Value**
Heat source mass flow rate $\dot{m}_{hs}$, kg/s	50
Heat source temperature $T_{hs,max}$, °C	550
Minimum heat source temperature $T_{hs,min}$, °C	150
Heat source specific heat $c_{p,hs}$, kJ/kgK	1.15
Minimum cycle temperature, °C	33
Minimum PHE pinch point $\Delta T_{pp,PHE}$,°C	25
Cooling water inlet temperature, °C	20
Cooling water temperature rise, °C	7
Cooling water Δp, bar	1.5
PHE CO_2 Δp, bar	2
HRU CO_2 $(\Delta p/p_{in})$	0.5%
Recuperators hot side $(\Delta p/p_{in})$ SRC/SRCB/TSF	1%
Recuperators hot side $(\Delta p/p_{in})$ RRC/RRCB	0.5%
Turbines isentropic efficiency, η_{turb}	85%
Compressors isentropic efficiency, η_{comp}	80%
Water pump efficiency, $\eta_{water\ pump}$	75%
Generator/motor efficiency $\eta_{me,t}$/ $\eta_{me,c}$	96.4%

The five cycle configurations are optimized by varying: (i) the working fluid minimum pressure, (ii) the cycle maximum pressure (iii) the turbine inlet temperature (iv) the recuperator(s) terminal cold and hot end temperature differences, (v) the recuperator(s) pinch point(s) temperature difference and (vi) the temperature difference between streams in the mixing process(es). In order to reduce the complexity of the numerical problem the parameters (i-iv) are optimized by a dedicated optimization algorithm while parameters (v-vi) are investigated with a sensitivity analysis and considered as a constraint to the optimization process. These last parameters should

be considered in order to catch the tradeoff between heat source heat recovery and cycle internal heat recovery effectiveness. Cycle minimum and maximum pressures are selected considering the trade-off between the need of having high cycle expansion ratio and the need to increase compressor fluid average density by exploiting the low compressibility factor of the CO_2 in the proximity of the critical point. An increase of cycle maximum temperature positively affects the cycle thermodynamic efficiency thanks to the increased turbine specific work but may negatively impact on the heat recovery factor for recuperative cycles.

The location of a selected pinch point temperature difference in sCO_2 cycle recuperator(s) is non-trivial since real gas effects on the cold and high-pressure CO_2 side involve a nonlinear trend of specific heat. Pinch point temperature difference can be located within the heat exchanger instead of being on the hot or cold end of the recuperator depending on the minimum and maximum pressure of the cycle. Moreover, for configurations provided by recuperator bypass (SRCB and RRCB) and for the TSF configuration it is possible to design the recuperator (HTR for RRCB and TSF) having the minimum temperature difference at cold end, at hot end, or at both extremities by tuning the bypass split ratio. For this reason, the terminal cold end and hot end temperature differences of recuperators are included as optimization variables while desired pinch point temperature differences are considered as constraints to the optimization algorithm and varied by an enumerative approach.

The optimization algorithm selected to maximize the net power output of the systems is the *patternsearch* algorithm available in the MATLAB optimization toolbox. *Patternsearch* is a direct search algorithm for constrained optimization problems which evaluates, at each iteration step, the objective function over an increasing/decreasing/rotating mesh of tentative solution and it does not require gradient calculation [61]. As result it can deal with non-continuous and non-differentiable functions and shows a good ability in avoiding local minimum/maximum. This algorithm has been preferred to simple *fmincon* and complex *genetic* or *particle swarm* algorithms because it shows a good compromise between computational time and accuracy of the solution. The number of free variables for each cycle configuration is reported in Table 3 and it increases with cycle complexity reaching six optimization variables plus four sensitivity analysis parameters for the RRCB configuration. Figure 2.a depicts the flow diagram at the base of the single simulation and the design optimization iterative procedure for the SRCB configuration. Scheme shows all the interconnections between the assumptions, the optimization variables and the calculation of the different thermodynamic points and quantities.

Table 3. Optimization variables for the different cycle layouts

	SRC	**SRCB**	**RRC**	**RRCB**	**TSF**	**Lower Bound**	**Upper Bound**
Parameters varied by sensitivity analysis and considered as constraints for the optimization algorithm							
$\Delta T_{pp,REC}$, °C	X	X				10	75
$\Delta T_{pp,LTR}$, °C			X	X	X	10	75
$\Delta T_{pp,HTR}$, °C			X	X	X	10	75
$\Delta T_{mix,REC,outlet}$ or $\Delta T_{mix,LTR,outlet}$, °C		X	X	X		-30	+30
$\Delta T_{mix,HTR,outlet}$, °C				X		-30	+30
Optimization variables varied by *patternsearch* optimization algorithm to maximize η_{plant} and respect recuperator(s) pinch point temperature difference and mixing process temperature difference constraints							
p_{min}, bar	X	X	X	X	X	75	150
p_{max}, bar	X	X	X	X	X	150	250
T_{max}, °C	X	X	X	X	X	200	525
$\Delta T_{cold-end,REC}$, °C	X	X				10	75
$\Delta T_{hot-end,REC}$, °C		X				10	75
$\Delta T_{cold-end,LTR}$, °C			X	X	X	10	75
$\Delta T_{hot-end,LTR}$			X	X		10	75
$\Delta T_{cold-end,HTR}$, °C					X	10	75
$\Delta T_{hot-end,HTR}$, °C				X	X	10	75

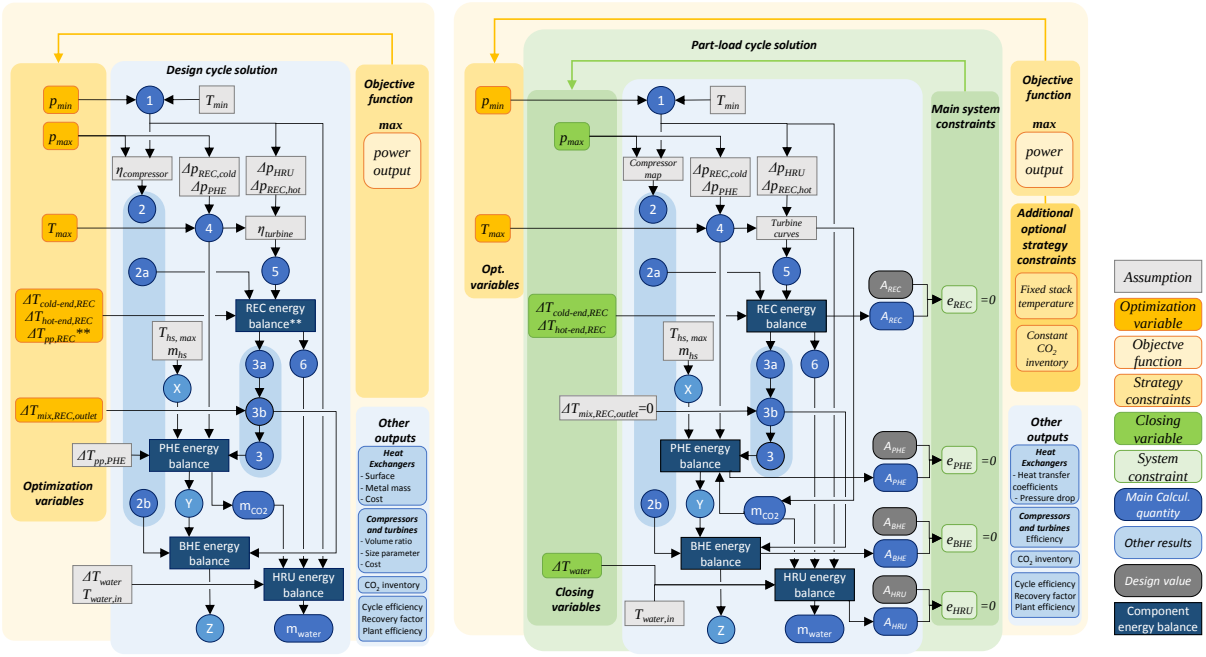

(a) SRCB Design optimization *(b) SRCB Part-load optimization*

Figure 2. Flow diagrams representing all the interconnections between assumptions, optimization variables and calculated quantities for the design optimization routine (a) and the part-load routine (b) referred to SRCB configuration.

Heat exchanger design is carried out with a dedicated set of numerical routines for the calculation of the heat transfer coefficients, the volume of fluid and the mass of the heat exchangers. The recuperators are modelled as printed circuit heat exchangers (PCHE) according to the model suggested in [62] integrated with manufacturer data already presented in [19] and reported in Table 4. The minimum temperature difference in each recuperator directly affects the thermal duty while the assumed hot side allowable pressure drop directly affects the CO_2 velocity in the heat exchanger, the heat transfer coefficients and the channels length. The numerical code assumes perfect counter-current flow arrangement and the same number of channel flows on both hot and cold side. Hot fluid velocity is varied in order to match the desired pressure drop and eventually, the global heat transfer coefficient referred to the internal surface (U_{int}) (Eq. 5), the actual heat transfer area (Eq. 6) and metal mass of the heat exchanger as well as the pressure drops on the cold side are computed. Each heat exchanger is discretized in 30 sections in order to catch local variations of fluid thermophysical properties and calculate the needed heat transfer area with higher accuracy The PHE and the BHE (if present) are modelled as finned tube heat exchangers with CO_2 inside the tubes and flue gas flowing outside the tubes bundles. The HRU is modelled as a shell and tubes (S&T) heat exchanger with the CO_2 flowing into the tubes while cold water flows in the shell. CO_2 pressure drop side in BHE is set equal to the cold side pressure drop of the bypassed recuperator, in order to limit the mixing irreversibilities at the end of the two components. In the HRU, the cooling water pressure drops are considered fixed and assumed equal to 1.5 bar, while in the PHE and BHE the hot gas side pressure drops are neglected. The HRU, PHE and BHE tubes thicknesses have been computed through Eq. 4 starting from the internal diameters reported in Table 4, adopting ASME allowable stress value (σ_{max}) [63] and considering a safety factor of 1.15.

$$t = 1.15\left[\frac{p \cdot d_{ext}}{2\sigma_{max}(T) + p} + 0.005 d_{ext}\right] \qquad \text{Eq. 4}$$

From the design of each heat exchanger, and assuming a connecting piping length value between the different cycle components, the nominal CO_2 plant inventory is calculated. The piping length is assumed equal to 15 m for each pipe connected to the PHE and the HRU while all other pipes are assumed to be 2 m long. The internal piping diameter has been computed considering a maximum CO_2 velocity equal to half the erosional one [64], while the external diameter and piping thickness has been computed through Eq. 4. For simplicity, the piping thermal losses and their pressure drops are neglected. Table 4 reports the main assumptions related to the heat exchangers design adopted in this work.

$$U_{int} = \left(\frac{1}{htc_{int}} + \frac{d_{int} \cdot \ln\left(\frac{d_{ext}}{d_{int}}\right)}{2k_{metal}} + \frac{1}{\frac{A_{ext,finned}}{A_{ext,plain}} \cdot \frac{A_{ext,plain}}{A_{int}} \cdot htc_{ext}} \right)^{-1} \quad \text{Eq. 5}$$

$$A_i^{des} = \sum_{n=1}^{30} \frac{Q_{i,n}}{U_{i,n}\Delta T_{i,n}}, \text{ with } i = [HRU, REC, LTR, HTR, BHE, PHE] \quad \text{Eq. 6}$$

Table 4. Main assumptions for the heat exchangers design.

REC/LTR/HTR	
HX type	PCHE
Thickness of plate, mm	1.5
Diameter of semi-circular channel, mm	2
Thickness of wall between channels, mm	0.4
Heat exchanger material	SS316L
Heat transfer correlation hot side	Gnielinski
Heat transfer correlation cold side	Gnielinski
PHE/BHE	
HX type	Finned tube HX
Tube internal diameter, mm	20
Ratio of tube pitch to external diameter	1.25
Ratio of finned to plain external area	12
Tube material	Inconel 617
Heat transfer coefficient flue gas side	125 W/m^{2}K
Heat transfer correlation CO_2 side	Dittus-Boelter
HRU	
HX type	S&T
Tube internal diameter, mm	20
Ratio of tube pitch to external diameter	1.25
Ratio of finned to plain external area	12
Tube/fin material	Copper/Aluminum
Heat transfer coefficient water side	7500 W/m^{2}K
Heat transfer correlation CO_2 side	Gnielinski

.

3. DESIGN RESULTS

In this section the results for the optimal design of the five investigated cycles configurations are presented and discussed. Not all the free variables reported in Table 3 have the same impact on cycle performance and for this reason their role is first discussed with separate sensitivity analyses on maximum cycle temperature, pinch point temperature difference in recuperators and streams temperature difference before mixing processes while minimum and maximum cycle pressures and recuperators terminal hot and cold end temperature differences are optimized at all times. Final optimal results are discussed at the end of this section.

3.1 Effect of maximum cycle temperature

In order to evaluate the effect of the maximum cycle temperature on plant performance, a sensitivity analysis is carried out optimizing both minimum and maximum cycle pressures for every considered maximum cycle temperature while considering fixed minimum temperature differences in the recuperators at the lower bound (10°C) and isothermal mixing. Figure 3 depicts the results of the sensitivity analysis on cycle maximum temperature for the simplest cycle configuration (SRC), for the most complex one (RRCB) and for the TSF configuration, to highlight the importance of optimizing this parameter independently of the cycle architecture.

The cycle maximum temperature affects both the cycle thermodynamic efficiency and the heat recovery factor: a tradeoff between these two figures is evident for both the SRC configuration (Figure 3.a1) and the RRCB configuration (Figure 3.a2). Cycle efficiency is positively affected by the increase of turbine inlet temperature as typical of gas cycles because of the increase of turbine specific work with respect to compressors specific consumption (Figure 3.b1 and b2). On the contrary, the heat recovery factor is penalized due to the higher CO_2 temperature at PHE inlet when maximum cycle temperature increases (Figure 3.c1 and c2) which entails a poor utilization of the available heat and eventually a lower CO_2 mass flow rate (Figure 3.b1 and b2). For both SRC and RRCB architectures, the turbine inlet temperature that maximizes the overall plant efficiency is fairly below the maximum limit (525°C) defined as the heat source inlet temperature minus the pinch point temperature difference at PHE (25°C). Optimal values are 391.8°C and 335.6°C for SRC and RRCB configurations respectively, giving the possibility to increase the plant efficiency by more than 3.05 and 6.94 points of efficiency with respect to the case with the highest possible value of turbine inlet temperature.

Different considerations can be stated for the TSF configuration: for this cycle architecture, the adoption of the maximum allowable turbine inlet temperature (525°C) does not imply a poor utilization of the available heat: χ is equal to 91.9% while the same figure is around 57.5% and 40% for the SRC and RRCB configurations respectively at the same maximum cycle temperature. This implies that the range of turbine inlet temperature to be investigated is narrower than for the other cycles and with a maximum temperature of 450°C a complete utilization of the available thermal power is obtained. In this temperature range (450°C-525°C) the cycle efficiency change is more marked than for the other two configurations because of the adoption of two turbines and larger than the relative increase of heat recovery factor χ, thus reducing the main turbine inlet temperature is not convenient from thermodynamic perspective.

3.2 Effect of recuperator temperature difference

The effect on the plant efficiency of assuming different recuperators pinch point temperature differences is not trivial: enhancing the effectiveness of the internal heat recovery process certainly allows to reduce the irreversibility of the compressed CO_2 heating process but, on the other hand, involves an increase of the PHE inlet temperature with a consequent limitation of heat source exploitation. In literature generally the recuperators pinch point temperature difference is always assumed equal to a fixed value (ranging generally from 5°C to 15°C) and rarely is subject to optimization. An exception is represented by the work of Held [33] where the heat exchangers UA value (overall heat transfer coefficient, *U*, multiplied by the heat transfer surface, *A*) is selected as an optimization variable rather than pinch point temperature differences. Figure 4 depicts the trend of the three figures of merit (η_{cycle}, χ and η_{plant}) as function of ΔT_{pp} of recuperator for non-recompressed cycle configurations (SRC and SRCB): turbine inlet temperature, minimum and maximum pressures are optimized at all times and isothermal mixing assumption at the exit of SRCB recuperator is adopted. For SRC plant (Figure 4.a), pinch point temperature difference can be located at recuperator cold end or within the heat exchanger depending on the cycle minimum and maximum pressure which changes from case to case. Adopting the minimum investigated ΔT_{pp} (i.e.10°C) the cycle efficiency is maximized while the heat recovery factor is around 83%. A better heat exploitation can be obtained by increasing the ΔT_{pp} but the overall effect on the plant efficiency is penalized by the contextual, and more marked reduction of cycle thermodynamic efficiency. All the optimal solutions have the pinch point temperature difference located at recuperator cold end because of the higher specific heat of cold high-pressure fluid with respect to the hot low pressure one. For SRCB plant the minimum temperature difference can be located within the recuperator, at cold end, at hot end or at both depending on the bypass mass flow rate and fluid pressures. For this configuration (Figure 4.c), the adoption of the recuperator bypass allows to totally exploit the heat source (which minimum allowable temperature is 150°C) even at minimum recuperator temperature differences, so any increase of this parameter simply contributes to a penalization of the net power output. From thermodynamic perspective, the solution with pinch point at both cold and hot ends is particularly attractive since

it allows to reach the highest internal heat recovery effectiveness without penalizing the heat recovery but, on the other hand, it entails a larger heat transfer area and investment cost.

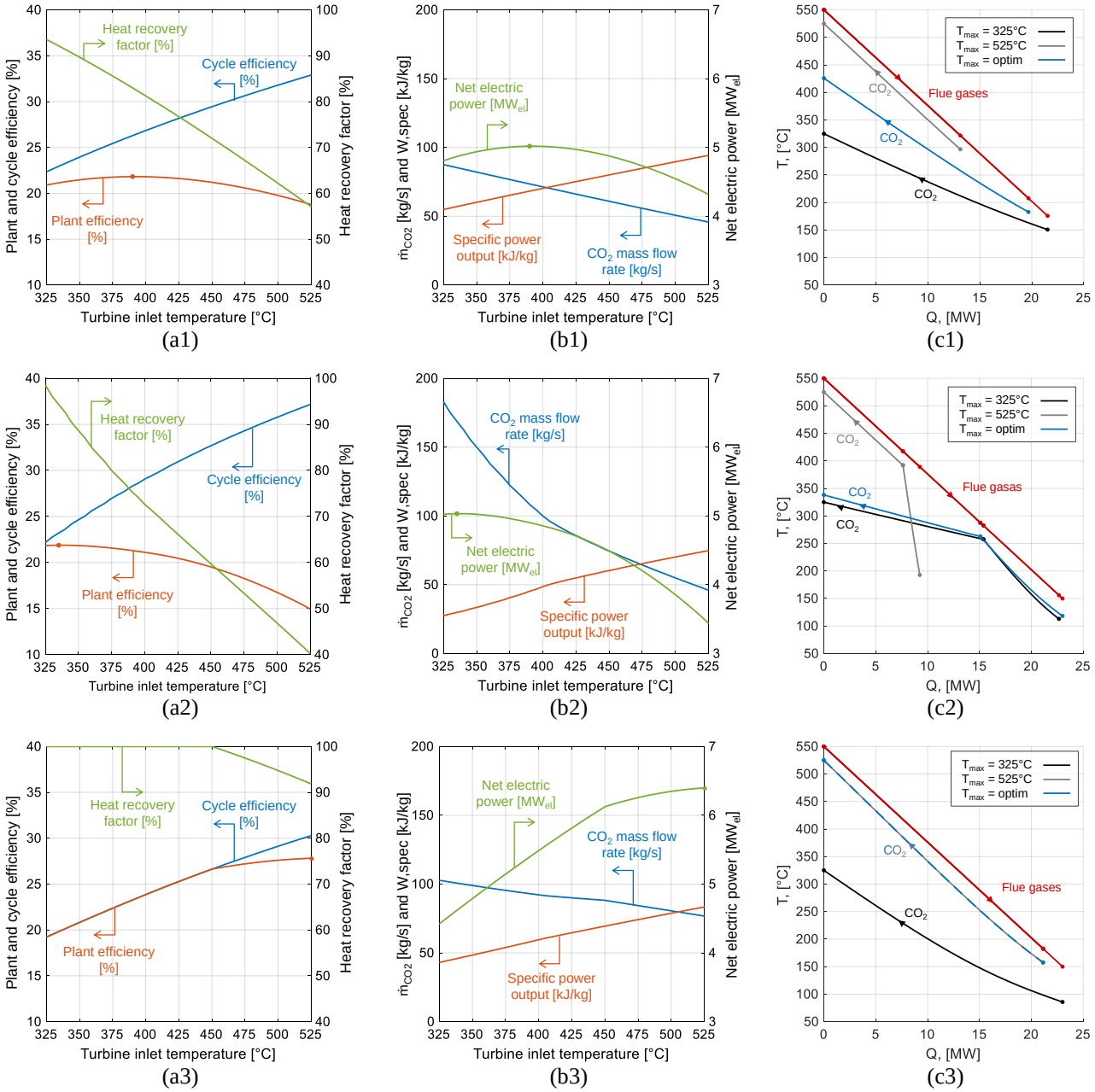

Figure 3. (a) Trends of the main system efficiencies and (b) of the net power output, of the CO_2 mass flow rate, of the specific power output as function of the maximum turbine inlet temperature. (c) T-Q diagrams of the CO_2-flue gas heat exchangers for two extreme cycles maximum temperatures and for the optimal one (blue line). The cycle configurations considered are (1) the simple recuperated cycle (SRC), (2) the recompressed recuperative cycle with HTR bypass (RRCB) and (3) the turbine split flow (TSF).

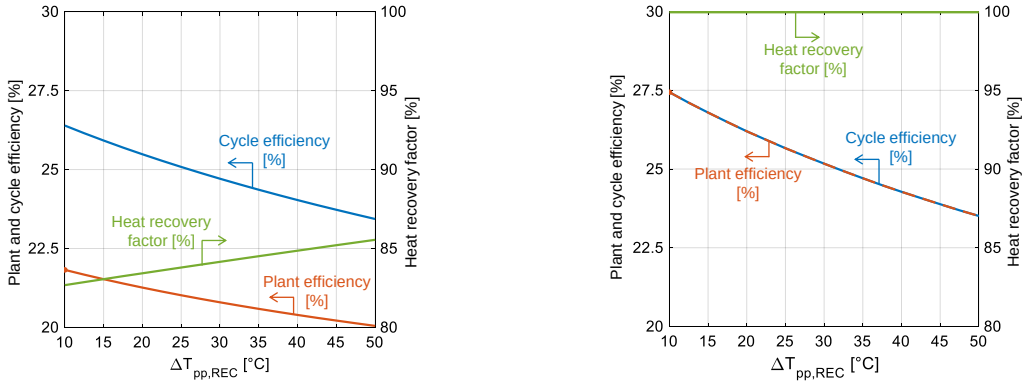

Figure 4. Trend of the three figures of merit (η_{cycle}, χ and η_{plant}) as function of ΔT_{pp} of recuperator for SRC (a) and SRCB (b) configurations.

The same analysis, applied to recompressed cycles configurations (RRC and RRCB), is less trivial because of the presence of two recuperators (LTR and HTR) and the possibility of varying both components minimum temperature differences. For the RRC cycle the heat capacity of the cold stream of the LTR is modulated by varying the split ratio at the entrance of the HRU towards the secondary compressor while the HTR works with the same mass flow rate on both sides. As result the pinch point temperature difference of the LTR may be located at cold end, at hot end or within the component while for the HTR the pinch point temperature difference is always at cold end because the high pressure cold fluid always has an average specific heat higher than the low pressure hot fluid. Considering the constraint of isothermal mixing it results that it is only possible to investigate designs with $\Delta T_{pp,HTR} \geq \Delta T_{pp,LTR}$ and the two temperature differences coincide when the pinch point is located at hot end of LTR and at cold end of HTR. Figure 5.a depicts the cycle thermodynamic efficiency, the heat recovery factor and the plant efficiency for the RRC configuration as function of HTR pinch point temperature difference while optimal $\Delta T_{pp,LTR}$ is always equal to the minimum value (10°C) because higher values lead to an increase of the thermal power released to the HRU with penalizing effects on cycle thermodynamic efficiency. For each point the performance is maximized by varying the cycle minimum and maximum pressure, the turbine inlet temperature, the $\Delta T_{cold\,end,LTR}$ and the $\Delta T_{hot\,end,LTR}$ (also equal to $\Delta T_{cold\,end,HTR}$ because of the constraint of isothermal mixing at LTR outlet). Adopting the minimum value of ΔT_{pp} for both LTR and HTR results in a very high thermodynamic efficiency (27.9%) but in a poor utilization of the heat source (69.2%) finally resulting in a plant efficiency of 19.3%. Increasing the $\Delta T_{pp,HTR}$ the HTR duty progressively decreases (Figure 5.b), reducing the boiler inlet temperature and increasing the heat exploitation. Results clearly show that the optimal RRC configuration collapses on the SRC configuration substantially eliminating both the HTR (by employing a very high ΔT_{pp}) and the secondary compressor (using split fraction close to 1) as reported in both Figure 6.b and in the Ts diagram in Figure 5.c.

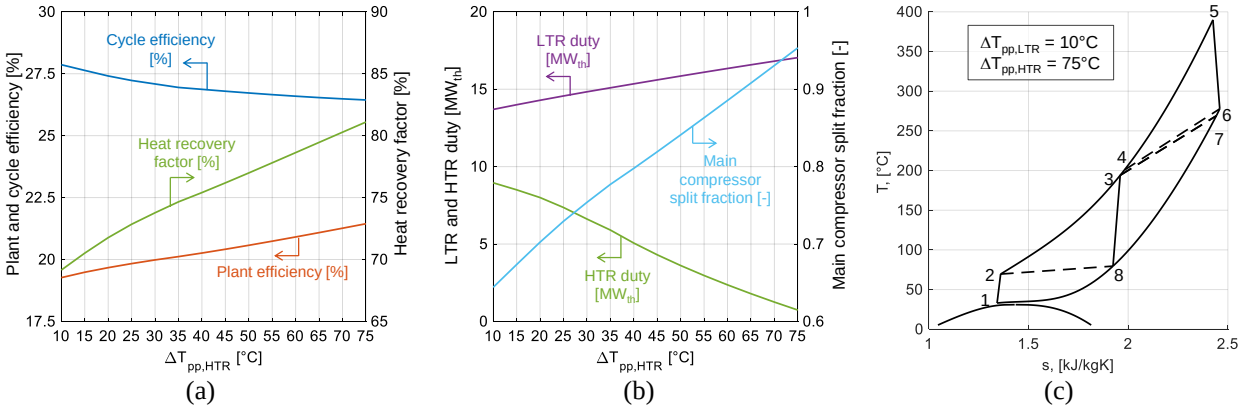

Figure 5. Results for the RRC configuration: (a) trend of η_{cycle}, χ and η_{plant} as function of ΔT_{pp} of HTR, (b) trend of recuperators duty and main compressor split fraction as function of ΔT_{pp} of HTR, (c) T-s diagram of optimal RRC configuration. Dashed lines in (c) represent the cold and hot extremities of the recuperators

For the RRCB configuration thanks to the HTR bypass it is possible to consider cases where the $\Delta T_{pp,HTR}$ is located at the hot end of the heat exchanger thus enabling the possibility to investigate solutions with HTR minimum temperature difference lower than the LTR value. Sensitivity analysis is carried out varying the pinch

point temperature difference of LTR and HTR and by optimizing the performance by varying the cycle maximum temperature, the cycle maximum and minimum pressures, the $\Delta T_{cold\text{-}end,LTR}$, the $\Delta T_{hot\text{-}end,LTR}$ and the $\Delta T_{hot\text{-}end,HTR}$ while always considering a isothermal mixing a both LTR and HTR recuperators. Best result is obtained adopting the minimum temperature difference (10°C) at LTR and HTR but adopting a larger value (15.6°C) for the $\Delta T_{cold\text{-}end,HTR}$. Maximum efficiency is 23.2% that is almost 1.3 points of efficiency higher than the performance attainable by adopting 10°C for all the three temperature differences.
On the contrary, the TSF configuration thanks to the very high heat recovery factor, benefits from adopting the low pinch point temperature difference in the recuperators and optimal solution is obtained considering 10°C for $\Delta T_{cold\text{-}end}$ of both recuperators and for $\Delta T_{hot\text{-}end,HTR}$.

3.3 Effect of imposing isothermal rather than non-isothermal mixing processes

General assumption in literature is to impose isothermal mixing for the recompressed cycle configuration (RRC and RRCB) at secondary compressor/LTR cold stream outlet and for the cycles with recuperator bypass (SRCB and RRCB) at recuperator/BHE outlet. This constraint involves the adoption of a specific value for the split or bypass ratio (depending on the cycle configuration) which may lead to suboptimal solutions. A sensitivity analysis is carried out in order to highlight the correctness of this assumption by varying the ΔT_{mix} (namely T_{3a}-T_{3b} and T_{4a}-T_{4b}) in a range of -30°C/+30°C thus investigating the effect of a non-isothermal mixing process. The results show that it is always beneficial to have ΔT_{mix} equal to zero at the outlet of high temperature recuperator bypass (namely at the outlet of REC in SRCB and HTR in RRCB configurations) while for the RRCB configuration optimal ΔT_{mix} at LTR recuperator outlet (T_{3a}-T_{3b}) is pushed towards negative values in order to reduce the duty in the LTR. This results in a final RRCB design that collapses on the SRCB configuration which has a higher efficiency. This numerical test shows also the stability of the numerical algorithm that, independently of the selected cycle configuration, when provided by a sufficient number of optimization variables, is able to optimize the system by excluding some components and to numerically converge to the optimal configuration.

3.4 Optimal selected cycles

Table 5 reports the overall results and the power balance of SRC, SRCB and TSF configurations optimal design while both recuperative RRC and RRCB configurations are discarded since their numerical optimization converge towards the simple cycles SRC and SRCB configurations respectively, as discussed in the previous sensitivity analysis. Figure 6 depicts the Ts diagram and the T-Q charts for heat introduction, internal heat recovery and heat rejection processes in the three selected cycle configurations. Finally, Table 6 reports the main results related to component preliminary sizing with a quantification of overall heat exchangers metal mass.
The two cycle configurations with the highest performance are the TSF and the SRCB with very similar plant efficiency equal to 27.8% and 27.4% respectively.
The TSF configuration reaches a higher cycle thermodynamic efficiency (30.3%) than the SRCB configuration (27.4%) with an almost total exploitation of the available thermal power (91.9%) while the SRCB configuration thanks to the use of the recuperator bypass can reach a total heat recovery factor confirming the crucial role of recuperator bypass for WHR systems exploiting a variable temperature heat source. Both TSF and SRCB configurations show a recuperator with ΔT_{pp} on both heat exchanger hot and cold ends thus maximizing the effectiveness of the internal heat recovery process.
TSF configuration can benefit from a more compact design of some heat exchangers: in particular, metal mass of the HRU and the recuperators (LTR+HTR) is 11.6% and 31.2% lower with respect to the SRCB. However, the metal mass of the PHE in TSF configuration is nearly twice than the sum of PHE and BHE in SRCB configuration, leading to an overall heat exchangers metal mass which is 30% higher in the TSF configuration. This implies a higher investment cost and a higher system footprint.
Results can be confirmed by verifying the correctness of turbomachinery efficiency assumptions against the results attainable with correlations developed for sCO_2 components as function of pressure ratio and size parameter [60]. Considering single-stage and multi-stage turbomachinery the efficiency for SRCB configuration ranges between 80.74% and 81.42% for the compressor and 84.32% and 87.68% for the turbine confirming that the calculated SRCB performance is realistic though a little conservative. On the contrary, TSF configuration adopts two turbines which size parameter is smaller than for the SRCB configuration because of the high pressure flow split: considering data from reference an efficiency below 85% for the primary turbine (below 82% considering a single-stage expander) and below 82% for the secondary turbine (below 79% considering a single-stage expander) is expected meaning that the calculated performance are not conservative and a realistic system efficiency is expected to be lower than the efficiency of the SRCB configuration. Considering the high performance, the lower overall metal mass and the need of a single expander the SRCB configuration looks the more promising one among the two.
With respect to RRC and SRCB configuration the SRC can reach a lower plant efficiency (21.8%) due to both lower thermodynamic efficiency (26.4%) and heat recovery factor (82.7%) but dramatically differ in required heat exchanger surface and metal mass. The recuperator metal mass in SRC is 4.7 times smaller than for the SRCB configuration because the lack of recuperator bypass does not allow to balance the heat capacity of cold and hot

side of the recuperator causing large temperature differences in the heat transfer process. Also heat introduction process of SRC configuration requires a lower heat transfer area and metal mass which is around 60% of the sum of PHE and BHE for the SRCB configuration. As result the overall metal mass of SRC configuration is less than half the metal mass required for the optimized SRCB. In conclusion, the SRC can be certainly considered as a possible solution when a low complexity, low capital cost and low footprint power plant is required by the end user or when the minimum exhaust temperature is high (e.g. 250°C-300°C) allowing to reach a plant performance of at least 28.6% and making this configuration an attractive solution against other WHR systems like ORC which efficiency generally ranges between 15-25% [31].

Considering the result of the optimization procedure for the three selected cycle configurations it is possible to highlight that the maximum pressure is pushed to the upper bound (250 bar) while minimum pressure is close to the CO_2 critical point (80 bar) for all cases in order to exploit real gas effects and high density during compression. Cycle pressure ratio results around 3 confirming the possibility to adopt compact turbomachinery with a limited number of stages. As final consideration, the results also highlight that the choice of sCO_2 cycle configuration must be always tailored to the considered application and that the adoption of configurations suggested for other applications (i.e. RRC and RRCB for high temperature cases like fossil fuel combustion or solar tower technology) may lead to questionable system design characterized by poor efficiency and very expensive equipment.

Table 5. Overall results and power balance for SRC, SRCB and TSF configurations optimal design.

	SRC	**SRCB**	**TSF**
Optimization variables optimal values			
Maximum cycle pressure p_2, bar	250	250	250
Minimum cycle pressure p_1, bar	79.19	79.88	79.18
Turbine inlet temperature, °C	391.78	411.17	525
$\Delta T_{pp,REC}$, °C	10	10	-
$\Delta T_{pp,LTR}$, °C	-	-	10
$\Delta T_{hot\ end,REC}$, °C	-	10	-
$\Delta T_{cold\ end\ HTR}$, °C	-	-	10
$\Delta T_{hot\ end\ HTR}$, °C	-	-	10
System performance			
Cycle thermodynamic efficiency, %	26.39	27.44	30.28
Heat recovery factor, %	82.68	100	91.86
Plant efficiency, %	21.82	27.44	27.82
Second law efficiency %	42.60	53.55	54.31
Power balance			
Thermal power recovered, MW_{th}	19.02	23.00	21.13
Main turbine electric power, MW_{el}	7.48	9.19	5.58
Secondary turbine electric power, MW_{el}	-	-	3.40
Main compressor electric power, MW_{el}	2.37	2.77	2.48
Heat rejection auxiliaries consumption, kW_{el}	95.28	113.55	100.00
Net electric power, MW_{el}	5.02	6.31	6.40
Mass flow rates			
CO_2 mass flow at turbine inlet, kg/s	73.13	87.18	76.75
CO_2 mass flow at bypass, kg/s	-	25.53	-
CO_2 mass flow at secondary turbine, kg/s	-	-	33.11
Cooling water mass flow rate, kg/s	462.12	550.71	484.94

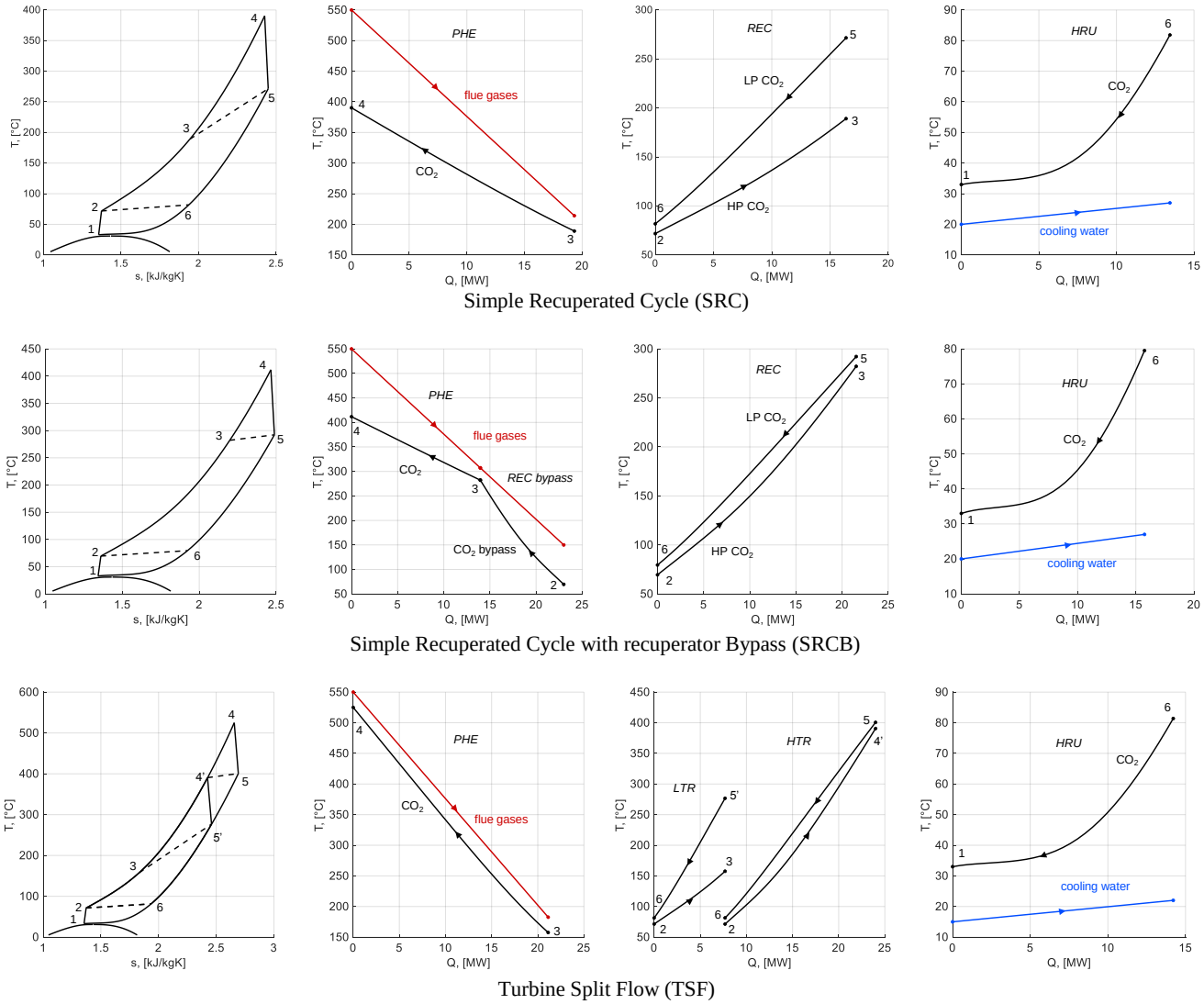

Figure 6. (a) T-s diagram of the best cycle design and corresponding T-Q diagrams of the heat source/CO2 heat exchangers (b), of the cycle recuperators (c) and of the heat rejection unit (d). Dashed lines in (a) represent the cold and hot extremities of the recuperators.

Table 6. Main results related to component preliminary sizing for SRC, SRCB and TSF configurations optimal design.

	SRC	**SRCB**	**TSF**
Total metal mass (piping excluded), kg	11455.41	24040.41	31018.84
Total metal mass (piping included) kg	17434.47	33570.24	35854.46
Total CO_2 inventory (piping excluded), kg	673.33	1224.14	1304.80
Total CO_2 inventory (piping included), kg	1338.68	2170.25	1929.89
HRU			
Duty, MW_{th}	13.54	16.14	14.21
ΔTmln, °C	27.32	27.00	27.33
U (int), W/m^2K	3752.51	3790.16	3748.78
A_{int}, m^2	153.28	180.39	161.02
A_{ext}, m^2	171.47	202.00	180.14
Metal mass, kg	1727.24	2052.59	1814.32

CO_2 mass, kg	245.93	297.47	257.83
REC (SRC, SRCB) or LTR (TSF)			
Duty, MW_{th}	17.13	22.52	7.69
ΔTmln, °C	48.69	18.38	63.45
U, W/m^2K	1446.24	845.44	1615.06
A, m^2	334.05	1557.92	112.18
Metal mass, kg	2083.02	9714.72	699.52
CO_2 mass, kg (hot/cold)	12.43/58.46	51.98/209.80	4.25/21.05
HTR (TSF)			
Duty, MW_{th}	-	-	16.31
ΔTmln, °C	-	-	24.66
U, W/m^2K	-	-	779.25
A, m^2	-	-	959.37
Metal mass, kg	-	-	5982.34
CO_2 mass, kg (hot/cold)	-	-	28.20/112.85
BHE (SRCB)			
Duty, MW_{th}	-	9.33	-
ΔTmln, °C	-	64.76	-
U (int), W/m^2K	-	718.47	-
A_{int}, m^2	-	224.31	-
A_{ext}, m^2	-	288.71	-
Metal mass, kg	-	6155.97	-
CO_2 mass, kg	-	432.21	-
PHE			
Duty, MW_{th}	19.02	13.67	21.13
ΔTmln, °C	94.25	82.30	32.00
U (int), W/m^2K	964.72	981.29	899.19
A_{int}, m^2	262.39	208.76	743.59
A_{ext}, m^2	341.82	272.27	976.52
Metal mass, kg	7645.15	6117.13	22522.66
CO_2 mass, kg	356.51	232.67	880.62
Turbine			
V_{in}, m^3/s	0.375	0.463	0.276
V_{out}, m^3/s	0.919	1.130	0.689
Z_{in}	1.011	1.017	1.042
Z_{out}	0.969	0.975	0.997
Vr	2.45	2.44	2.49
Δh, kJ/kg	106.06	109.32	132.62
PR	3.08	3.06	3.08
SP	0.050	0.055	0.041
Secondary turbine (TSF)			
V_{in}, m^3/s	-	-	0.168
V_{out}, m^3/s	-	-	0.415
Z_{in}	-	-	1.011
Z_{out}	-	-	0.969
Vr	-	-	2.47
Δh, kJ/kg	-	-	106.50
PR	-	-	3.11
SP	-	-	0.034
Compressor			
V_{in}, m^3/s	0.123	0.143	0.129
V_{out}, m^3/s	0.100	0.118	0.105
Z_{in}	0.230	0.226	0.230
Z_{out}	0.526	0.523	0.526
Vr	1.22	1.21	1.23
Δh, kJ/kg	31.19	30.60	31.20
PR	3.16	3.13	3.16
SP	0.028	0.030	0.022

3.5 Economic analysis

Finally, an evaluation of the capital investment cost for the three selected cycle configurations is carried out. Each component is described by a specific cost correlation obtained from literature, however for some components different references are available leading to a different evaluation of equipment cost and thus plant specific cost. Two main sets of cost correlations, the first one from Weiland [65] and the second from Carlson [66], are adopted in this analysis and integrated with cost correlation for sCO_2/exhaust heat exchanger (BHE and PHE) from [42][43]. Main differences between the two sets rely in the cost of turbomachinery: for the same turbine (e.g. 10 MW) Carlson correlations estimates a specific cost which is around 30% higher than the specific cost of Weiland radial turbine and around triple with respect to Weiland axial turbine (including gearbox and generator cost). Similarly, Carlson compressor cost (e.g. 5 MW) is almost two times the Weiland estimation (including motor). On the contrary, heat exchangers cost calculated with Carlson reference is 40% lower with respect to the Weiland one for the HRU and 24% lower for the recuperator. It is important to highlight that the turbine size of this paper is below the minimum size of cost correlations from literature (10 MW for axial turbine and 8 MW for radial turbine) and thus the cost of this piece of equipment is extrapolated with possible inaccuracy in economic evaluation. However, minimum turbine size is 3.4 MW for the TSF configuration while for the SRCB the turbine power output (9.19 MW) is very close to the correlation range of validity and so the economic results reported in Table 7 can be considered reliable taking into account the ±30% accuracy suggested by the authors for the cost correlations. Table 7 reports the cost breakdown of the capital investment cost of the three selected configurations carried out considering Weiland and Carlson set of correlations and using both axial and radial correlation in case of Weiland reference. Despite the different cost share obtained with the different correlations, the range of calculated specific cost is relatively narrow and comparable among the three selected configurations. Specific cost is lower for SRC configuration that benefits from very compact heat exchangers which low cost is not totally balanced by the reduction of power output, on the contrary TSF configuration shows the highest specific cost because of the larger heat transfer area and the smaller turbine size. SRCB specific cost ranges between 1617 $\$/kW_{el}$ (Weiland with axial turbine) and 2223 $\$/kW_{el}$ (Carlson): values of waste heat recovery ORC for the same range of power output are around 2000 $€/kW_{el}$ [67].

Table 7. Cost breakdown of the capital investment cost of SRC, SRCB and TSF configurations optimal design.

	SRC			SRCB			TSF		
	Weiland (axial)	Weiland (radial)	Carlson	Weiland (axial)	Weiland (radial)	Carlson	Weiland (axial)	Weiland (radial)	Carlson
PHE	1.27	1.27	1.27	1.02	1.02	1.02	3.34	3.34	3.34
BHE	-	-	-	0.80	0.80	0.80			
Turb1	0.57	2.09	3.57	0.64	2.47	4.11	0.48	1.65	2.92
GB Turb 1	0.29	0.29	-	0.31	0.31	-	0.27	0.27	-
Turb 2	-	-	-	-	-	-	0.37	1.11	2.08
GB Turb 2	-	-	-	-	-	-	0.24	0.24	-
Generator	0.33	0.33	-	0.37	0.37	-	0.36	0.36	-
Compressor	1.71	1.71	3.02	1.82	1.82	3.41	1.74	1.74	3.14
Motor comp	0.36	0.36	-	0.40	0.40	-	0.37	0.37	-
Recuperator	0.98	0.98	0.66	2.05	2.05	1.65	-	-	-
LTR	-	-	-	-	-	-	0.47	0.47	0.28
HTR	-	-	-	-	-	-	1.34	1.34	0.97
HRU	1.09	1.09	0.76	1.25	1.25	0.89	1.13	1.13	0.80
Contingency	0.46	0.57	0.65	0.61	0.73	0.83	0.71	0.84	0.95
Engineering	0.73	0.89	1.02	0.95	1.15	1.31	1.11	1.32	1.49
Total IC [M$]	7.78	9.58	10.95	10.20	12.36	14.03	11.95	14.21	15.97
Specific cost [$/KW]	1550.86	1908.45	2181.98	1616.89	1958.39	2223.29	1867.75	2220.94	2496.75

4 PART-LOAD METHODOLOGY

The part load operation of a sCO_2 system strongly depends on the cycle configuration and on the type of components installed. The part-load strategy usually aims at maximizing the plant performance while respecting a set of constraints on the components and on the sub-systems connected to the power block like the main industrial process upstream or possible thermal users downstream the WHR system. Real part-load operation inevitably refers to the direct control of some physical quantities of the system while the thermodynamic of the cycle spontaneously follows and adapts to the new operating condition. The numerical approach to part-load operation acts on different variables by imposing quantities that usually result from real plant operation (like components efficiency and temperature differences in heat exchangers) and by calculating quantities that are usually imposed in real plant (like the fluid inventory) but inevitably the final results must coincide.
The power plant part-load strategy is briefly proposed below, then the numerical approach adopted in this work is presented to provide a full explanation of the methodology and of the algorithms employed.

4.1 Real power plant part-load operation

In a real power plant, the off-design operation strategy is strongly linked to system dynamic and control. When a variation of the boundary conditions occurs, the system goes through a controlled transient to ensure proper operation of the different components and to maximize the performance in the new steady-state operative condition. The study of the dynamic and the control of sCO_2 power plants is beyond the scope of this paper, but the actions that can be reasonably done to control the system are listed below. This list of actions shall not be considered as a sequence of operation since all of them must be taken simultaneously.

- Cooling water pump rotational speed is varied to control the inlet temperature at the main compressor. Considering the very low nominal minimum temperature of the cycle (2°C above the critical point) it is seems reasonable to control the cooling medium mass flow rate to keep the minimum cycle temperature equal to the nominal one[1]. Increasing this temperature, (i.e. reducing the cooling water mass flow rate) is generally detrimental from an efficiency perspective since it involves an increase of main compressor specific work due to the CO_2 density reduction. On the other hand, reducing the main compressor inlet temperature (i.e. increasing the cooling water mass flow rate) may improve the efficiency of the system but it could possibly involve issues related to cavitation in the compressor due to vapor bubbles formation during fluid acceleration in the compressor distributor and stator [68].
- Turbine is not controlled with rotational speed, Inlet Guide Vanes (IGV) or variable degree of admission, but it is its sliding pressure operative curve (i.e. corrected mass flow vs pressure ratio) which determines the cycle maximum pressure as function of turbine inlet temperature and mass flow rate. The use of a more complex turbine design provided with features that allow to vary the machine operative curve may help to reach higher efficiencies in part load but are not strictly recommended for sCO_2 power plants. For TSF configuration the mass flow rate repartition between main and secondary turbine in part load can be different from the nominal value possibly resulting in different inlet pressures to the expanders. In this case the compressor outlet pressure is set equal to the highest value and control valves are required to guarantee a correct fluid repartition.
- Main compressor volumetric mass flow rate is varied in order to obtain the desired turbine inlet temperature while for RRC and RRCB configurations the secondary compressor mass flow rate is varied in order to ensure a desired ΔT_{mix} between the temperature of the streams at LTR and secondary compressor exit (T_{3a}-T_{3b}).
- Both main and secondary compressor operating points are set acting on available control strategies (IGV aperture and/or rotational speed variation) in order to provide the desired mass flow rate at the correct pressure while maximizing compressor adiabatic efficiency within the component operative map. These features look particularly effective for WHR sCO_2 power plants where the expected operative range is relatively wide [69]. Compressor operability is ensured by an anti-surge bypass loop which activates if the compressor operative point falls too close to the surge line.
- Recuperator bypass and HTR bypass split ratio, for SRCB and RRCB respectively, are varied to ensure a desired ΔT_{mix} between the streams at recuperator (REC or HTR) and BHE outlets (T_{3a}-T_{3b} for SRCB and T_{4a}-T_{4b} for RRCB).
- Fluid inventory is varied in order to achieve a specific objective. Considering sliding pressure turbines, when CO_2 mass flow rate is reduced also cycle maximum pressure decrease and, without an active control on fluid inventory, the minimum cycle pressure would increase to compensate the density reduction of gas in high pressure side of the cycle. The adoption of a pressurized CO_2 storage vessel may allow to

[1] Controlling the HRU operation measuring main compressor inlet temperature may lead to difficulties and system instability as small variations of temperature around the critical point, due to delay in response or measurements errors, result in dramatic variations of fluid density and thus in volumetric flow at compressor inlet. For this reason, a HRU control based on the direct measure of density at main compressor inlet with Coriolis mass flow and density meter looks more reliable [74].

vary the CO_2 mass in the system, freely vary the minimum pressure of the cycle. Fluid inventory can be varied in order to maximize plant performance or to satisfy a specific constraint like the need to control the flue gas minimum temperature due to downstream process specifications or because the need of avoiding acid condensation or fouling deposition on heat transfer surface. The CO_2 inventory storage can be constituted by a system of small vessels in parallel in order to limit the safety risk and to maintain the storage pressure nearly constant independently of stored mass. The storage system can be designed to operate with a pressure between the actual cycle maximum and minimum pressure. In this manner it is possible to depressurize the system and store fluid opening a throttling valve on the high-pressure side of the plant towards the storage and increase the fluid inventory by opening a throttling valve towards the low-pressure side of the plant. Another option is to design the inventory storage with a pressure between saturation pressure at ambient temperature and critical pressure (57 bar-73.8 bar) in order to condensate the fluid mass removed from the cycle and store it in liquid phase with less issues regarding leakages, however in this case a pump is required to fill again the system.

4.2 Numerical approach to part load operation

The numerical part load analysis is carried out varying the flue gas mass flow rate coming from the main upstream process between 30-100% of the nominal value and by imposing a set of cycle parameters: some of them are kept constant for the whole part-load operation while others are varied in order to maximize plant performance or to satisfy a specific constraint.

- Heat source maximum temperature (*fixed*): always equal to the design value thus neglecting variation of upstream main process gas cooling at part load condition. This assumption can be valid for a generic industrial or chemical process while it may not be accurate for gas turbine WHR since turbine outlet temperature can sensibly increase at part load as result of pressure ratio reduction and turbine efficiency decay, unless the gas turbine is controlled keeping the Turbine Outlet Temperature (TOT) constant [70][71].
- Cooling water minimum temperature (*fixed*): always equal to the design value according to the focus of this work on the part load analysis. Variation of minimum temperature of the cooling medium on nigh-day and seasonal base can clearly affect system performance but the penalizing effect on annual energy yield can be rather limited when water cooled or wet and dry HRU solutions are adopted [57].
- Main compressor inlet temperature (*fixed*): always equal to the design value according to the need of exploiting real gas effects in main compressor without issues related to cavitation.
- Temperature difference at mixing processes (*fixed*): always equal to zero in order to limit the irreversibility of the mixing process in SRCB, RRC and RRCB configurations.
- Main compressor inlet pressure (*varied*): this parameter affects the cycle pressure ratio with consequent effect on turbine and compressors operating point and it can be varied in order to maximize the cycle efficiency or to match a specific constraint. An example can be the need of keeping the minimum flue gas temperature at PHE/BHE outlet above a certain threshold.
- Turbine inlet temperature (*varied*): this parameter can be set constant or varied in part load in order to maximize plant performance. For example, a reduction of the TIT at part load could lead to an increase in the power output if the benefit related to the increase of CO_2 mass flow rate outweighs the detrimental effect related to the reduction of the turbine specific power.

Once the aforementioned parameters are set, the steady-state part load operating condition is obtained by solving a system of nonlinear equations each one representing the part load behavior of a component in the system (system constraints in Table 8). Table 8 also reports the selected closing variables of the off-design problem, namely those quantities, unknown a priori, that are varied by the solving algorithm in order to verify system constraints. Once the off-design problem is solved, the power output is computed and the fluid inventory variation within the system is calculated knowing the internal volume of each component, the connecting piping volume and the thermodynamic conditions of sCO_2. Table 8 only refers to the SRCB configuration which is the one selected for part load operation detailed analysis. Figure 2.b depicts the flow diagram for the SRCB part load analysis: only the first four closing variables and system constraints (referred to heat exchangers constant area) are reported in the diagram while the other ones (referred to pressure drops and turbomachinery efficiency) are omitted for sake of clarity.

Table 8. Numerical constraints and closing variable for the system of non-linear equations representing the part load (*pl*) numerical problem for the SRCB configuration. * labels closing variables directly handled by the solving numerical algorithm.

SRCB	
System constraint	**Closing variable**
$A_{HRU}^{pl} = A_{HRU}^{des}$	$\Delta T_{cooling\ water}^{pl-(*)}$
$A_{REC}^{pl} = A_{REC}^{des}$	$\Delta T_{cold\ end\ REC}^{pl-(*)}$
$A_{BHE}^{pl} = A_{BHE}^{des}$	$\Delta T_{hot\ end\ REC}^{pl-(*)}$
$A_{PHE}^{pl} = A_{PHE}^{des}$	$p_{max}^{pl-(*)}$
$\Delta p_{REC,cold}^{pl-(*)} = \Delta p_{REC,cold}^{pl-calc}$	$\Delta p_{REC,cold}^{pl-(*)}$
$\Delta p_{REC,hot}^{pl-(*)} = \Delta p_{REC,hot}^{pl-calc}$	$\Delta p_{REC,hot}^{pl-(*)}$
$\Delta p_{BHE,cold}^{pl-(*)} = \Delta p_{BHE,cold}^{pl-calc}$	$\Delta p_{BHE,cold}^{pl-(*)}$
$\Delta p_{PHE,cold}^{pl-(*)} = \Delta p_{PHE,cold}^{pl-calc}$	$\Delta p_{PHE,cold}^{pl-(*)}$
$\Delta p_{HRU,hot}^{pl-(*)} = \Delta p_{HRU,hot}^{pl-calc}$	$\Delta p_{HRU,hot}^{pl-(*)}$
$\eta_{main\ comp}^{pl-(*)} = \eta_{main\ comp}^{pl-calc}$	$\eta_{main\ comp}^{pl-(*)}$
$\eta_{turbine}^{pl-(*)} = \eta_{turbine}^{pl-calc}$	$\eta_{turbine}^{pl-(*)}$

As reported in Table 8, main closing variables are the temperature differences in the recuperators that are varied in order to match the calculated heat transfer area in part load (*pl*) operation with the design value (*des*). Off design heat transfer area of each heat exchanger is imposed equal to the design value and calculated considering the same discretization of the component in order to catch local variations of thermodynamic properties as reported in Eq. 5 and Eq. 6.

Pressure drops and heat transfer coefficients on the CO_2 side are computed by adopting the same correlations used for the cycle design using the average stream properties in each heat exchanger subsection; for flue gas and cooling water, Eq. 7 and Eq. 8 are used for pressure drops and heat transfer coefficients respectively [72]. As CO_2 side pressure drops directly affect fluid thermodynamic and transport properties, thus influencing both the heat exchanger duty and the heat transfer coefficients, from the numerical stability point of view it is preferable to include them as closing variables and constraints in the system of equations representative of the off-design problem as reported in Table 8.

$$\Delta p_{pl} = \Delta p_{des} \left(\frac{\rho_{des}}{\rho_{pl}}\right) \left(\frac{\dot{m}_{pl}}{\dot{m}_{des}}\right)^2 \qquad \text{Eq. 7}$$

$$htc_{X,pl} = htc_{X,des} \left(\frac{\dot{m}_{X,pl}}{\dot{m}_{X,des}}\right)^{\alpha} \quad \text{with} \begin{cases} X = gas & \alpha = 0.6 \\ X = water & \alpha = 0.8 \end{cases} \qquad \text{Eq. 8}$$

Turbomachinery design can be assumed coherent with the design proposed by Baker Hughes General Electric (BHGE) in the framework of sCO2-Flex project [29] adopting the following design criteria and off design performances.

Both main and secondary compressor are designed as multistage centrifugal compressors, each one mounted on a dedicated high-speed shaft driven by a variable speed electrical motor. In addition, compressors are provided by Inlet Guide Vanes (IGV) which are close to fully open position in nominal condition. Compressors efficiency variation at part-load is evaluated as function of normalized volumetric flow rate and normalized enthalpy rise ratios with respect to the nominal values, adopting dimensionless operative maps provided by BHGE [73].

Compressors maps have been developed considering the possibility to act on both shaft rotational speed and IGV aperture in order to maximize the compressor efficiency for any operating condition. Main compressor map is reported in Figure 7 highlighting the iso-efficiency levels.

In part load conditions the compressor can be operated in a high efficiency region down to low volumetric flow rates by contextually reducing the cycle pressure ratio and controlling the compressor mainly through speed variation and adjusting the IGV aperture only when rotational speed is close to lower or upper limit. However, if the variation of enthalpy head is too high, the operative point moves towards the choked flow region characterized by low turbomachinery performance (path A). On the contrary, if the enthalpy head remains fairly constant at part load, the compressor operative point approaches the surge line and the surge safety limit computed considering a 10% margin with respect to the volumetric flow rate that causes an incipient surge condition for a given enthalpy head. If the volumetric flow rate falls below this limit, the anti-surge loop is activated to maintain a proper compressor inlet volumetric flow rate and avoid instability issues (path B). When compressor anti-surge bypass

is activated, a fraction of CO_2 mass flow rate is recirculated from the outlet of the compressor, throttled down to cycle minimum pressure and cooled in order to keep compressor inlet conditions unchanged.
The power plant HRU is used to cool down the main compressor bypass while an additional gas cooler is employed for the secondary compressor bypass for both RRC and RRCB cases. As result, the compressor elaborates a mass flow rate higher than the one required by the system, leading to an increase of the power plant internal consumption, HRU auxiliary consumptions and eventually involving a penalization of the plant overall efficiency. The compressors antisurge loops are depicted in green in Figure 1.
The expander is designed as a full admission axial turbine, mounted on a high-speed shaft according to the very high machine power density and the small turbine diameter. High speed shaft is eventually connected through a gearbox to the 3000 RPM generator shaft.
Turbine part load operative curve and off design performance is derived from BHGE calculations carried out in the frame of sCO2-Flex project [29]. Raw data on corrected mass flow rate and efficiency as function of the turbine pressure ratio (at fixed outlet pressure) have been normalized with respect to nominal quantities. Then the turbine off-design behavior has been implemented as the normalized corrected mass flow rate and the normalized efficiency (Figure 7.b) against the normalized load coefficient (Eq. 9) which is proportional to the normalized enthalpy drop for a fixed rotational speed turbine. Part load isentropic turbine efficiency remains fairly constant until the pressure ratio is above half of the critical value. Compressors and the turbine efficiencies affect the thermodynamic of the cycle and, as for the heat exchanger pressure drops, it is preferable to include them as unknown quantities in the system of equations representing the off-design problem as reported in Table 8.

$$k_{is*} = \frac{\Delta h_{is}^{pl}}{\Delta h_{is}^{des}} \left(\frac{u_{is}^{des}}{u_{is}^{pl}} \right)^2 \qquad \text{Eq. 9}$$

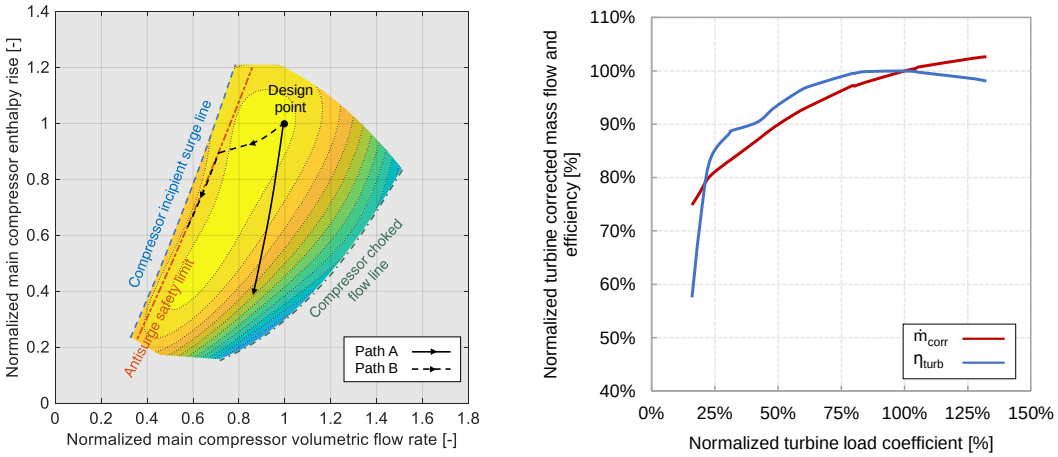

(a) (b)

Figure 7. Normalized operative map of main compressor (a) and normalized operative curve of the turbine (b) (normalized corrected mass flow rate (red) and the normalized efficiency (blue) vs. the normalized load coefficient).

5. PART-LOAD RESULTS

Part load analysis is carried out only for the SRCB configuration which represents a good compromise between design efficiency, system complexity and specific cost. Different part-load cycle operation strategies can be implemented in order to optimize the power production and/or to meet specific operational constraints. Two main parameters have been identified as optimization variables in part-load strategy definition namely the compressor inlet pressure, i.e. the cycle minimum pressure, and the turbine inlet temperature, i.e. the cycle maximum temperature. In addition, two main part-load operation constraints can be identified: the first one is related to the minimum stack temperature to be respected in order to avoid acid condenses while the second one is related to the inventory variation that can be imposed equal to zero to simulate a totally sealed cycle without the need of CO_2 storage vessel. No additional constraint is introduced to limit the maximum cycle pressure to the design value (250 bar), anyhow, the maximum value obtained in all the investigated cases is 256 bar which should not entail any safety issue.

Table 9 summarizes the different investigated strategies: strategies from S1 to S3 are obtained through CO_2 inventory change while strategies S4 and S5 with fixed CO_2 mass within the cycle. The activation of a specific strategy constraint involves an additional closing variable: as result one strategy control variable must be calculated to satisfy the additional constraint instead of being varied with the aim at maximizing power output. Maximum flue gas temperature, minimum coolant temperature and compressor inlet temperature are constant and equal to the nominal value while performance are calculated by varying the flue gas mass flow rate from 100% down to 30%.

Table 9. Summary of the different investigated part-load operation strategies.

Strategy	**Strategy control variables**		**Strategy constraints**	
	Turbine inlet temperature	*Compressor inlet pressure*	*Minimum stack temperature*	*Constant inventory*
S1	Equal to nominal	Equal to nominal	Not active	Not active
S2	optimized	optimized	Not active	Not active
S3	optimized	calculated	Active	Not active
S4	optimized	calculated	Not active	Active
S5	calculated	calculated	Active	Active

5.1 Part-load of cycles with CO_2 storage vessel

With reference to Table 9, three different strategies (S1-S2-S3) can be identified for plants that can implement inventory variation. Figure 8 reports the trends of the most relevant quantities as function of the flue gas mass flow rate: cycle maximum pressure and cycle minimum pressure (Figure 8.a), turbine inlet temperature and stack temperature (Figure 8.b), heat recovery factor and difference against S1 strategy (Figure 8.c), cycle thermodynamic efficiency and difference against S1 strategy (Figure 8.d), net power output and difference against S1 strategy (Figure 8.e), cycle pressure ratio and fluid inventory variation (Figure 8.f).

- Strategy S1 is the simplest one, it does not include any optimization in order to maximize power output and it is reported here as term of comparison: both maximum temperature and cycle minimum pressure are not varied from nominal condition with the aim of not penalizing turbine power output and keeping the main compressor inlet condition in a region with marked real gas effects. Reducing the flue gas mass flow rate, the cycle maximum pressure decreases (from 250 bar to slightly below 135 bar at minimum load, Figure 8.a) because of the sliding pressure operation of the turbine leading to a reduction of the cycle pressure ratio (Figure 8.f) from 3.13 to 1.67 with a consequent penalization of the thermodynamic cycle efficiency (Figure 8.d). Moreover, main compressor outlet temperature decreases while turbine outlet temperature increases enhancing the internal heat recovery process. Recuperator is oversized at part-load operation as it features a thermal duty lower than the nominal one leading to an increase in heat transfer effectiveness, partially balancing the detrimental effect caused by the reduction of pressure ratio on the cycle thermodynamic efficiency. For this reason, cycle thermodynamic efficiency (Figure 8.d) is above the nominal value for flue gas mass flow rates between 85% and 100% and below the nominal one for normalized flue gas mass flow rate values below 85%: at minimum load thermodynamic cycle efficiency loss is around 6.2 points. The reduced flue gas and working fluid mass flow rates involve also a higher effectiveness of PHE and BHE which operate with lower average temperature differences, involving a reduction of stack temperature (Figure 8.b) and thus a heat recovery factor higher than 100% (Figure 8.c). Minimum stack temperature is around 139°C for a flue gas mass flow rate equal to 43% of the nominal one. This aspect must be carefully considered in case of the presence of a minimum stack temperature limit due to acid condenses formation or requirements of downstream processes (other industrial heat use or flue gas treatment section). Power output (Figure 8.e) always decreases with a trend which is determined by both heat recovery factor and cycle thermodynamic efficiency trends in part load. Fluid inventory (Figure 8.f) is progressively reduced because of the lower cycle maximum pressure with

a minimum value at the minimum flue gas mass flow rate corresponding to -21% (-470 kg_{CO2}) of fluid inventory with respect to the inventory in nominal conditions.

- Strategy S2 aims at optimizing cycle power output by varying both minimum pressure (compressor inlet) and maximum cycle temperature (turbine inlet). Figure 9.a depicts the trend of power output variation against strategy S1 attainable by the adoption of different cycle maximum temperatures and by optimizing the cycle minimum pressure (Figure 9.b) at all times. Results show that in part-load it is always convenient to reduce both the cycle minimum pressure and maximum temperature in order to increase the main compressor volume flow rate and to limit the reduction of cycle pressure ratio. Only the optimal results of strategy S2, namely the envelope of iso-maximum temperature lines of Figure 9, are reported in Figure 8. By optimizing both the cycle maximum temperature and minimum pressure it is possible to increase the plant power output with respect to S1 strategy for any value of flue gas mass flow rate. For nominal flue gas mass flow rate, it is possible to increase the power output of 25 kW_{el} (Figure 8.e) thanks to the adoption of a slightly higher maximum pressure (255.8 bar vs. 250 bar) (Figure 8.a), a higher minimum pressure (81.7 bar vs. 79.9 bar) (Figure 8.a) and a lower cycle maximum temperature (400.3°C vs. 411.2°C) (Figure 8.b) while keeping nearly the same pressure ratio (Figure 8.b). As result, the cycle thermodynamic efficiency decreases (-0.4%) (Figure 8.d) while the heat recovery factor increases at 101.9% with a consequent slightly positive effect on power output. For a flue gas mass flow rate lower than the nominal one, it is convenient to reduce both cycle minimum pressure (Figure 8.a) and cycle maximum temperature (Figure 8.b) which are 77.0 bar and 378.1°C respectively at minimum load. In this manner it is possible to operate the compressor in a region of high efficiency and to further reduce the stack temperature with a minimum value of 125.9°C (Figure 8.b). At minimum load the power output is around 93 kW_{el} higher with respect to S1 strategy. Plant CO_2 inventory is higher than strategy S1 for flue gas mass flow rates above 50% of the nominal one and lower (-692 kg_{CO2} with respect to nominal baseline fluid inventory) at minimum load.
- Strategy S3 aims at optimizing the power output at any load also respecting the constraint of a minimum stack temperature equal to the nominal value (Figure 8.a). Only cycle maximum temperature is optimized while cycle minimum pressure is calculated in order to respect the stack temperature constraint[2]. Heat recovery factor (Figure 8.c) is always equal to the nominal value (100%) and the overall plant efficiency is thus equal to the cycle thermodynamic efficiency (Figure 8.d). Since the algorithm cannot further reduce the flue gas stack temperature, it pushes the cycle thermodynamic efficiency at the maximum attainable with values that are always higher than the ones found both with S1 and S2 strategies. It should be mentioned that for a nominal flue gas mass flow rate the cycle operation differs from design point because the optimization algorithm slightly increases both the maximum cycle temperature (413.0°C vs. 411.2°C) (Figure 8.b) and the cycle minimum pressure (81.3 bar vs. 79.9 bar) (Figure 8.a) with respect to the nominal values in order to get a power output increment lower than 1 kW_{el} thanks to a slightly higher compressor efficiency: this solution proves the capability of the optimization procedure but also highlights that very similar values of net power output can be obtained with different combinations of cycle maximum temperature and minimum pressure. Cycle maximum pressure (Figure 8.a) decreases at lower flue gas mass flow rates with a trend similar to both strategies S1 and S2 while cycle minimum pressure is always below the one of case S2 and higher than the nominal one only for flue gas mass flow rates above 91% of the nominal one. Power output (Figure 8.e) is lower than the nominal for flue gas mass flow rates between 48% and 100% of the nominal one (with a maximum difference of -28 kW_{el}) but reaches similar values of S2 strategy at minimum load, performing better than S1 strategy (+85 kW_{el}).

[2] The same result can be obtained by optimizing cycle minimum pressure and calculating the cycle maximum temperature.

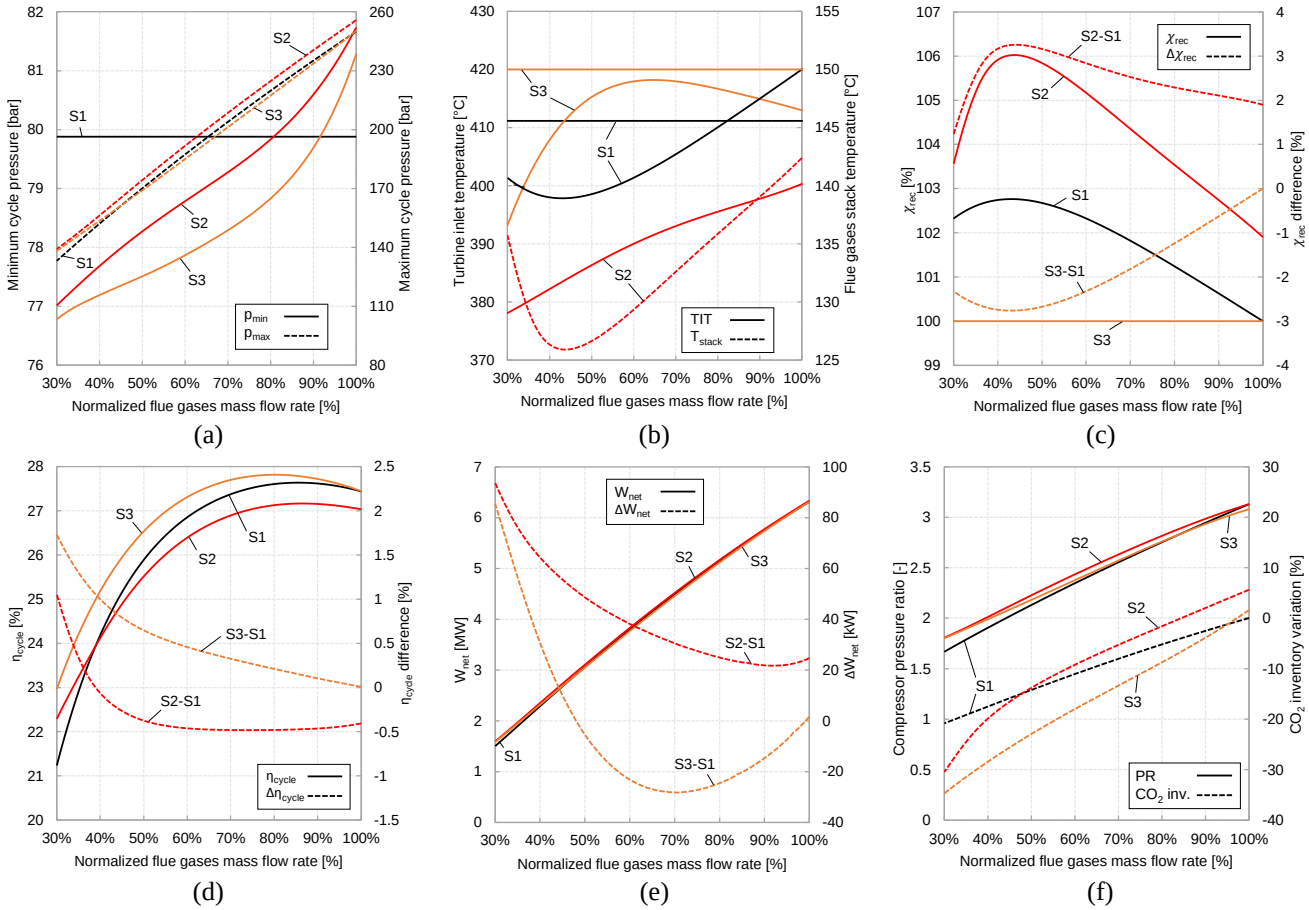

Figure 8. Trend of cycle maximum pressure and cycle minimum pressure (a), turbine inlet temperature and stack temperature (b), heat recovery factor (c), cycle thermodynamic efficiency (d), net power output (e), cycle pressure ratio and fluid inventory variation (f) against normalized flue gas mass flow rate for the strategy S1, S2 and S3.

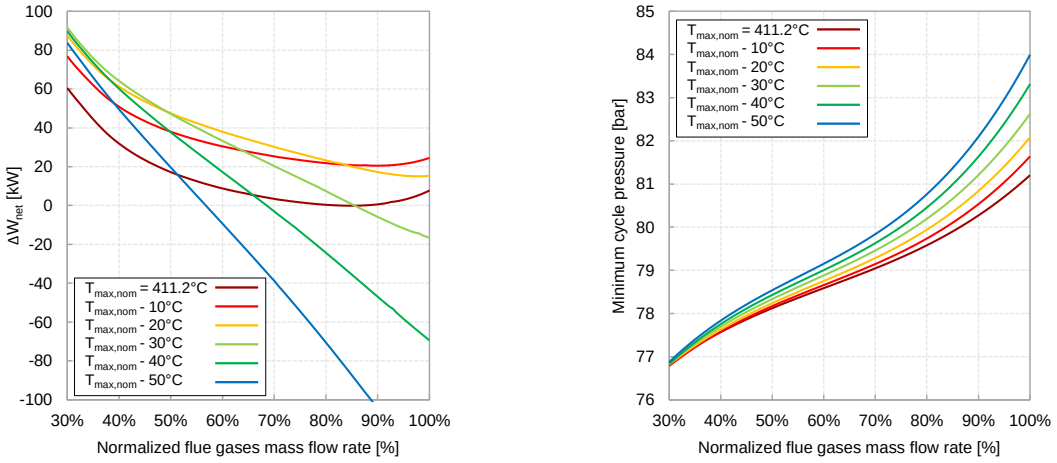

Figure 9. (a) Net power output variation with respect to S1 strategy attainable by varying cycle maximum temperatures and optimizing cycle minimum pressure at all times, (b) corresponding optimal compressor inlet pressure for the different cycle maximum temperatures.

Figure 10.a reports the main compressor operative points path on the compressor map for strategies S1, S2 and S3: each marker represents a 10% reduction of normalized flue gas mass flow rate, ranging from 100% to 30%. It is possible to highlight that the main compressor operative points for the three operating strategies are almost overlapped in the 100%-60% range, while, for further reductions of flue gas mass flow rates, S1 path drifts away from S2 and S3 paths approaching the lower limit of the compressor operative map and getting close to anti-surge limit. S2 and S3 strategies, tuning the cycle minimum pressure, allow to increase the cycle pressure ratio keeping

the main compressor operative point closer to nominal one, leading to a lower turbine efficiency penalization (Figure 10.b).

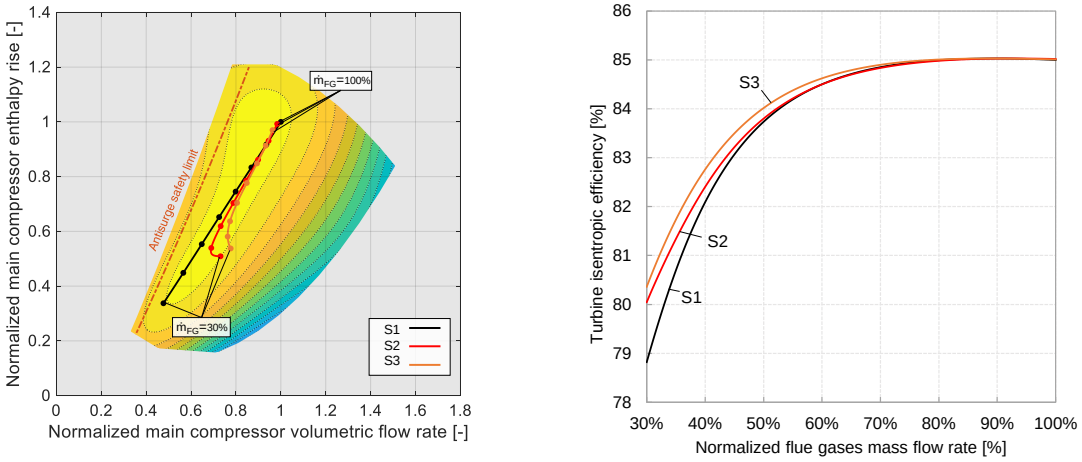

(a) (b)

Figure 10. a) S1, S2 and S3 strategies main compressor operative points and b) turbine efficiency in the range 100%-30% normalized flue gas mass flow rate.

5.2 Part-load of cycles without CO_2 storage vessel

Inventory variation involves an inevitable increase of system complexity and its control represents a non-trivial challenge because of the transients related to charging and discharging operation of the carbon dioxide vessels. Moreover, considering the relatively small size of WHR applications in industrial facilities and the need of ease installation and simplicity of operation, the possibility to design a totally sealed system that does not require inventory variation during part load looks particularly attractive. Results are shown in Figure 11 comparing the results of the two proposed constant inventory strategies (S4 and S5) against the corresponding variable CO_2 inventory strategy: namely S4 against S2 (both without active constraint on minimum stack temperature) and S5 against S3 (both with active constraint on minimum stack temperature). Strategy S4 aims at maximizing plant power output through optimization of cycle maximum temperature while keeping constant the fluid inventory by variation of cycle minimum pressure. On the contrary, strategy S5 aims at keeping the inventory constant and the stack minimum temperature above the nominal value: as a consequence, both cycle maximum temperature and cycle minimum pressure are computed to satisfy these constraints and power output cannot be maximized. Main compressor operative points and turbine efficiency values as function of normalized flue gas mass flow rate are reported in Figure 12. Considerations common to both strategies regard the trend of cycle minimum pressure (Figure 11.a) which increases at part load given the need to compensate the fluid density reduction on high pressure side of the cycle due to the sliding pressure operation of the turbine. As result, cycle pressure ratio (Figure 11.f) decreases more than in variable inventory strategies (S1-S3) leading to main compressor operative point very close to map lower bound with a penalization of compressor efficiency (Figure 12.a) and a larger drop of turbine efficiency (Figure 12.b) with respect to strategies S1-S3. The effect is more marked for S5 strategy due to the need of limiting the stack temperature variation (Figure 11.b) which involves a higher cycle maximum temperature (Figure 11.b) and consequently a higher cycle minimum pressure. On the contrary, S4 strategy is optimized by decreasing the cycle maximum temperature and the stack temperature, thus leading to a heat recovery factor greater than 100% (Figure 11.c). Imposing a constant CO_2 inventory strongly penalizes cycle thermodynamic efficiency[3] (Figure 11.d) because of the stronger reduction of pressure ratio and turbomachinery efficiencies: performance are fairly constant down to 75% of normalized flue gas mass flow rate while at minimum load the plant efficiency results to be 18.3%, equivalent to a drop of around 9.1 percentage points with respect to the nominal case (-33% on relative base). From the point of view of net electric power output (figure 11.e) both S4 and S5 strategies are penalized with a maximum loss of net power output equal to 124 kW_{el} (-7.8%) and 347 kW_{el} (-15.2%) for S4 and S5 strategies respectively when compared to S2 and S3 strategies.

[3] For S5 strategy, this parameter is proportional to system efficiency because of constant heat recovery factor.

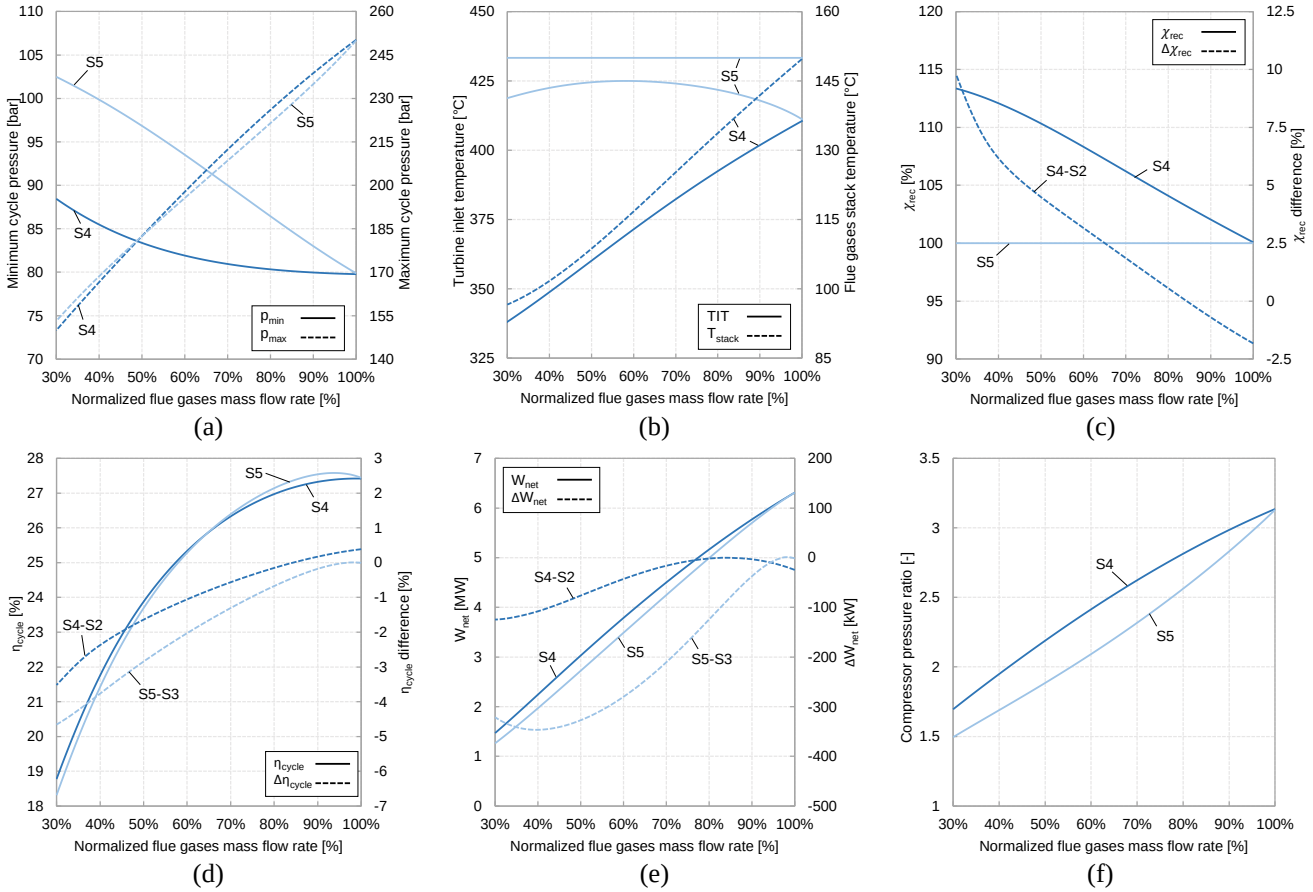

Figure 11. Trend of cycle maximum pressure and cycle minimum pressure (a), turbine inlet temperature and stack temperature (b), heat recovery factor (c), cycle thermodynamic efficiency (d), net power output (e), cycle pressure ratio (f) against normalized flue gas mass flow rate for the strategy S4 and S5.

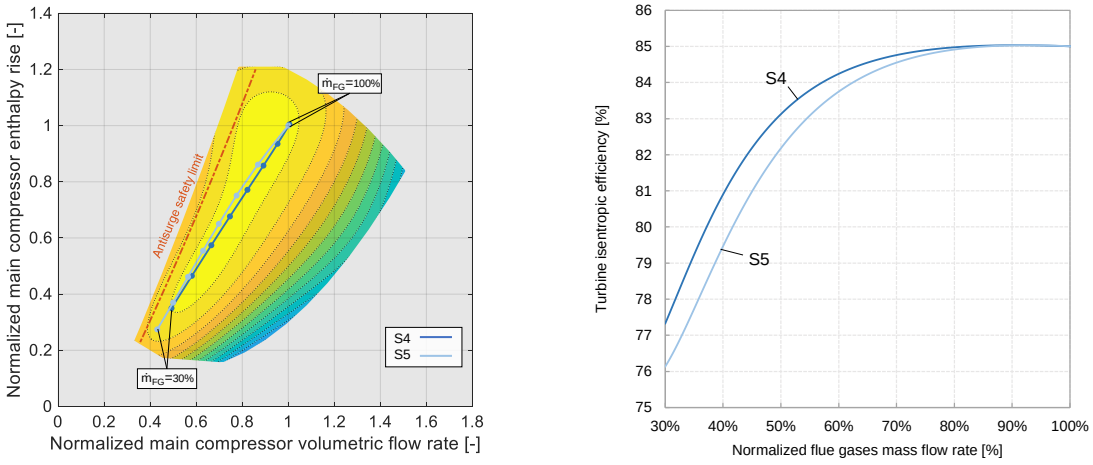

Figure 12. S4 and S5 strategies main compressor operative points (a) and turbine efficiency (b) in the range 100%-30% normalized flue gas mass flow rate.

5.3 Final comparison

Among the five proposed part load strategies, S3 and S5 have been selected as the most relevant ones as they respect the minimum stack temperature limit, avoiding an excessive cooling of the flue gases at part load. Figure 13 depicts the temperature-specific entropy diagrams for S3 and S5 strategies at 70%, 50% and 30% of normalized flue gas mass flow rate. It is possible to appreciate the fact that both strategies keep the cycle maximum temperature close to the nominal one while cycle minimum pressure is higher for S5 strategy pushing main compressor inlet condition to the left of the critical point. Finally, Table 10 reports the main results for S3 and S5 strategies at different normalized flue gas mass flow rates: it is possible to appreciate that, even if plant efficiency is fairly similar for both strategies ($\Delta\eta_{plant}$=1.3%) down to 70% normalized flue gas mass flow rate, at minimum

load the adoption of a constant CO_2 inventory strongly penalizes the plant efficiency which for S5 strategy results 4.7% points lower than for S3 strategy (-20% on relative base).

Figure 14 reports the breakdown of CO_2 inventory variation within the plant components against normalized flue gas mass flow rate for strategies S3 and S5. It is possible to highlight that for strategy S3 both maximum and minimum pressures decrease leading to a homogeneous reduction of fluid inventory in all the plant components. At minimum load about one-third of the overall CO_2 inventory needs to be stored in an external CO_2 vessel.

On the contrary, in strategy S5, as no external CO_2 vessel is considered, the cycle maximum pressure reduction due to the turbine sliding pressure operation involves a shift of the CO_2 from the high-pressure side components (cold side REC, BHE, PHE, and piping to/from PHE) to the low-pressure side components (hot side REC, HRU and piping to/from HRU) of the plant. The higher amount of CO_2 can fit in the low-pressure side of the system thanks to the reduced average temperature of the HRU and thanks to the increase of the minimum cycle pressure.

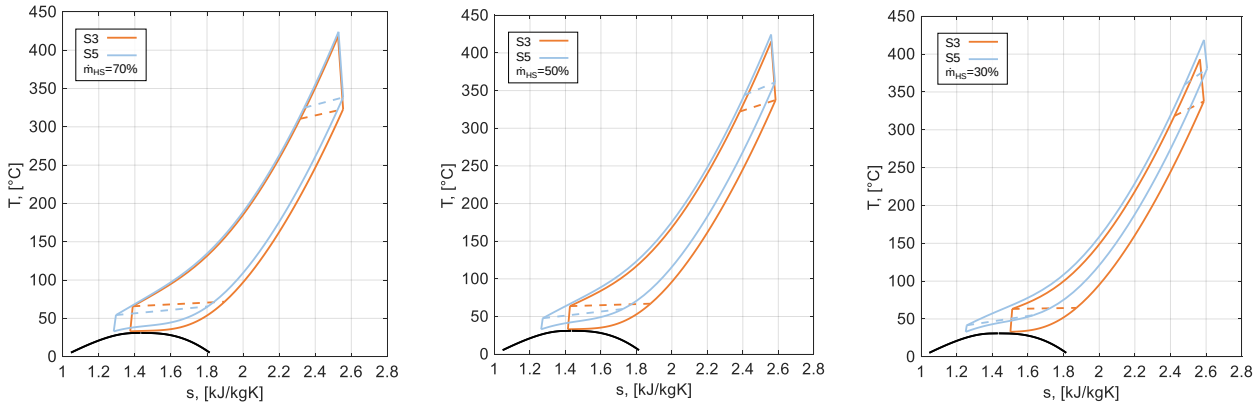

(a) (b) (c)

Figure 13. Comparison between optimized Ts diagrams of constant stack temperature S3 (variable inventory) and S5 (constant inventory) strategies for 70% (a), 50% (b), and 30% (c) normalized flue gas mass flow rate.

Table 10. main results for S3 and S5 strategies at different normalized flue gas mass flow rates.

	S3 strategy				S5 strategy			
Normalized flue gas mass flue rate [%]	90.0%	70.0%	50.0%	30.0%	90.0%	70.0%	50.0%	30.0%
Normalized electric power output [%]	90.9%	70.7%	48.4%	25.1%	90.3%	67.3%	43.2%	20.0%
Plant efficiency [%]	27.7%	27.7%	26.5%	23.0%	27.5%	26.4%	23.7%	18.3%
Gross power output [MW]	5.81	4.49	3.06	1.59	5.76	4.26	2.73	1.26
HRU consumption [MW]	0.07	0.03	0.01	0.00	0.06	0.01	0.00	0.00
Net power output [MW]	5.74	4.46	3.05	1.58	5.70	4.25	2.72	1.26
Turbine inlet temperature [°C]	414.93	417.96	415.24	393.18	417.90	424.02	424.48	418.77
Maximum cycle pressure [bar]	233.64	201.20	169.04	138.16	234.94	208.52	182.48	153.16
Minimum cycle pressure [bar]	79.69	78.29	77.51	76.78	83.00	90.00	96.85	102.50
Compressor pressure ratio [-]	2.93	2.57	2.18	1.80	2.83	2.32	1.88	1.49
Turbine isentropic efficiency [%]	85.0%	84.9%	84.0%	80.4%	85.0%	84.5%	82.2%	76.1%
Compressor isentropic efficiency [%]	80.2%	80.1%	80.0%	79.5%	80.2%	80.0%	80.0%	79.1%
Inventory variation [kg]	-87.05	-303.03	-521.29	-788.99	0.00	0.00	0.00	0.00
Inventory variation [%]	-3.8%	-13.3%	-22.9%	-34.7%	0.0%	0.0%	0.0%	0.0%

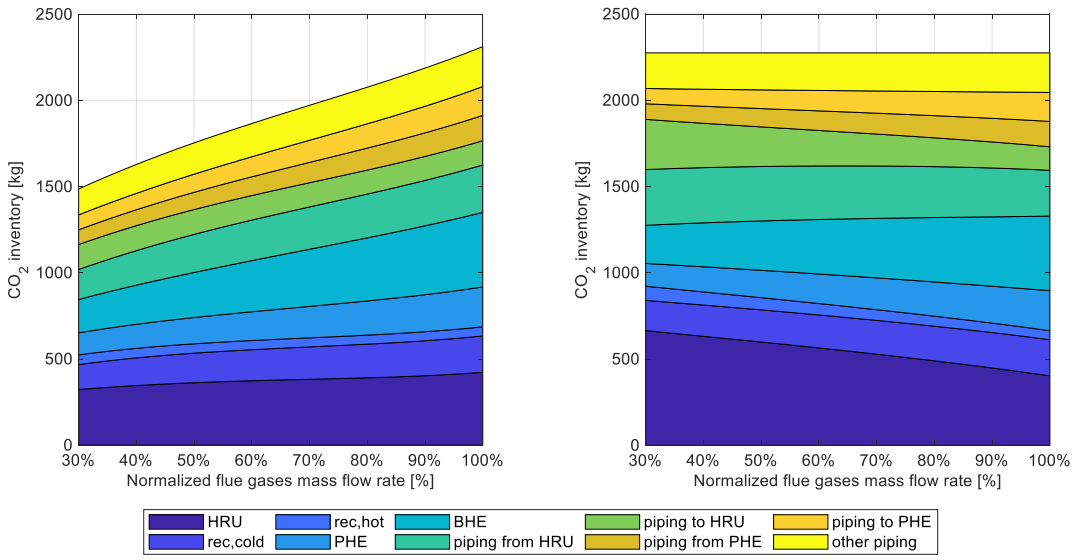

(a) (b)

Figure 14. Breakdown of CO_2 inventory variation within the plant components against normalized flue gas mass flow rate for strategy S3 (a) and S5 (b). For S3 strategy (a) the difference between actual CO_2 inventory and nominal fluid inventory correspond to the CO_2 mass sent to the storage.

6. CONCLUSIONS

In this work the numerical optimization of sCO_2 power plants for a WHR application has been performed and the best control strategies in part load operation have been identified. Assuming as heat source a flue gas stream of 50 kg/s at 550°C with a minimum stack temperature of 150°C, a preliminary sizing heat exchanger and the definition of turbomachinery main parameters has been also carried out, as well as an analysis on the system investment cost. The main outcome of the study is that sCO_2 cycles are a viable technical solution for industrial waste heat recovery applications showing nominal efficiencies higher than ORC, comparable plant specific costs and nearly stable part-load performance down to 50% of the thermal input. More detailed conclusions can be listed referring to design and part-load results.

Conclusions on cycle design optimization

- Not all the cycle configurations are appropriate for WHR applications. In particular, recompressed cycles, due to their effective internal heat recovery, show a poor utilization of the heat source and thus a lower overall plant efficiency.
- Cycle minimum pressure needs to be optimized for any operating conditions according to the assumptions on all the other cycle parameters. As a general observation, the variation of the optimal cycle minimum pressure between the different configurations is rather limited in order to allow the operation of the main compressor in the proximity of the CO_2 critical point in order to benefit from the consequent marked real gas effects.
- Sensitivity analysis demonstrates that optimal turbine inlet temperature can be significantly lower than the maximum allowable cycle temperature: in most of the cycles it is convenient to reduce this parameter in order to improve waste heat utilization, while for the TSF configuration the cycle maximum temperature is pushed to the upper bound as this does not limit the heat recovery factor.
- Adopting the minimum allowable pinch point temperature difference in the recuperators and minimizing the temperature difference at mixing processes is generally correct unless it leads to a poor exploitation of the heat source. This is the case for the recompressed RRC and the RRCB configurations which optimization collapse towards SRC and SRCB configurations respectively when those quantities are optimized.
- The three best cycle configurations are the SRC, the SRCB and TSF. Overall plant efficiency of SRCB and TSF is relatively similar (around 27.5%) but the first one can benefit from the adoption of a single turbine, a more compact heat exchangers design and eventually a lower system specific cost. The plant efficiency of the SRC configuration (22%) is significantly lower than the one of SRCB but also allow for lower Capex investment.
- At a similar plant specific cost, sCO_2 power plants can reach a higher overall conversion efficiency with respect to ORCs, as organic compounds feature a limited maximum allowable temperature due to thermal stability and decomposition issues.

Conclusions on cycle part load analysis

- Different part load strategies can be implemented depending on the equipment installed in the system and on the choice of part-load active constraints. In particular both variable and constant inventory systems are analyzed.
- Best result is obtained by optimizing at each part-load condition both the cycle minimum pressure and the cycle maximum temperature by actively controlling the cycle inventory. Imposing a limit in heat source minimum temperature (in order to avoid condensed formation or because specific needs of downstream processes) involves a very little penalization of the power output and thus is a viable option in industrial field.
- The use of an external CO_2 storage vessel and thus the possibility of varying the CO_2 inventory in the cycle components has a positive impact on part-load system performance. In particular at low flue gas mass flow rates (30% of nominal one), an increase of power output equal to 20% can be attained with respect to constant inventory strategies.
- Totally sealed cycles with constant inventory can be attractive thanks to their easiness of installation and operation but are more penalized in part-load due to the increase of cycle minimum pressure and the marked reduction of cycle pressure ratio. However, they can operate with nearly constant efficiency for industrial processes characterized by rather high minimum load (>75%)

Future works

Future steps of the present research will focus on the techno-economic optimization of different cycle configurations and fixed Capex comparison among different cycle architectures. Moreover, the analysis will be extended to different type of waste heat recovery applications, as well as on a deeper comparison with state-of-art technologies for the conversion of these sources.

1106 **NOMENCLATURE**

Symbols

A	Area (m^2)
cp	Specific heat capacity (J/kgK)
d	Diameter (m)
h	Specific enthalpy (kJ/kg)
htc	Heat transfer coefficient (W/m^2K)
k	Thermal conductivity (W/mK)
$\dot{m}$	Mass flow rate (kg/s)
mln	Logarithmic mean
p	Pressure (bar)
PR	Pressure ratio
$\dot{Q}$	Thermal power (W)
s	Specific entropy (kJ/kgK)
SP	Size parameter (m)
T	Temperature (°C)
U	Overall heat transfer coefficient (W/m^2K)
V	Volumetric flow rate (m^3/s)
Vr	Volumetric ratio
u	peripheral blade speed (m/s)
$\dot{W}$	Power (W)
Z	Compressibility factor
η	Efficiency (%)
χ	Heat recovery factor (%)

Acronyms

APH	Air Preheater
BHE	Bypass Heat Exchanger
CSP	Concentrating Solar Power
GB	Gearbox
HRU	Heat Rejection Unit
HTR	High Temperature Recuperator
HTRB	High Temperature Recuperator Bypass
HX	Heat Exchanger
IGV	Inlet Guide Vanes
LTR	Low Temperature Recuperator
ORC	Organic Rankine Cycle
PCHE	Printed Circuit Heat Exchanger
PHE	Primary Heat Exchanger
REC	Recuperator
RRC	Recompressed Recuperated Cycle
RRCB	Recompressed Recuperated Cycle with HTR bypass
sCO_2	Supercritical CO_2
S&T	Shell &Tube
SR	Split Ratio
SRC	Simple Recuperated Cycle
SRCB	Simple Recuperated Cycle with Recuperator Bypass
TIT	Turbine Inlet Temperature
TOT	Turbine Outlet Temperature
TSF	Turbine Split Flow Cycle
WHR	Waste Heat Recovery

AKNOWLEDGEMENTS

The sCO2-Flex project has received funding from the European Union's Horizon 2020 research and innovation programme under grant agreement N° 764690.

REFERENCES

[1] European Parliament, "Directive 2018/2002/EU amending Directive 2012/27/EU on Energy Efficiency," *Off. J. Eur. Union*, vol. 328, no. November, pp. 210–230, 2018.
[2] C. Forman, I. K. Muritala, R. Pardemann, and B. Meyer, "Estimating the global waste heat potential," *Renew. Sustain. Energy Rev.*, vol. 57, pp. 1568–1579, 2016.
[3] M. Papapetrou, G. Kosmadakis, A. Cipollina, U. La Commare, and G. Micale, "Industrial waste heat: Estimation of the technically available resource in the EU per industrial sector, temperature level and country," *Appl. Therm. Eng.*, vol. 138, no. July 2017, pp. 207–216, 2018.
[4] G. P. Hammond and J. B. Norman, "Heat recovery opportunities in UK industry," *Appl. Energy*, vol. 116, pp. 387–397, 2014.
[5] G. Bianchi *et al.*, "Estimating the waste heat recovery in the European Union Industry," *Energy, Ecol. Environ.*, vol. 4, no. 5, pp. 211–221, 2019.
[6] D. Vance *et al.*, "Estimation of and barriers to waste heat recovery from harsh environments in industrial processes," *J. Clean. Prod.*, vol. 222, pp. 539–549, 2019.
[7] E. Macchi and M. Astolfi, *Organic Rankine Cycle (ORC) Power Systems*. Elsevier Science, 2016.
[8] T. Tartière and M. Astolfi, "A World Overview of the Organic Rankine Cycle Market," *Energy Procedia*, vol. 129, pp. 2–9, 2017.
[9] C. M. Invernizzi and D. Bonalumi, "Thermal stability of organic fluids for Organic Rankine Cycle systems," in *Organic Rankine Cycle (ORC) Power Systems: Technologies and Applications*, 2017.
[10] G. Angelino, "Carbon Dioxide Condensation Cycles For Power Production," *J. Eng. Power*, vol. 90, no. 3, pp. 287–295, Jul. 1968.
[11] E. G. Feher, "The supercritical thermodynamic power cycle," *Energy Convers.*, vol. 8, no. 2, pp. 85–90, 1968.
[12] V. Dostal, "A supercritical carbon dioxide cycle for next generation nuclear reactors," Massachusetts Institute of Technology, 2004.
[13] T. Neises and C. Turchi, "A comparison of supercritical carbon dioxide power cycle configurations with

an emphasis on CSP applications," *Energy Procedia*, vol. 49, pp. 1187–1196, 2014.
[14] T. Neises and C. Turchi, "Supercritical carbon dioxide power cycle design and configuration optimization to minimize levelized cost of energy of molten salt power towers operating at 650 °C," *Sol. Energy*, vol. 181, no. November 2018, pp. 27–36, 2019.
[15] M. D. Carlson, B. M. Middleton, and C. K. Ho, "Techno-Economic Comparison of Solar-Driven SCO2 Brayton Cycles Using Component Cost Models Baselined With Vendor Data and Estimates," in *ASME 2017 11th International Conference on Energy Sustainability*, 2017, pp. 1–5.
[16] S. P. Kao, "Application of supercritical CO2 Brayton cycle for small modular light water reactors," *Int. Congr. Adv. Nucl. Power Plants, ICAPP 2016*, vol. 3, no. September, pp. 1647–1656, 2016.
[17] J. Floyd *et al.*, "A numerical investigation of the sCO2 recompression cycle off-design behaviour, coupled to a sodium cooled fast reactor, for seasonal variation in the heat sink temperature," *Nucl. Eng. Des.*, vol. 260, no. March, pp. 78–92, 2013.
[18] M. Mecheri and Y. Le Moullec, "Supercritical CO2 Brayton cycles for coal-fired power plants," *Energy*, vol. 103, pp. 758–771, 2016.
[19] D. Alfani, M. Astolfi, M. Binotti, S. Campanari, F. Casella, and P. Silva, "Multi Objective Optimization of Flexible Supercritical CO2 Coal-Fired Power Plants," in *Volume 3: Coal, Biomass, Hydrogen, and Alternative Fuels; Cycle Innovations; Electric Power; Industrial and Cogeneration; Organic Rankine Cycle Power Systems*, 2019, vol. 3, pp. 1–11.
[20] R. Allam *et al.*, "Demonstration of the Allam Cycle: An Update on the Development Status of a High Efficiency Supercritical Carbon Dioxide Power Process Employing Full Carbon Capture," *Energy Procedia*, vol. 114, no. November 2016, pp. 5948–5966, 2017.
[21] R. Scaccabarozzi, M. Gatti, and E. Martelli, "Thermodynamic Optimization and Part-load Analysis of the NET Power Cycle," *Energy Procedia*, vol. 114, no. November 2016, pp. 551–560, 2017.
[22] P. Huck, S. Freund, M. Lehar, and P. Maxwell, "Performance comparison of supercritical CO2 versus steam bottoming cycles for gas turbine combined cycle applications," *5th Int. Symp. - Supercrit. CO2 Power Cycles*, pp. 1–14, 2016.
[23] V. T. Cheang, R. A. Hedderwick, and C. McGregor, "Benchmarking supercritical carbon dioxide cycles against steam Rankine cycles for Concentrated Solar Power," *Sol. Energy*, vol. 113, pp. 199–211, 2015.
[24] J. D. Miller *et al.*, "Comparison of Supercritical CO2 Power Cycles to Steam Rankine Cycles in Coal-Fired Applications," in *Volume 9: Oil and Gas Applications; Supercritical CO2 Power Cycles; Wind Energy*, 2017, pp. 1–12.
[25] J. Marion, M. Kutin, A. McClung, J. Mortzheim, and R. Ames, "The STEP 10 MWe SCO2 pilot plant demonstration," in *Proceedings of the ASME Turbo Expo*, 2019.
[26] J. Gary, C. Turchi, and N. Siegel, "CSP and the DOE SunShot Initiative," *System*, 2011.
[27] M. Mehos *et al.*, "Concentrating Solar Power Gen3 Demonstration Roadmap," *Nrel/Tp-5500-67464*, 2017.
[28] "SOLARSCO2OL: Unlocking the potential of integrating sCO2 in all kinds of CSP plants. Available online at: https://www.rina.org/en/media/casestudies/solarsco2ol." .
[29] "sCO2-Flex: Supporting the electricity system By making fossil fuel based electricity production more flexible. Available online at: http://www.sco2-flex.eu." .
[30] K. Brun, P. Friedman, and R. Dennis, *Fundamentals and Applications of Supercritical Carbon Dioxide (SCO2) Based Power Cycles*. 2017.
[31] M. Astolfi, D. Alfani, S. Lasala, and E. Macchi, "Comparison between ORC and CO2 power systems for the exploitation of low-medium temperature heat sources," *Energy*, vol. 161, pp. 1250–1261, Oct. 2018.
[32] "Echogen Power Systems: Waste Heat Recovery Power Generation. Available online at: https://www.echogen.com/." .
[33] T. J. Held, "Supercritical CO2 cycles for gas turbine combined cycle power plants," in *Power Gen International*, 2015.
[34] U.S. Department of Energy, "Waste Heat Recovery: Technology Opportunities in the US Industry," 2008.
[35] B. Egilegor *et al.*, "ETEKINA: Analysis of the potential for waste heat recovery in three sectors: Aluminium low pressure die casting, steel sector and ceramic tiles manufacturing sector," *Int. J. Thermofluids*, vol. 1–2, p. 100002, 2020.
[36] M. Persichilli, A. Kacludis, E. Zdankiewicz, and T. Held, "Supercritical CO2 Power Cycle Developments and Commercialization: Why sCO2 can Displace Steam Ste am," *Power-Gen India Cent. Asia*, pp. 1–15, 2012.
[37] A. Kacludis, S. Lyons, D. Nadav, and E. Zdankiewicz, "Waste Heat to Power (WH2P) Applications Using a Supercritical CO 2 -Based Power Cycle," *Power-Gen Int.*, vol. 2, no. December, pp. 1–10, 2012.

[38] M. Mohagheghi and J. Kapat, “Thermodynamic Optimization of Recuperated S-Co2 Brayton Cycles for Waste Heat Recovery Applications,” *4th Int. Symp. - Supercrit. CO2 Power Cycles*, vol. 53, no. 9, pp. 1689–1699, 2013.
[39] G. S. Martínez, D. Sánchez, F. Crespi, and G. Gavagnin, “A global approach to assessing the potential of combined cycles using supercritical technology,” *1st Glob. Power Propuls. Forum*, pp. 1–8, 2017.
[40] L. Moroz, P. Pagur, O. Rudenko, M. Burlaka, and C. Joly, “Evaluation for Scalability of a Combined Cycle Using Gas and Bottoming SCO2 Turbines,” pp. 1–10, 2015.
[41] G. Kimzey, “Development of a Brayton bottoming cycle using supercritical carbon dioxide as the working fluid,” *Electr. Power Res. Institute, Univ. Turbine Syst. Res. Program, Gas Turbine Ind. Fellowship, Palo Alto, CA*, 2012.
[42] S. A. Wright, C. S. Davidson, and W. O. Scammell, “Thermo-Economic Analysis of Four sCO2 Waste Heat Recovery Power Systems,” *5th Int. Symp. - Supercrit. CO2 Power Cycles*, pp. 1–16, 2016.
[43] M. Marchionni, G. Bianchi, and S. A. Tassou, “Techno-economic assessment of Joule-Brayton cycle architectures for heat to power conversion from high-grade heat sources using CO2 in the supercritical state,” *Energy*, vol. 148, pp. 1140–1152, 2018.
[44] M. Marchionni, G. Bianchi, S. S. Saravi, and S. A. Tassou, “Modelling and performance analysis of a supercritical CO2 system for high temperature industrial heat to power conversion at off-design conditions,” in *Proceedings of the 3rd European supercritical CO2 Conference*, 2019, pp. 1–10.
[45] “I-ThERM: Industrial Thermal Energy Recovery Conversion and Management. Available online at: http://www.itherm-project.eu/.” .
[46] G. Manente and M. Costa, “On the conceptual design of novel supercritical CO2 power cycles for waste heat recovery,” *ECOS 2019 - Proc. 32nd Int. Conf. Effic. Cost, Optim. Simul. Environ. Impact Energy Syst.*, pp. 2219–2231, 2019.
[47] The MathWorks Inc., “MATLAB version R2019b.” 2019.
[48] E. W. Lemmon, M. L. Huber, and M. O. McLinden, “NIST Standard Reference Database 23: Reference Fluid Thermodynamic and Transport Properties (REFPROP), Version 9.0,” *Phys. Chem. Prop. …*, 2010.
[49] R. Span and W. Wagner, “A new equation of state for carbon dioxide covering the fluid region from the triple-point temperature to 1100 K at pressures up to 800 MPa,” *J. Phys. Chem. Ref. Data*, 1996.
[50] F. Crespi, G. Gavagnin, D. Sánchez, and G. S. Martínez, “Supercritical carbon dioxide cycles for power generation: A review,” *Appl. Energy*, vol. 195, pp. 152–183, 2017.
[51] D. Alfani, M. Astolfi, M. Binotti, P. Silva, and E. Macchi, “Off-design Performance of CSP Plant Based on Supercritical CO2 Cycles,” in *AIP Conference Proceedings*, 2020, vol. 2303, no. i.
[52] M. Binotti, M. Astolfi, S. Campanari, G. Manzolini, and P. Silva, “Preliminary assessment of sCO2 cycles for power generation in CSP solar tower plants,” *Appl. Energy*, vol. 204, pp. 1007–1017, 2017.
[53] C. S. Turchi, Z. Ma, T. W. Neises, and M. J. Wagner, “Thermodynamic study of advanced supercritical carbon dioxide power cycles for concentrating solar power systems,” *J. Sol. Energy Eng. Trans. ASME*, vol. 135, no. 4, pp. 1–7, 2013.
[54] D. Alfani, M. Astolfi, M. Binotti, and P. Silva, “Part Load Strategy Definition and Annual Simulation for Small Size sCO2 Based Pulverized Coal Power Plant,” in *Proceedings of ASME Turbo Expo 2020 Turbomachinery Technical Conference and Exposition GT2020 June 22-26, 2020, London, England*, 2020, pp. 1–10.
[55] Y. Ahn *et al.*, “Cycle layout studies of S-CO 2 cycle for the next generation nuclear system application,” *Trans. Korean Nucl. Soc. Autumn Meet. Pyeongchang*, pp. 2–5, 2014.
[56] T. Koji, “Kawasaki L20A Gas Turbine,” 2004.
[57] D. Alfani, M. Astolfi, M. Binotti, and P. Silva, “Effect of the ambient temperature on the performance of small size sCO2 based pulverized coal power plants,” in *The 4th European sCO2 Conference for Energy Systems March 23-24, 2021, Online Conference*, 2021, pp. 1–10.
[58] J. S. Noall and J. J. Pasch, “Achievable Efficiency and Stability of Supercritical CO2 Compression Systems,” *Supercrit. CO 2 Power Cycle Symp.*, 2014.
[59] C. K. Ho, M. Carlson, P. Garg, and P. Kumar, “Technoeconomic Analysis of Alternative Solarized s-CO2 Brayton Cycle Configurations,” *J. Sol. Energy Eng. Trans. ASME*, vol. 138, no. 5, 2016.
[60] A. Romei, P. Gaetani, A. Giostri, and G. Persico, “The Role of Turbomachinery Performance in the Optimization of Supercritical Carbon Dioxide Power Systems,” *J. Turbomach.*, 2020.
[61] C. Audet and J. E. Dennis, “Analysis of generalized pattern searches,” *SIAM J. Optim.*, 2003.
[62] V. Dostal, P. Hejzlar, and M. J. Driscoll, “The supercritical carbon dioxide power cycle: Comparison to other advanced power cycles,” *Nucl. Technol.*, vol. 154, no. 3, pp. 283–301, 2006.
[63] ASME, “An International Code - ASME Boiler and Pressure Vessel Code,” *Am. Soc. Mechnical Eng.*, 2015.
[64] American Petroleum Institute, “Recommended Practice for Design and Installation of Offshore Production Platform Piping Systems,” *Am. Pet. Inst. Recomm. Pract. 14E*, 1991.

[65] N. T. Weiland, B. W. Lance, and S. R. Pidaparti, “SCO2 power cycle component cost correlations from DOE data spanning multiple scales and applications,” *Proc. ASME Turbo Expo*, vol. 9, pp. 1–17, 2019.
[66] M. D. Carlson, B. M. Middleton, and C. K. Ho, “Techno-economic Comparison of Solar-Driven sCO2 Brayton Cycles Using Component Cost Models Baselined With Vendor Data,” *Proc. ASME 2017 Power Energy Conf.*, pp. 1–7, 2017.
[67] S. Lemmens, “A perspective on costs and cost estimation techniques for organic Rankine cycle systems,” *Proc. 3rd Int. Semin. ORC Power Syst.*, no. 2010, pp. 1–10, 2015.
[68] G. Persico, P. Gaetani, A. Romei, L. Toni, E. F. Bellobuono, and R. Valente, “Implications of Phase Change On the Aerodynamics of Centrifugal Compressors for Supercritical Carbon Dioxide Applications,” *J. Eng. Gas Turbines Power*, 2021.
[69] D. Alfani, M. Astolfi, M. Binotti, E. Macchi, and P. Silva, “Optimization of the Part-load Operation Strategy of sCO2 Power Plants,” in *5th International Seminar on ORC Power Systems*, 2019, no. i, pp. 1–10.
[70] J. M. Muñoz De Escalona, D. Sánchez, R. Chacartegui, and T. Sánchez, “Part-load analysis of gas turbine & ORC combined cycles,” *Appl. Therm. Eng.*, vol. 36, no. 1, pp. 63–72, 2012.
[71] M. P. Boyce, *Gas Turbine Engineering Handbook*. 2006.
[72] F. Crespi, D. Sánchez, K. Hoopes, B. Choi, and N. Kuek, “The conductance ratio method for off-design heat exchanger modeling and its impact on an SCO2 recompression cycle,” *Proc. ASME Turbo Expo*, vol. 9, pp. 1–11, 2017.
[73] A. M. Bigi *et al.*, “sCO2-Flex D3.13 – First turbomachinery models and report,” 2020.
[74] F. Casella, G. Mangola, and D. Alfani, “Density-Based Control of Air Coolers in Supercritical CO 2 Power Cycles,” in *21st IFAC World Congress, Germany, July 12-17, 2020*, 2020.